AFWAL-TR-84-3104

METHODOLOGIES FOR THE DIRECT DIGITAL
CONTROL OF HIGHLY FLEXIBLE VEHICLES

Duane McRuer
Richard F. Whitbeck
Raymond E. Magdaleno

Systems Technology, Inc.
13766 S. Hawthorne Blvd.
Hawthorne, CA   90250

February 1985

Final Report for Period July 1982 - September 1984

FLIGHT DYNAMICS LABORATORY
AIR FORCE WRIGHT AERONAUTICAL LABORATORIES
AIR FORCE SYSTEMS COMMAND
WRIGHT PATTERSON AIR FORCE BASE, OHIO   45433

DTIC
ELECTE
SEP 3 1985

B

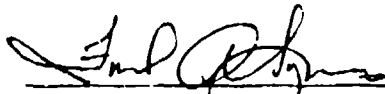This technical report has been reviewed and is approved for publication.

DAVID K. BOWSER
Project Engineer
Control Dynamics Branch
Flight Control Division

VERNON O. HOEHNE, Chief
Control Dynamics Branch
Flight Control Division

FOR THE COMMANDER

FRANK A. SCARPINO
Chief, Flight Control Division

REPORT DOCUMENTATION PAGE		READ INSTRUCTIONS BEFORE COMPLETING FORM
1. REPORT NUMBER AFWAL-TR-84-3104	2. GOVT ACCESSION NO. 4 - 11/ 44	3. RECIPIENT'S CATALOG NUMBER
4. TITLE (and Subtitle) METHODOLOGIES FOR THE DIRECT DIGITAL CONTROL OF HIGHLY FLEXIBLE VEHICLES		5. TYPE OF REPORT & PERIOD COVERED Final July 1982–September 1984
		6. PERFORMING ORG. REPORT NUMBER STI TR-1193-1
7. AUTHOR(s) Duane McRuer Richard F. Whitbeck Raymond E. Magdaleno		8. CONTRACT OR GRANT NUMBER(s) F33615-82-C-3614
9. PERFORMING ORGANIZATION NAME AND ADDRESS Systems Technology, Inc. 13766 S. Hawthorne Blvd. Hawthorne, CA 90250		10. PROGRAM ELEMENT, PROJECT, TASK AREA & WORK UNIT NUMBERS P.E. 61102F 2304 N3 27
11. CONTROLLING OFFICE NAME AND ADDRESS Flight Dynamics Laboratory (AFWAL/FIGC) Air Force Wright Aeronautical Laboratories Wright Patterson AFB, OH 45433		12. REPORT DATE February 1985
		13. NUMBER OF PAGES 136
14. MONITORING AGENCY NAME & ADDRESS(if different from Controlling Office)		15. SECURITY CLASS. (of this report) Unclassified
		15a. DECLASSIFICATION/DOWNGRADING SCHEDULE

16. DISTRIBUTION STATEMENT (of this Report)

Approved for public release; distribution unlimited

17. DISTRIBUTION STATEMENT (of the abstract entered in Block 20, if different from Report)

18. SUPPLEMENTARY NOTES

19. KEY WORDS (Continue on reverse side if necessary and identify by block number)

digital flight control systems
w-transforms
hybrid frequency response
flexible vehicle control

large space structures
optimal control
comparisons of optimal and
classical control

20. ABSTRACT (Continue on reverse side if necessary and identify by block number)

This report presents methodologies for the direct digital control of vehicles with flexible modes. The techniques yield robust control system designs with modest or minimal requirements on the number of sensors and control actuators. The digital system techniques used include primarily the w-transform, for direct design and stability assessment, and the "hybrid" frequency response, for assessment and understanding of digital system peculiarities. The "sawtooth Bode" is used as the basic control system design concept. These three elements are
Continued

20. ABSTRACT

applied to several examples, including a comprehensive case study for a fighter aircraft flight and flexible mode control system. Both continuous and discrete system designs are considered and the continuous system characteristics are contrasted with an optimal control design. This comparison pinpoints some of the features needed to make optimal control procedures more practical and mature for flexible vehicle control applications. An important step is taken in this direction by determining the nature of performance criteria which yield, for an example case, a highly robust, extremely simple controller derived from an optimal control procedure.

FOREWORD

The research described in this report was performed by Systems Technology, Inc., Hawthorne, CA under Air Force Contract F33615-82-C-3614. The Task Number 2304N3, mathematics of flight control, was under project number 2304, mathematics. The work was directed by the Control Dynamics Branch, Flight Control Division, Flight Dynamics Laboratory, Air Force Wright Aeronautical Laboratories, Air Force Systems Command, Wright-Patterson Air Force Base, Ohio. The Air Force Technical Manager was Mr. David K. Bowser.

Richard F. Whitbeck and Duane McRuer were the Systems Technology, Inc. Project Engineers and Principal Investigators. The STI Technical Director was Duane McRuer.

This report covers work performed from July 1982 through September 1984. The report was submitted by the authors in September 1984.

DTIC
ELECTE
SEP 3 1985
B

A-1

iii

TABLE OF CONTENTS

LIST OF FIGURES

Page

LIST OF TABLES

SECTION I

INTRODUCTION

Current trends in aircraft and space vehicle structural design have significantly increased the possibility for interaction between flight control and structural characteristics. In aircraft, to achieve the full benefits of possible drag and weight reduction, the vehicle may be designed for normal operation around neutral or negatively stable c.g. locations with active control systems to stabilize the rigid body modes. Because the basic (unaugmented) aircraft can be divergent, the closed-loop system will have a minimum bandwidth requirement which can be greater, whe adequate margins are provided, than the bandwidth needed to augment a stable aircraft. This is all too likely to intrude on the lower frequency flexible modes, with effects which must be considered in the control system design. The flexible modes can either be stabilized or have their effects on the system reduced by appropriate filtering. Because low frequency effective lags are minimized, direct stabilization of the lower frequency flexible modes is often a superior strategy in contrast to signal suppression via notch or low pass filters. In other cases direct control of the flexible modes is essential, as in the direct reduction of wing root bending moment by control of aircraft wing bending modes, or the alleviation of flutter characteristics by active stabilization. Similarly in space vehicles, structures are projected which have very large physical dimensions, light damping, and low rigidity. Such systems inherently possess many degrees of freedom, some characterized by eigenvalues of low frequency and damping which may also be highly cross-coupled. There can be an overlap of the body and bending modal frequencies, requiring explicit consideration of the bending modes in the control system synthesis.

From the standpoint of the flight control system designer the status of the vehicle's flexible characteristics has fundamentally changed. Previously these high frequency properties were ordinarily nuisances to be countered by notch or low pass filtering. While these techniques are still valuable for some modern and future craft, the flexible properties

1

of the vehicle will be central issues in most new designs. In these cases the object will be to actively intervene with the flexible modes using control techniques. Another technology trend is in the control apparatus, which has become dominantly discrete or digital in character in recent years. Digital systems are now commonplace in flight control although most of the applications have not yet had to cope in a significant way with direct control of flexible modes. Instead most of the systems have again relied on the equivalent of low pass or notch filtering and antialiasing filtering to reduce the impact of any flexible mode effects on the primarily rigid body flight control system.

Following these trends in vehicle dynamics and controller technology the study reported here is primarily concerned with the direct digital control of highly elastic vehicles, including the exertion of positive influences on the elastic modes themselves. The approach that is taken in most of the report is to carefully select existing theory and well-proven flexible vehicle control concepts. The case study method will be used throughout to illustrate the applications. They are arranged in order of increasing complexity, ending finally with a relatively complete design study of a digital automatic flight control system for flexible and rigid body control of a fighter aircraft.

The next section of this report reviews the principal analytical tools to be used for digital design. These are the w-domain transfer function for direct digital analysis stability assessment; the "hybrid" frequency response for response assessment and indication of digital system peculiarities; and the "sawtooth Bode" as the key control system design concept.

Section III provides a detailed case study illustrating the hybrid frequency response. Some of the peculiar features of digital, as contrasted with continuous, control systems are revealed in a clear cut way in this example.

Section IV presents two control system design examples for rigid body and flexible control of a typical fighter aircraft. The aircraft control problems are initially addressed with a continuous control system design. Topics such as the control system feedback loop architecture, the most favorable control loops, sensitivity and robustness

2

considerations, and the closed-loop system design assessment are addressed. Then the design is redone using the discrete systems analysis tools. The overall feedback control architecture is the same as in the continuous system since this is appropriate from the standpoint of the basic physics of the aircraft and flexible mode control tasks. The digital design is conducted first with a w-domain transfer function treatment which emphasizes the effects of sampling rate. Stability properties are explored both in the w and z-domain. Then the hybrid frequency response is examined over a wide range of sampling conditions.

Section V brings in the subject of optimal control. In the first article the flight control system design of Section IV is contrasted with a previously accomplished set of optimal control designs for the same vehicle. This comparison leads to many insights, such as the much simpler, generally superior, and more practical features of the conventionally designed system over the optimal version. This reflects the relative maturity of the two techniques and is particularly useful in illuminating some of the problems which optimal formulations must overcome to result in practical systems. The latter portion of this section is an attempt to overcome some of the difficulties encountered with optimal control approaches for flexible structures. An extensive literature shows that continuous or discrete regulators based on quadratic indices and/or maximum likelihood estimators often lead to controller transfer functions which are not only equal to the order of the system being controlled but are also sometimes unstable and very often non-minimum phase. Thus optimal controllers for flexible vehicles are inherently very sensitive to both the modelling process and demand a precise knowledge of the vehicle parameters. We illustrate by a simple example that the control system complexity, e.g., the feedback of all significant state vector components, can be somewhat relieved by using physical rather than generalized coordinates. The tendency for optimal approaches to yield nonrobust and occasionally nonminimum phase controllers is more troublesome. By another example we are able to show that the adoption of an unusual optimal control performance index will yield an extraordinarily robust and simple control system akin to those illustrated earlier using the more conventional procedures.

3

SECTION II

REVIEW OF ANALYTICAL AND CONCEPTUAL PRELIMINARIES

This study is primarily concerned with digital control systems for flexible vehicles. The focus is on the application of existing discrete systems analysis techniques and flexible vehicle control concepts rather than the development of new theory. The bulk of the report is made up of examples which illustrate behavioral features of digital controllers as applied to flexible vehicles. So that the details of the examples can be easily followed we will present, in this section, reviews of pertinent sampled data system analysis and flexible mode control concepts. These will include:

- w-domain transfer functions as the primary tool for direct digital design and stability;

- the "hybrid" or "complete" frequency response as the primary tool for response assessment and understanding;

- the "sawtooth Bode" as the key to establishing "phase stabilized" control systems for flexible vehicles.

These topics will be treated in the above sequence in the following articles.

A. THE w-DOMAIN

1. s, z, and w Transforms

The use of discrete (digital) flight controllers makes the augmented aircraft a sampled data system, that is, a discretely controlled continuous system. The analysis and design of such systems requires procedures and tools beyond those of continuous feedback control system design. Since the late 1940's much work has been done in this area and a wide range of methods for analysis and synthesis of sampled data systems are available. This includes z- and w- transform techniques,

and procedures for multi-rate systems (e.g., Refs. 1-4). Because our focus is on the special class of controllers appropriate to flexible aircraft flight control system design, there are methods and approaches that are of principal interest and value. These particular sampled data methods were selected because of their power in connecting peculiarities introduced by the digital features to the well understood dynamics of the aircraft. This is especially desirable because of two considerations. The first appears naturally in FCS development simulations, where digital controllers are being assessed with simulated aircraft dynamics. Most simulation laboratories have now been converted to digital computers, so the continuous aircraft dynamics are conventionally simulated as "digital" aircraft. Because of the complexity of complete aircraft equations, simulation up-date rates for the vehicle are often quite low when compared with those of the controller. Consequently, the dominant "digital system" in a simulation may be the aircraft itself! The second consideration is the ever present concern with achieving good flying qualities. The FCS designer needs sampled data analysis tools which are not only good computational algorithms but which can aid in dealing with the impact of the digital controller on flight control system simulation and flying qualities issues which are often more qualitative than quantitative. To this end one of the more important uses of a digital analysis method is to aid in the interpretation of AFCS simulations and of pilot ratings in simulations or flight tests. Consequently discrete systems analysis techniques which parallel familiar continuous procedures to the maximum extent are most desirable.

The behavioral complexities introduced by discrete controllers arise from the implementation of the control laws as difference equations in the flight control computer and through the sampler and data hold elements required at the analog/digital interfaces. Thus for linear transform analysis the Laplace transforms of the continuous case become pulse transforms for the sampled data aircraft. A logical point of departure is to consider how the sampling operation may be analyzed. Figure 1a indicates the action of the sampler idealized as a switch which closes for an instant every T seconds. When the continuous function of time

5

f(t) shown at the left in Fig. 1b is sampled a time series represented by the points at T intervals, as shown on the right side of Fig. 1b, is generated. The information in this time series can conveniently be represented by a discrete function $f^T(t)$ which is related to the continuous function f(t) by

$$f^T(t) = f(0)\delta(t) + f(T)\delta(t - T) + f(2T)\delta(t - 2T) + \ldots \quad (1)$$

$$= \sum_{n=0}^{\infty} f(nT)\delta(t - nT)$$

where δ is the Dirac delta (or unit impulse) function and the superscript T notation indicates that f(t) is sampled every T seconds. The impulse train serves to establish the sampling times for the time series, while the area of a particular impulse sets the time series' value at that instant. Sampling may thus be viewed as impulse (amplitude) modulation, i.e., $f^T(t)$ is produced by modulating a train of unit impulses with f(t) as indicated in Fig. 1c.

The sampled signal may be Laplace transformed (Ref. 1) to give

$$F^T(s) \equiv \mathcal{L}\left[f^T(t)\right] = \sum_{n=0}^{\infty} f(nT)e^{-snT} \quad (2)$$

This does not lead immediately to a transfer-function-like quantity because Eq. 2 is not a rational polynominal but rather is transcendental in s. The traditional solution to this problem has been the use of the z-transform. This is accomplished by mapping the complex variable s into the complex variable z according to

$$z = e^{sT} \quad (3)$$

6
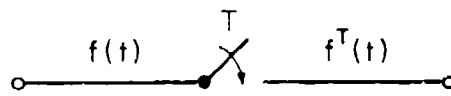
(a)
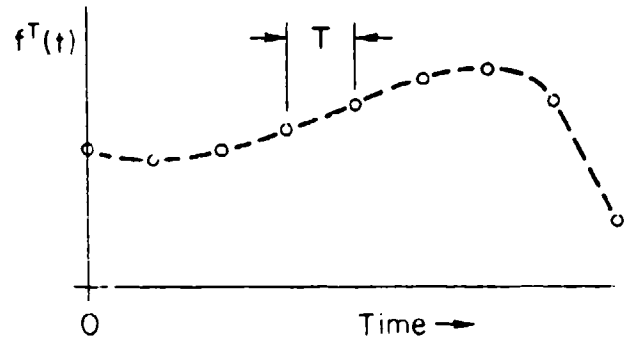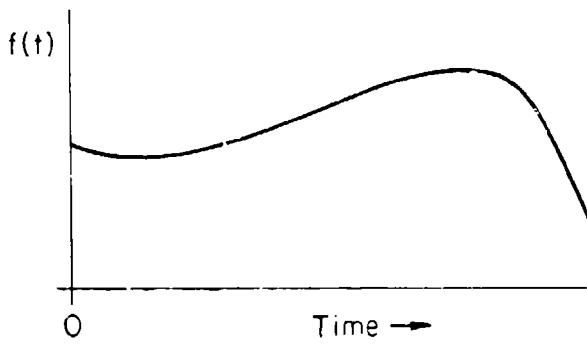
(b)
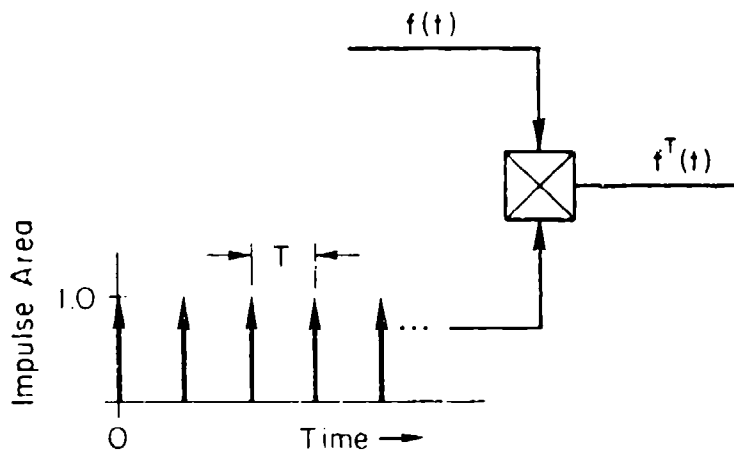
(c)

Figure 1.   The Idealized Sampler

The z-transform, $Z[f^T(t)]$, is then defined as the transformation which maps a time domain function (the sequence $f^T(t)$) into a complex valued function $F(z)$, of the complex variable z, according to

$$F(z) = Z[f^T(t)]$$

$$\equiv \sum_{n=0}^{\infty} f(nT)z^{-n} \qquad (4)$$

$$= \left[F^T(s)\right]_{e^{sT}=z}$$

z-transforms can be expressed as rational polynomials (and thus as poles and zeros) in the z-domain. For example consider $f(t) = e^{-at}$,

$$F(z) = \sum_{n=0}^{\infty} e^{-anT} z^{-n}$$

$$= 1 + e^{-aT} z^{-1} + e^{-2aT} z^{-2} + \ldots \qquad (5)$$

$$\equiv 1 + \left(\frac{e^{-aT}}{z}\right) + \left(\frac{e^{-aT}}{z}\right)^2 + \ldots$$

$$= \frac{1}{1 - \left(e^{-aT}/z\right)} = \frac{z}{z - e^{-aT}}$$

While the z-transform method is quite usable from a purely computational standpoint, it has certain disadvantages for aircraft FCS design. The s-plane is distorted by the $z = e^{sT}$ mapping as shown in Fig. 2. The unit circle replaces the imaginary axis as the stability boundary and in large order systems poles tend to cluster near this circle, giving the designer very little insight about degree of stability. Simple boundary contours of ω_n, ζ, etc., in the s-plane are quite distorted in the z-plane, which means that familiar flight control system and flying qualities specifications (e.g., those of the MIL-Specs) must be transformed and reinterpreted.
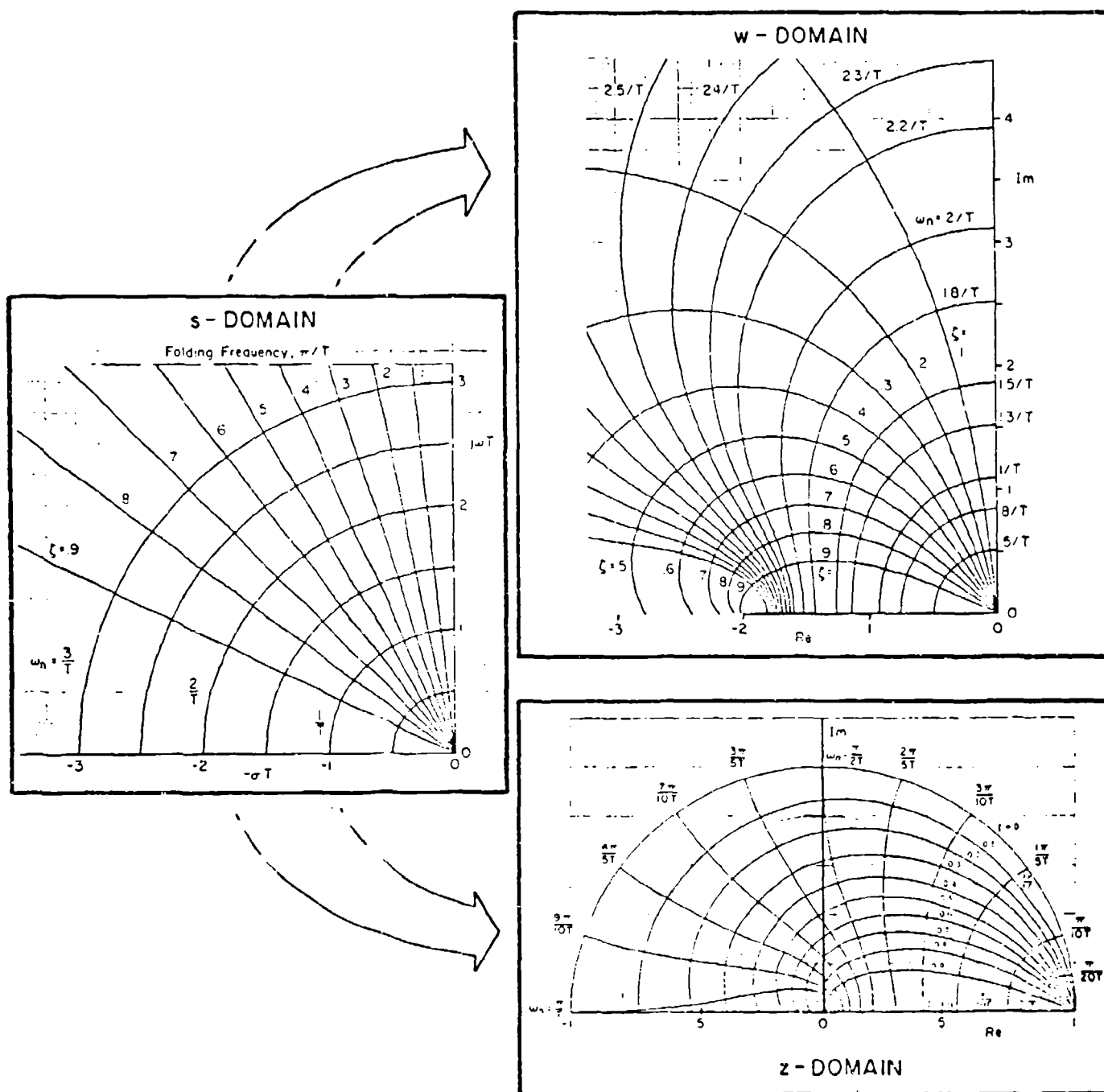
Figure 2.   Mapping s-Domain Contours into the z- and w-Domains

9

A much more serious objection to the z-transform is the loss of immediate connections between the z-domain poles and zeros and the aircraft configuration parameters -- stability derivatives. For many applications of digital control to complex plants the designer may not have a well developed physical insight for the plant, but the aircraft FCS dynamicist evolves a FCS design based on an intimate understanding of the aircraft-alone poles and zeros and the factors which influence them. For instance, the physical insights and literal approximate factors which derive from the s-domain Bode magnitude asymptotes are especially valuable, yet are not available in the z-domain. Fortunately most of these objections can be eliminated by using the w-transform instead of the z-transform for sampled data analysis.

The complex variable w can be developed from the complex variable z through the bilinear transform,

$$w = \frac{2}{T} \left(\frac{z - 1}{z + 1} \right) \tag{6}$$

z is also a bilinear transform of w, i.e.,

$$z = - \frac{w + 2/T}{w - 2/T} \tag{7}$$

w can also be determined directly from s by noting

$$w = \frac{2}{T} \left(\frac{z - 1}{z + 1} \right) = \frac{2}{T} \frac{e^{sT} - 1}{e^{sT} + 1} \tag{8}$$

$$= \frac{2}{T} \tanh \frac{Ts}{2}$$

The mapping of s into either the z or w domain is illustrated in Fig. 2. These transformation diagrams are given with a larger scale in Appendix B.

The w-transform, $W[f^T(t)]$, is defined as the transformation which maps the sequence $f^T(t)$ into a complex valued function $F(w)$ of the complex variable w according to

$$F(w) = W[f^T(t)]$$

$$\equiv \sum_{n=0}^{\infty} f(nT) \left(\frac{1 + Tw/2}{1 - Tw/2}\right)^{-n} \tag{9}$$

$$= \left[F(z)\right]_{z = -\frac{w + 2/T}{w - 2/T}}$$

The last expression in Eq. 9 provides a practical way of obtaining the w-transform if the z-transform is available (say from a z-transform table) by using Eq. 7 to replace the z's with w's.

The correspondence between a given $F(s)$ and its $F(z)$ equivalent can be summarized in convenient transform tables (e.g., Ref. 1). The first two columns of Table 1 provide a rudimentary version of such a table. If a transfer function $G(s)$ is isolated by samplers as shown in Fig. 3a, then $G(z)$ can be found either directly or via partial fraction expansion from the elemental forms of $G(s)$ given in Table 1.

In practical systems the continuous elements are not subjected to impulse train inputs. Instead a data hold of some type is present, as shown in Fig. 3b. The data hold is a physical device which takes the input signal samples, R^T, and constructs a continuous signal which then forces the continuous system represented by $G(s)$. It is a coupler between discrete and continuous system elements, and typically includes digital to analog conversion. When this coupler is a zero-order hold, its transfer function (see Fig. 3c) is,

$$M_0(s) = \frac{1 - e^{-sT}}{s} \tag{10}$$

The presence of the hold will modify the z transform of interest. Consider the earlier example where $f(t) = ae^{-at}$. If this is presumed to

TABLE 1. AN ABBREVIATED TRANSFORM TABLE.

s-PLANE	z-PLANE	z-PLANE (ZOH)	w-PLANE (ZOH)
$\dfrac{1}{s}$	$\dfrac{z}{z-1}$	$\dfrac{T}{z-1}$	$\dfrac{-\frac{T}{2}w+1}{w}$
$\dfrac{1}{s^2}$	$\dfrac{Tz}{(z-1)^2}$	$\dfrac{T^2}{2}\dfrac{(z+1)}{(z-1)^2}$	$\dfrac{-\frac{T}{2}w+1}{w^2}$
$\dfrac{1}{s^3}$	$\dfrac{T^2 z(z+1)}{2(z-1)^3}$	$\dfrac{T^3}{6}\dfrac{(z^2+4z+1)}{(z-1)^3}$	$\dfrac{(-\frac{T}{2}w+1)(-\frac{T}{\sqrt{12}}w+1)(\frac{T}{\sqrt{12}}w+1)}{w^3}$
$\dfrac{a}{s+a}$	$\dfrac{az}{z-e^{-aT}}$	$\dfrac{1-e^{-aT}}{z-e^{-aT}}$	$\dfrac{2}{T}\left[\dfrac{(1-e^{-aT})}{(1+e^{-aT})}\right](-\frac{T}{2}w+1)}{w+\frac{2}{T}\left[\dfrac{(1-e^{-aT})}{(1+e^{-aT})}\right]}$
$\dfrac{b}{s^2+b^2}$	$\dfrac{zS}{z^2-(2C)z+1}$	$\dfrac{\frac{(1-C)}{b}(z+1)}{z^2-(2C)z+1}$	$\dfrac{\frac{4}{T^2}\left[\frac{1-C}{b(1+C)}\right](-\frac{T}{2}w+1)}{w^2+\frac{4}{T^2}\left[\frac{1-C}{1+C}\right]}$
$\dfrac{s}{s^2+b^2}$	$\dfrac{z(z-C)}{z^2-(2C)z+1}$	$\dfrac{(\frac{S}{b})(z-1)}{z^2-(2C)z+1}$	$\dfrac{\frac{2}{T}\left[\frac{S}{b(1+C)}\right](w)(-\frac{T}{2}w+1)}{w^2+\frac{4}{T^2}\left[\frac{1-C}{1+C}\right]}$
$\dfrac{b}{(s+a)^2+b^2}$	$\dfrac{ze^{-aT}S}{z^2-(2e^{-aT}C)z+e^{-2aT}}$	$\dfrac{\frac{b-e^{-aT}(aS+bC)}{a^2+b^2}z+\frac{be^{-2aT}-e^{-aT}(bC-aS)}{a^2+b^2}}{z^2-(2e^{-aT}C)z+e^{-2aT}}$	$\dfrac{\frac{2}{T}\left[\frac{b(1-e^{-2aT})-2bSe^{-aT}}{(a^2+b^2)(1+2e^{-aT}C+e^{-2aT})}\right]\left(w+\frac{2}{T}\left[\frac{b(1+e^{-2aT})-2bCe^{-aT}}{b(1-e^{-2aT})-2bSe^{-aT}}\right]\right)(-\frac{T}{2}w+1)}{w^2+\frac{4}{T}\left[\frac{1-2e^{-aT}C+e^{-2aT}}{1+2e^{-aT}C+e^{-2aT}}\right]}$
$\dfrac{s+a}{(s+a)^2+b^2}$	$\dfrac{z(z-e^{-aT}C)}{z^2-(2e^{-aT}C)z+e^{-2aT}}$	$\dfrac{\frac{a+e^{-aT}(bS-aC)}{a^2+b^2}z+\frac{ae^{-2aT}-e^{-aT}(bS+aC)}{a^2+b^2}}{z^2-(2e^{-aT}C)z+e^{-2aT}}$	$\dfrac{\frac{2}{T}\left[\frac{a(1-e^{-2aT})+2bSe^{-aT}}{(a^2+b^2)(1+2e^{-aT}C+e^{-2aT})}\right]\left(w+\frac{2}{T}\left[\frac{a(1+e^{-2aT})-2aCe^{-aT}+2bSe^{-aT}}{a(1-e^{-2aT})+2bSe^{-aT}}\right]\right)(-\frac{T}{2}w+1)}{w^2+\frac{4}{T}\left[\frac{1-2e^{-aT}C+e^{-2aT}}{1+2e^{-aT}C+e^{-2aT}}\right]}$

$S = \sin bT$

$C = \cos bT$
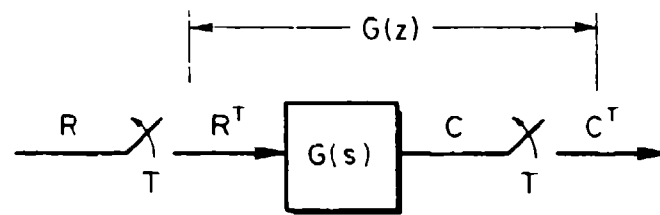
a) Correspondence Between Continuous and Pulse Transfer Functions
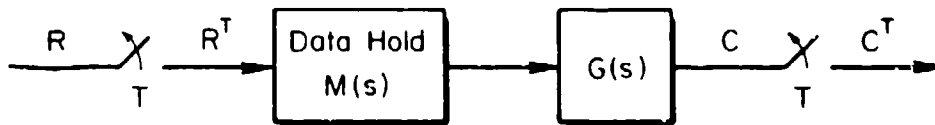
b) Sampled System With Data Hold
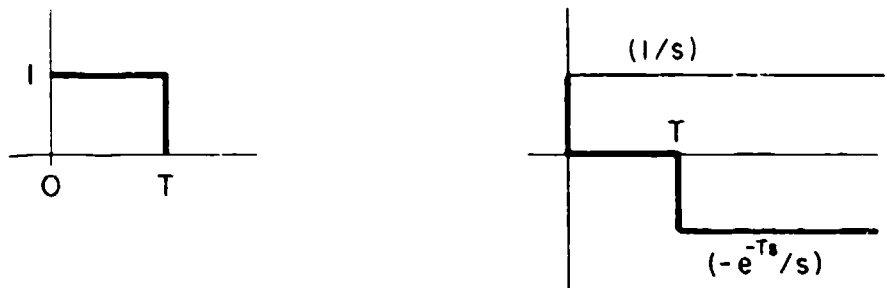
c) Impulse Response of Zero-Order Data Hold

Figure 3. Sampling and Zero Order Hold Operations

be the impulse response of a system element having a transfer function $G(s)$, then

$$G(s) = \frac{a}{s + a} \qquad (11)$$

As developed in Eq. 5 and shown in the fourth row, second column of Table 1 the z-transform is

$$G(z) = \frac{az}{z - e^{-aT}}$$

When the data hold is included

$$G(s) M(s) = \frac{a(1 - e^{-sT})}{s(s + a)} \qquad (12)$$

The z transform of this is

$$[GM]^T = \left[\frac{a(1 - e^{-sT})}{s(s + a)}\right]^T$$

$$\qquad (13)$$

$$= \left[(1 - e^{-sT}) \left(\frac{1}{s} - \frac{1}{s + a}\right)\right]^T$$

The factor $(1 - e^{-sT}) \equiv (z - 1)/z$, and is unaffected by the sampling operator, so

$$[GM]^T = \left(\frac{z - 1}{z}\right) \left[\frac{1}{s} - \frac{1}{s + a}\right]^T$$

$$= \left(\frac{z - 1}{z}\right) \left(\frac{z}{z - 1} - \frac{z}{z - e^{-aT}}\right) \qquad (14)$$

$$= \frac{(1 - e^{-aT})}{z - e^{-aT}}$$

This result corresponds to the "z-plane (ZOH)" entry in the third column of Table 1. The entries in this column are converted to the w transform

14

form, in the fourth column, using Eq. 9. In its now complete form, Table 1 illustrates several examples of the connection between s, z, and w-domain transfer functions. A key point to notice there is that the w transforms, when viewed as transfer function-like entities, all exhibit a right-half plane zero at $w = 2/T$. This, of course, stems from the sample and hold. When loops are closed around w transfer functions this zero has the expected but unfortunate property of drawing the loci from some system pole(s) toward or into the unstable region.

The three great appeals of the w-domain are:

- Stability boundaries are again associated with the entire left half plane rather than the unit circle.

- w approaches s as the sampling interval approaches zero, i.e.,

$$w = \frac{2}{T} \tanh \frac{Ts}{2}$$

$$\rightarrow \frac{2}{T} \left[\frac{Ts}{2} - \frac{1}{3} \left(\frac{Ts}{2} \right)^3 + \frac{2}{15} \left(\frac{Ts}{2} \right)^5 - \ldots \right] \tag{15}$$

$$\rightarrow s, \text{ as } T \rightarrow 0$$

- The poles and zeros in the w-domain are very close to those in the s-domain for poles or zeros which have magnitudes much less than $2/T$.

As an example of the last point consider the first-order lag $a/(s + a)$ plus zero-order hold as converted to the w-domain.

$$\frac{a}{s + a} \quad \longrightarrow \quad \frac{\frac{2}{T} \left(\frac{1 - e^{-aT}}{1 + e^{-aT}} \right) \left(1 - \frac{Tw}{2} \right)}{w + \frac{2}{T} \left(\frac{1 - e^{-aT}}{1 + e^{-aT}} \right)}$$

$$= \frac{a' \left(1 - \frac{Tw}{2} \right)}{w + a'}$$

where $a' = (2/T)(1 - e^{-aT})/(1 + e^{-aT}) = (2/T) \tanh (aT/2)$. Using the hyperbolic tangent series expansion the value of a' becomes,

$$a' = a\left[1 - \frac{1}{3}\left(\frac{aT}{2}\right)^2 + \frac{2}{15}\left(\frac{aT}{2}\right)^4 - \ldots\right]$$

For sampling rates which are high relative to the s-plane pole magnitude a, i.e., for aT/2 << 1, a' is very close to a and the s-plane pole at s = -a is an excellent approximation to the w-plane pole at w = -a'. At lower rates (or larger values of "a") the effect of sampling is to reduce the magnitude a' of the w-plane pole relative to the s-plane pole magnitude, a. The close connection between w and s poles and zeros which are much less than 2/T in magnitude, and the "distortion" for other conditions can be seen in Fig. 2. Here ζ and ω_n contours mapped into the w-domain are only slightly distorted near the origin (e.g., below 1/T).

As a consequence of these features, many continuous system design procedures and representations can be carried over into the digital world. Bode diagrams, conventional and Bode root loci, transfer-function based multiloop analysis procedures, and many rules of thumb will all work well using w as the complex variable in place of s.

If these concepts are now applied to FCS analysis considerations the first-order effect of sampling is to introduce the rhp numerator zero at 2/T, while the second-order effects are to change the magnitude of the poles and zeros in the w transfer functions from those of the s-domain transfer function. Ordinarily the FCS sampling rate will be large relative to the FCS frequencies of interest (except, perhaps, for flexible modes) so the addition of a zero at w = +2/T to the regular continuous transfer functions with w substituted for s will often provide an adequate approximation for FCS stability and dominant mode response purposes. When higher frequency modes impinge on the sampling region these approximations no longer apply and the more exact w-domain poles and zeros must be used.

16

With the high sample rates of next generation digital FCS for manned aircraft the sampling effects noted above are not as likely to cause trouble on the actual aircraft as they are earlier in the simulation phase of development. There are particular concerns with closed-loop man-in-the-loop simulation with actual hardware. In a typical simulation the aircraft characteristics may be programmed onto a digital computer which may also run a moving-base apparatus and parts of a visual display attachment. As already mentioned the mathematical models of the vehicle may be very complex and include many nonlinear characteristics, lots of lookup tables, and so forth. The result often is a simulation which represents a continuous airframe by a fundamentally digital characterization with relatively low update rates. Now, when an actual digital flight controller with a frame rate of 80-100/s is used in conjunction with a 20/s digital simulation of a continuous airplane, the simulated stability and control properties of the aircraft will suffer phasing and timing shifts. If these "digital airplane" effects are not properly accounted for the basic aircraft/augmenter system ay exhibit difficulties which are really only imaginary. There have been times when the actual airplane was needed to fully appreciate the FCS capabilities!

2. An Elementary Roll Control System Example

To illustrate some of the features of the w-domain analysis procedures we will consider the elementary roll controller shown in Fig. 4a as an example. The actuator and sensor dynamics are assumed to be negligible, and the aircraft is represented by an idealized ϕ/δ_a transfer function in which the spiral mode is neutral, the quadratic numerator term cancels the Dutch roll denominator term, and the roll subsidence time constant, T_R, equals $1/a$. The flight control computer, actuator, and other elements comprise a gain, sampler, and first-order hold.
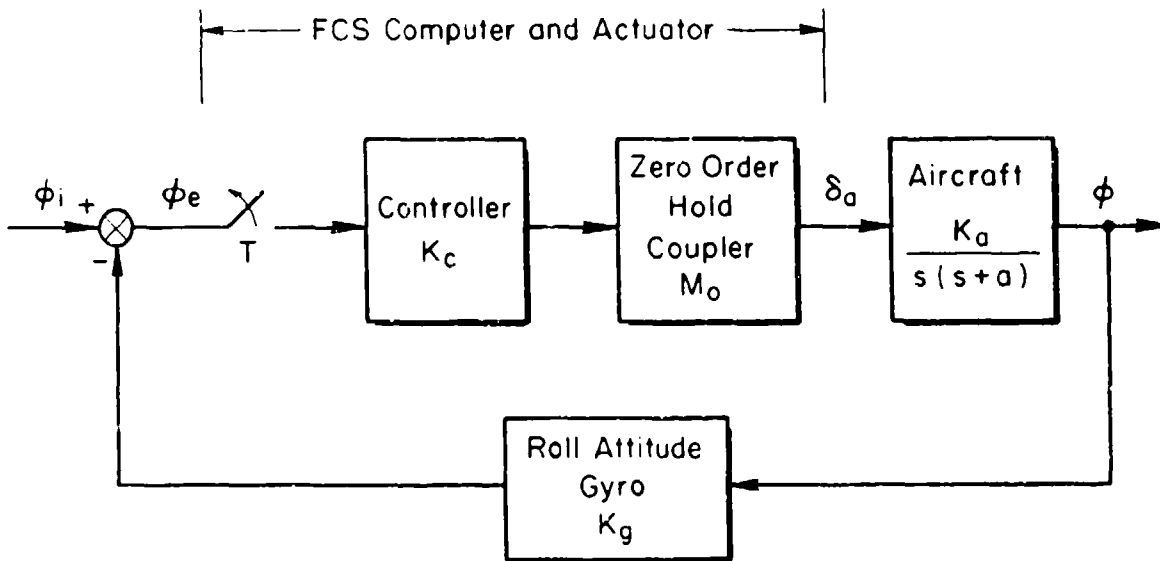
a) Elementary Roll Control System
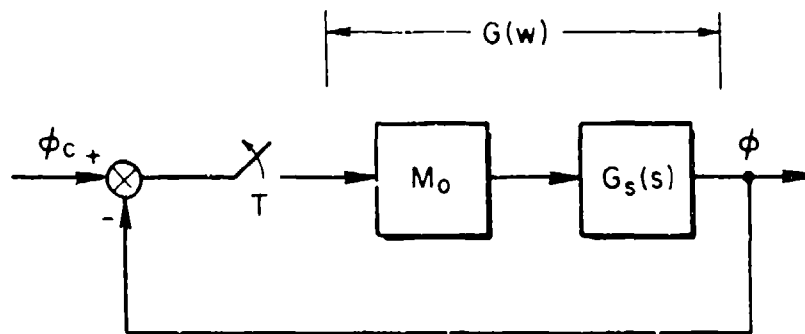
$$G_s(s) = \frac{K}{s(s+a)} \quad ; \quad K = K_c K_a K_g \quad ; \quad \phi_c = \frac{\phi_i}{K_g}$$

b) Simplified System

Figure 4. Elementary Roll Control System Example

18

a. Open-Loop Transfer Function Characteristics

When the system is presented in its simplest terms it appears as Fig. 4b. The effective open-loop system s-domain transfer function is,

$$G_8(s) = \frac{K}{s\,(s + a)}$$

(16)

$$= \frac{K}{a}\left(\frac{1}{s} - \frac{1}{s + a}\right)$$

This does not include the zero-order hold because the conversion from the s to the w-domain will be accomplished using Table 1 which takes this into account. The partial fraction form of Eq. 16, and the entries of column 4, rows 1 and 4 of Table 1 yields the w-domain transfer function which, after some manipulation, becomes

$$G(w) = \frac{(K/a)\left[w\left(1 - \frac{2}{aT}\tanh\frac{aT}{2}\right) + \frac{2}{T}\tanh\frac{aT}{2}\right]\left(-\frac{T}{2}w + 1\right)}{w\left(w + \frac{2}{T}\tanh\frac{aT}{2}\right)}$$

(17)

$$= \frac{K/a\left[w\left(1 - (\tanh u)/u\right) + a\,(\tanh u)/u\right]\left(-\frac{T}{2}w + 1\right)}{w\left(w + a\,(\tanh u)/u\right)}$$

where $aT/2 \equiv u$. When viewed as an open-loop transfer function analogous to $G_8(s)$, the major effects of the sampling and hold exhibited in $G(w)$ are

- A right half plane zero at $2/T$ is introduced;

- A second zero, $-z_1$, is also introduced, resulting in a transfer function numerator which is the same order in w as the denominator;

- A sampling effect scaling parameter, $u = aT/2$, appears and affects the system's poles and zeros.

The first point was anticipated from the development of the w-transform with zero-order hold. The second point is typical of G(w) transfer functions which can be considered to be generalizations of the continuous system transfer functions. The additional zeros introduced by the sample and hold operations tend towards infinity as the sampling interval approaches zero.

Both the second and third features are made even more evident if the w-domain pole, -a (tanh u)/u, is called -a'. Then G(w) becomes,

$$G(w) = \frac{(K/a) \left[w \left(1 - a'/a\right) + a'\right] \left(-\frac{T}{2} w + 1\right)}{w \left(w + a'\right)}$$

$$= - \left[\frac{K}{a^2} u \left(1 - \frac{a'}{a}\right)\right] \frac{(w + z_1) (w - 2/T)}{w (w + a')}$$

(18)

where

$$z_1/a = \frac{a'/a}{1 - a'/a} = \frac{(\tanh u)/u}{1 - [(\tanh u)/u]}$$

The relative "pole-zero" orders are such that $z_1 > 2/T > a'$. Considered as an open-loop transfer function analogous to $G_e(s)$, the very-low "frequency" gain [sometimes called the Bode gain], is K/a for both G(s) and G(w). The very-high "frequency", or root-locus, gains are quite different, being simply K for the continuous domain, and

$$- \frac{K}{a^2} u \left(1 - \frac{a'}{a}\right) = - \frac{KT}{2a} \left(1 - \frac{\tanh u}{u}\right)$$

(19)

for the w domain.

The variations of the normalized magnitudes of the poles and zeros with the normalized sampling interval (aT/2) for the G(w) transfer function are shown in Fig. 5. Note that the open-loop pole is shifted less than 10 percent even when the sampling rate in hertz (1/T) is equal to

20
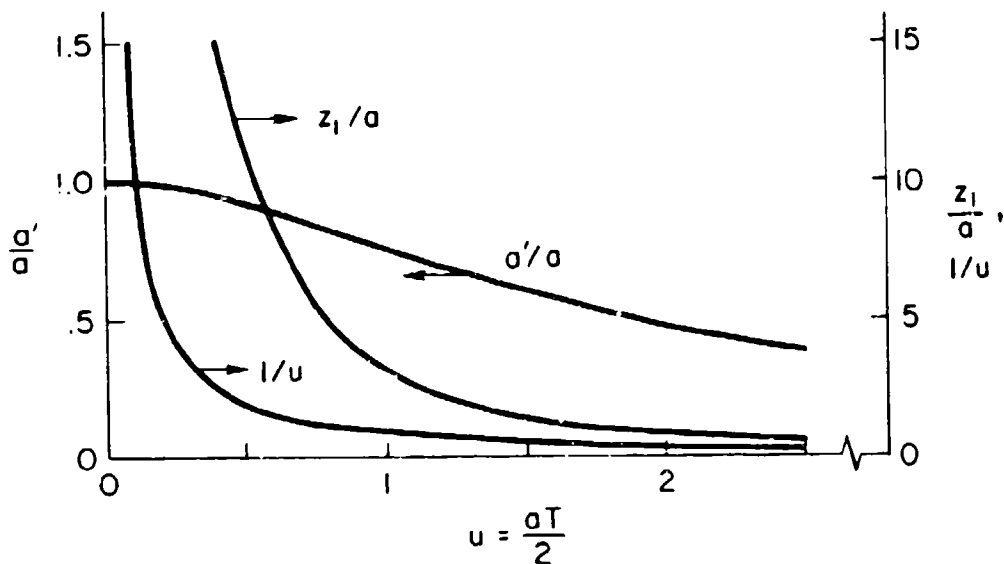
Figure 5. Variation of Open-Loop Poles and Zeros
with Normalized Sampling Interval

the magnitude of the pole (i.e., at $u = aT/2 = 1/2$). At this same normalized sampling frequency the high "frequency" minimum phase zero, $-z_1/a > 11$. So these two quantities are not shifted, in a practical sense, very far from their continuous values at this quite low sampling frequency. The non-minimum phase zero at $2/T$, on the other hand, is very much in the picture at this value of u, and will have a major impact on the closed-loop system properties.

b. **System Stability**

Because the left-half of the w-plane corresponds to stability the closed-loop characteristic equation, $1 + G(w) = 0$, can be examined for stability just as for the continuous case. Forming $1 + G(w)$,

$$G(w) + 1 = Aw^2 + Bw + C = 0 \tag{20}$$

21

where,

$$A = 1 - \frac{KT}{2a} \left(1 - \frac{a'}{a}\right) = 1 + \frac{KT}{2a} \left(\frac{\tanh u}{u} - 1\right)$$

$$B = \left(a' + \frac{K}{a}\right) - \frac{K}{a} \frac{a'}{a} \left(1 + \frac{aT}{2}\right)$$

$$= a \frac{\tanh u}{u} + \frac{K}{a} \left[1 - \frac{\tanh u}{u} \left(1 + u\right)\right]$$

(21)

$$C = K \frac{a'}{a} = K \frac{\tanh u}{u}$$

The coefficient C is always positive for a stable continuous system, for which the only criterion is $K > 0$ (assuming the roll subsidence inverse time constant, "a", is positive). The leading coefficient, A, approaches 1 as the sampling rate approaches infinity, so A is positive for high sampling rates. A transition from $A > 0$ to $A < 0$ will occur when,

$$1 + \frac{KT}{2a} \left(\frac{a'}{a}\right) = \frac{KT}{2a}$$

(22)

A will be zero when

$$\frac{a^2}{K} = u - \tanh u$$

(23)

An instability criterion based on A changing from positive to negative then becomes

$$\frac{K}{a^2} > \frac{1}{u - \tanh u}$$

(24)

This criterion is shown as a stability boundary in Fig. 6.

22
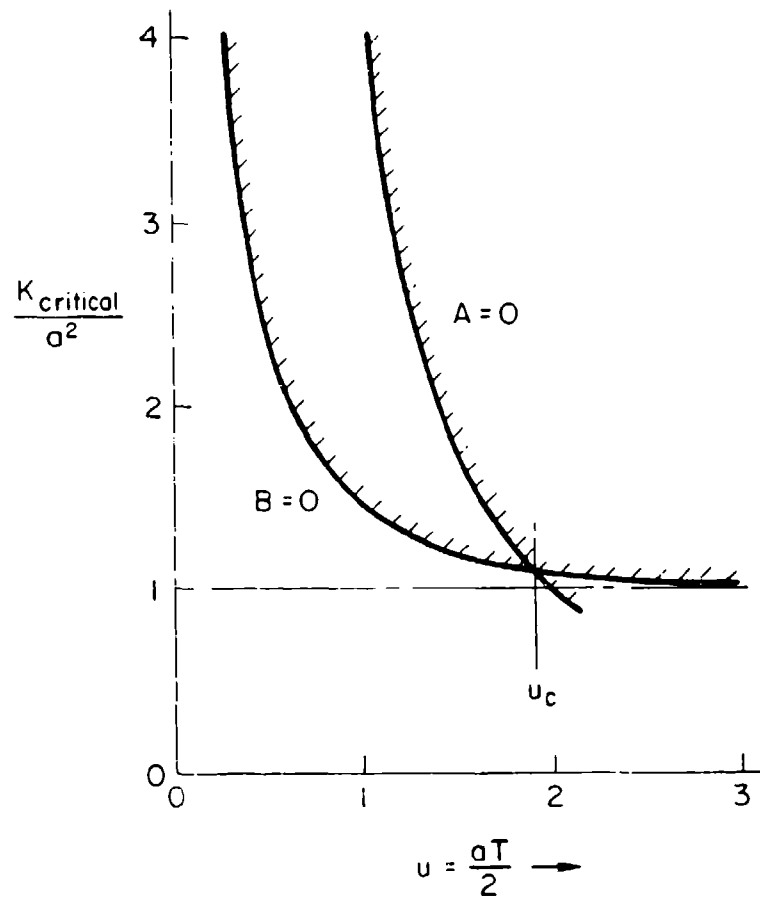
Figure 6. Stability Boundaries

Another stability boundary can be found by determining when the "closed-loop w-plane damping" coefficient, B, becomes zero. This is given by

$$\frac{K}{a^2} = \frac{\tanh u}{(1 + u) \tanh u - u} \tag{25}$$

This boundary is also shown on Fig. 6. The two boundaries intersect when the normalized sampling parameter $u = u_c$.

When u is less than u_c, the governing stability boundary is given by B = 0. Then any instability will show up as a negatively damped quadratic in the w-plane. A root locus sketch showing this situation is

23

given in Fig. 7b. Because the B = 0 boundary is asymptotic to 1, in this case any gain less than $K/a^2 = 1+$ will result in a stable system without further conditions.

When the normalized sampling interval is $u > u_c$, the governing stability criterion will be A = 0. The critical value of u will occur at the transitional condition where A = B. This can be shown to be

$$\tanh^2 u + \tanh u - u = 0 \tag{26}$$

Solving Eq. 26, the critical value for u is

$$u_c \doteq 1.860 \tag{27}$$

When the A = 0 boundary applies the instability is indicated by a closed-loop right half w-plane real root. This can occur at relatively low values of gain. In fact, as can be seen by examining Fig. 6, gains for instability corresponding to the A = 0 boundary will ordinarily be $K/a^2 < 1+$.

The same transitional conditions can be interpreted using the w-plane root loci. These start from the w-plane open-loop poles at zero and $-a'$. The zeros at $2/T$ and $-z_1$ (as well as the pole at $-a'$) depend on the normalized sampling parameter, u. When u is such that the constellation is as shown in Fig. 7c, there is a perfectly balanced symmetry among the poles and zeros. For this case as gain is increased from zero the closed-loop poles will progress from the two poles towards each other, rendezvous, and proceed along a straight line parallel to the imaginary axis. At the transitional gain, corresponding to the A = B point in Fig. 6, the closed-loop poles are at infinity, where they split into two real roots. Then at higher gains still these real roots will drive from plus and minus infinity along the positive and negative real axes towards the zeros.
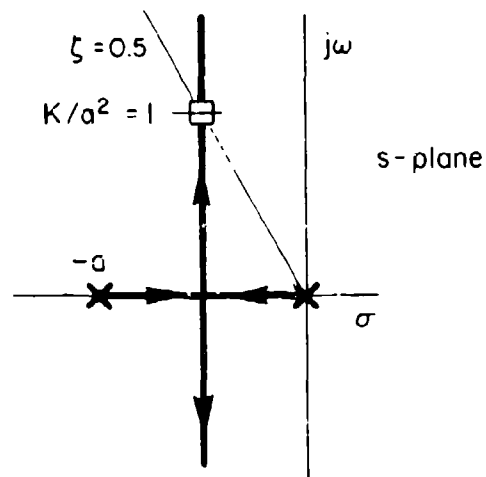
a) s-plane Root Locus for $G_s(s) = \dfrac{K}{s(s+a)}$
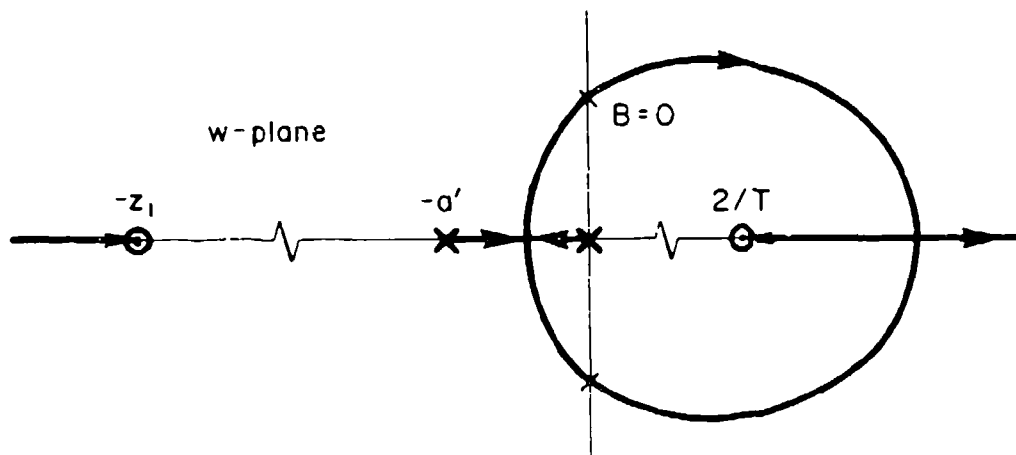
b) w-plane Root Locus for $G(w)$; $u < u_c$
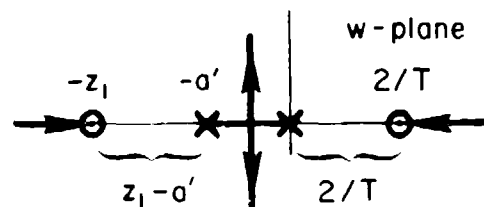
c) w-plane Transitional Conditions, $(z_1 - a') = 2/T$

Figure 7. Roots of w-plane Constellation for
Transitional ($A=B$; $u=u_c$) Conditions

25

This example is very instructive in that it demonstrates a great deal of interesting behavioral possibilities introduced by sampling. At the outset, as already remarked, the continuous system cannot be unstable for positive "a" and K (see Fig. 7a). The most common instability of the sampled system, corresponding to relatively high sampling rates (i.e., $u < u_c$) results in negatively damped w-plane closed-loop roots (Fig. 7b). These can only occur at quite high gains, i.e., $K/a^2 > 1$. It is worth noting that the closed-loop damping ratio in the continuous case corresponding to the lower gain bound for this condition ($K = a^2$) is $\zeta = 1/2$, which is approaching marginal conditions. Of course, the same gain for a sampled condition will result in a smaller effective w-plane damping ratio because of the tendency of the zero at 2/T to suck the closed-loop quadratic into the right half plane (a tendency which is not present in the s domain at all). The possibility of an instability corresponding to a w-plane real root (for the A < 0 case) has no parallel in the continuous case.

B. THE HYBRID FREQUENCY RESPONSE

Use of the w-domain permits many of the key problems of digital controller design to be addressed in a direct and effective way. In particular, stability issues and system compensation possibilities can be examined with techniques, such as w-plane and Bode root locus methods, which are analogous to continuous system analysis procedures. The effects on stability of lags and "new" leads introduced by sampling can be identified, assessed, and accounted for exactly.

While stability is well-handled using the w-domain and conventional techniques, digital systems introduce other effects which do not have continuous system parallels. In a continuous system the features (e.g., system poles and zeros) affecting stability and the features affecting system response are the same. This is not quite the situation in a digital system. For example, in a constant-coefficient linear system, a sinusoidal input will force a component of output response which is also sinusoidal at the same frequency. In the sampled system a sinusoidal

input will beget an output component at the same frequency plus an infinity of frequencies which are sums and differences of the forcing and integral multiples of the sampling frequency. This is a direct consequence of the impulse train modulation feature of sampling, and the appropriate analogy is amplitude modulation (as in carrier servo systems).

The w-domain deals exactly, but specifically, with the system's characteristics only at the sampling instants. The modulation products, on the other hand are primarily exhibited during the inter-sampling intervals. Accordingly, the assessment of the total response characteristics, including the "control roughness" or inter-sample ripple introduced when the discrete system elements are coupled with the continuous components via data holds requires another approach.

These effects are most easily considered using the "hybrid frequency response" developed in Refs. 2 and 4. The name "hybrid frequency response" is used to emphasize that it is a continuous frequency response of a continuous plant with a discrete controller. It, therefore, by definition involves the complete spectrum of the output of the continuous elements of the system -- all of the higher frequency sum and difference frequencies generated by the modulation are included as well as the fundamental output which corresponds directly to the input. [The hybrid frequency response should not be confused with the "sampled spectrum," in which one finds the lowest frequency sine wave that fits the sampled response at the sampling instants.]

The hybrid frequency response function permits one to determine the amplitude ratio and phase shifts imparted to a sinusoid inserted at the input as it is converted to an output component, and also provides data on the infinity of modulation products generated in the process. Construction of the actual output time response requires consideration of all of the components.

When contrasted with the frequency response for a system with a continuous controller the hybrid frequency response is very similar at

27

lower frequencies. There is a significant difference in the low frequency phase, amounting to a phase lag increment for the discrete system which is given by

$$\Delta\phi \doteq \frac{\omega T}{2} \tag{28}$$

This phase lag effect is just what is expected as the low-frequency consequence of the non-minimum phase zero at $w = -2/T$. Because the low-frequency phase shows clearly the delay introduced by the sampling and hold processes, and the amplitude ratio and phase includes all of the modulation products, the hybrid frequency response reflects all of the important effects introduced by the digital controller.

To develop the hybrid frequency response assume that a unit sinusoid, $r(t) = 1 \sin bt$, is applied at the input of the sampled system with data hold given in Fig. 3b. Then, following Ref. 4, the Laplace transform $C(s)$ of the <u>continuous</u> output will be

$$C(s) = G(s)M(s) \frac{1}{T} \sum_{n=-\infty}^{\infty} \frac{\omega_n}{s^2 + \omega_n^2} \tag{29}$$

where $\omega_n = b + 2\pi n/T$, and $M(s)$ and $G(s)$ are the transfer functions of the data hold and the continuous system respectively. The partial fraction expansion of Eq. 29 may be written as

$$C(s) = \sum_{n=-\infty}^{\infty} \frac{A_n(\omega_n)}{s^2 + \omega_n^2} + \frac{B_n s}{s^2 + \omega_n^2} + [\text{Transient modes of GM}] \tag{30}$$

Multiply each side by $s^2 + \omega_n^2$ and evaluate at $s = j\omega_n$:

$$C(s)\left(s^2 + \omega_n^2\right) = A_n\omega_n + B_n j\omega_n$$

$$= G(s)M(s)(1/T)\omega_n \tag{31}$$

$$A_n + jB_n = (1/T)G(s)M(s)\big|_{s=j\omega_n} \,, \quad n = 0, \pm1, \pm2, \ldots$$

Thus the continuous spectrum contains, because of the summation from $-\infty$ to $+\infty$, both positive and negative modulation product frequencies.

As an example, consider a zero-order hold for $M(s)$ and a continuous system given by a first order lag, $G(s) = 1/(s + 1)$. Then,

$$A_n + jB_n = \frac{1 - e^{-sT}}{sT} \cdot \frac{1}{s + 1}\Bigg|_{s=j\omega_n} \tag{32}$$

This is seen to be the frequency response of the continuous system, $1/(j\omega + 1)$, multiplied by a "frequency response" corresponding to the sample and hold, i.e.,

$$\frac{1 - e^{-j\omega T}}{j\omega T} = \left(e^{-j\omega T/2}\right) \frac{\left(e^{j\omega T/2} - e^{-j\omega T/2}\right)}{2(j\omega T/2)}$$

$$= \frac{\sin \omega T/2}{\omega T/2} \, e^{-j\omega T/2} \tag{33}$$

The incremental phase, $\Delta\phi = \omega T/2$ is the predominant low frequency effect due to the sampling and hold operations. The amplitude ratio, $(\sin \omega T/2)/(\omega T/2)$, introduces an infinity of notches, located at $\omega = 2\pi/T, \, 4\pi/T, \, 6\pi/T, \, \ldots$ etc.

The Bode plot of this hybrid frequency response is presented in Fig. 8 for $T = 1$ second.

To interpret Fig. 8 suppose a unit sine wave at 1 rad/sec is inserted to the sampler. Then, if sine waves with the amplitudes and phases corresponding to those shown at 1, $1 + 2\pi/T$, $1 - 2\pi/T$, $1 + 4\pi/T$, $1 - 4\pi/T \ldots$ are added together, the resultant waveform will be an exact match of the actual steady-state output waveform. In Fig. 8, one may plot the negative frequency modulation products on a "positive frequency" Bode plot by taking advantage of the fact that the magnitude is an even function of frequency and the phase is an odd function of frequency.

29
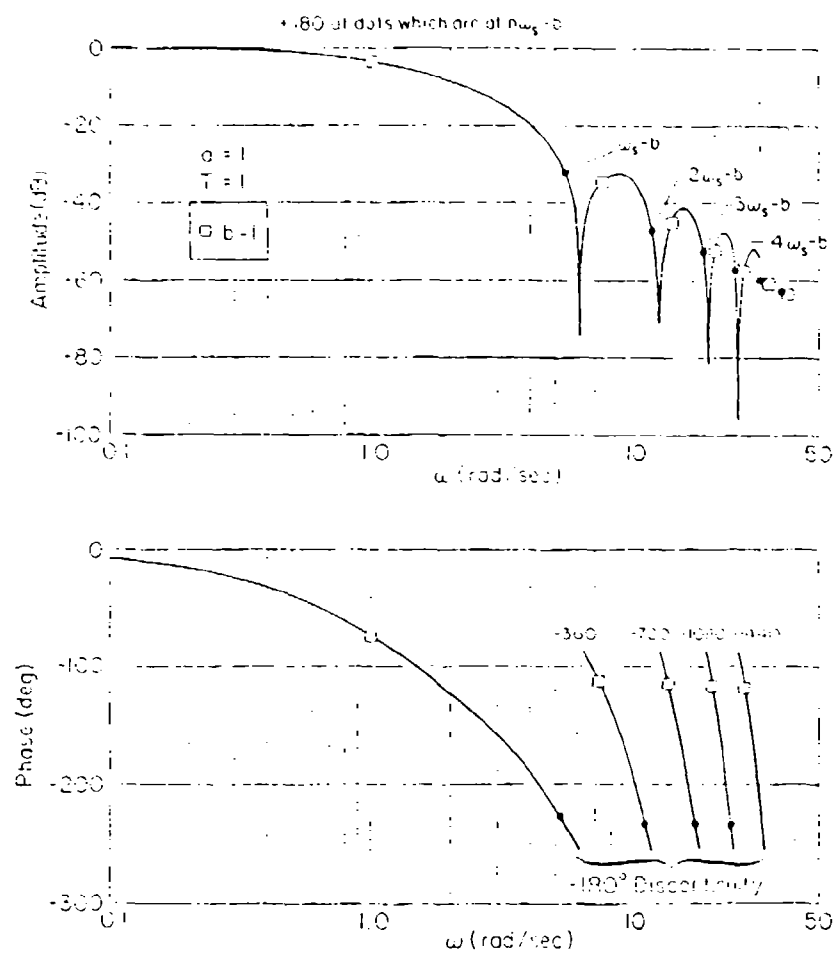
Figure 8. Frequency Response and Spectral
Components of Output for $G(s) = 1/(s+1)$
and Zero Orders Hold
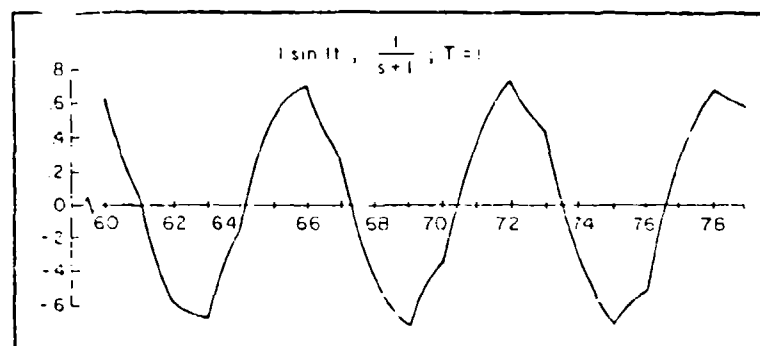
Figure 9. "Steady-State" Output Response

30

One might expect this waveform to be relatively clean, since the first modulation product is 30 dB lower than the input component. However, the output response itself does not bear out this conjecture, as can be seen in Fig. 9. The reason that the higher frequency terms are important is that they are not "harmonic" terms which slightly distort periodic waveforms but are rather modulation components which add together to match conditions at the T transition points. It can also be seen that the "steady state" does not necessarily take on the additional attribute of periodicity. This occurs only when the input frequency and the sampling frequency bear an integer relationship with respect to one another.

C. SAWTOOTH BODE - QUADRATIC DIPOLES

The basis for flexible mode stabilization in continuous control systems is thoroughly explored and exemplified in many sources, including Refs. 5 and 6. The basic idea for achieving simple and robust stabilization is to insure an appropriate "Sawtooth Bode" situation for the open-loop characteristics. This will be reviewed below for the simplest example possible -- a quadratic dipole representing the dynamics of a flexible mode.

Quadratic dipoles in the crossover region of some feedback loop or other are ubiquitous in flight control practice (Ref. 7). Among the applications are flexible mode control. The essence of what can happen is indicated in Fig. 10. This considers an open-loop system which can be approximated in the region of crossover by:

$$G(s) = \frac{K\left[s^2 + 2\zeta_N \omega_N s + \omega_N^2\right]}{s\left[s^2 + 2\zeta_D \omega_D s + \omega_D^2\right]} = \frac{K\left[\zeta_N, \omega_N\right]}{s\left[\zeta_D, \omega_D\right]} \quad (34)$$

In the idealized situations illustrated the closed-loop quadratic mode $\left[\zeta_D', \omega_D'\right]$ progresses as open-loop gain is increased from the open-loop pole $\left[\zeta_D, \omega_D\right]$ to the open-loop zero $\left[\zeta_N, \omega_N\right]$, in a counterclockwise direction along a circular segment. Thus, when the pole is smaller than the zero, the closed-loop roots depart toward the right-half plane and

31

$$G(s) = \frac{c_e}{\epsilon} = \frac{K\left[s^2 + 2\zeta_N\omega_N s + \omega_N^2\right]}{s\left[s^2 + 2\zeta_D\omega_D s + \omega_D^2\right]} = \frac{K\left[\zeta_N, \omega_N\right]}{s\left[\zeta_D, \omega_D\right]}$$

$$\Delta\phi_{MAX} \cong -\tan^{-1}\frac{\zeta_N + \zeta_D}{2\zeta_N\zeta_D}\left(\frac{\omega_N}{\omega_D}-1\right)$$
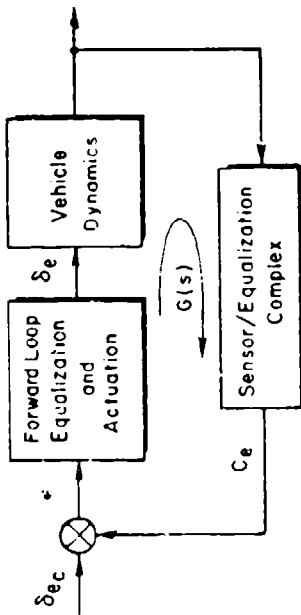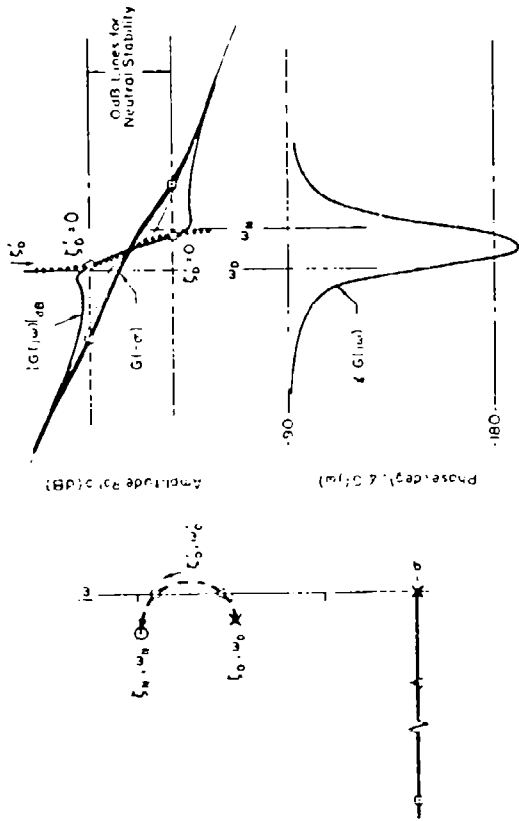
a) Log-Lead Dipole $\left(\frac{\omega_N}{\omega_D} > 1\right)$
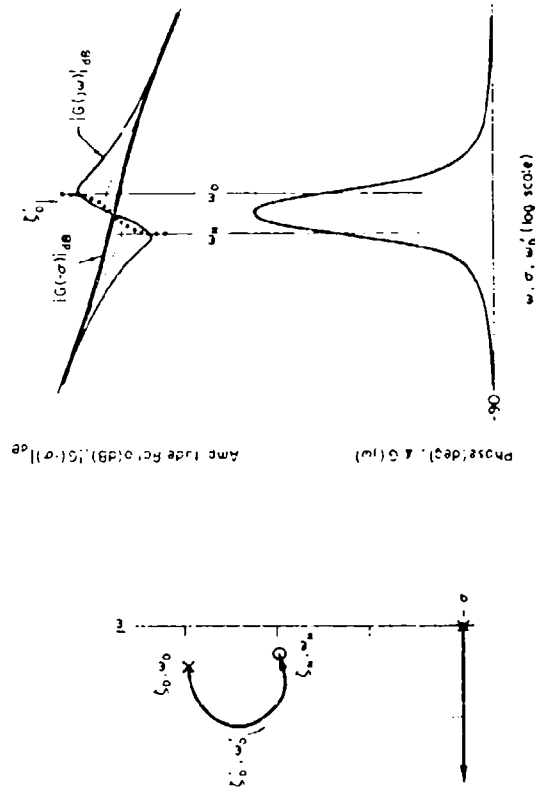
b) Lead-Log Dipole $\left(\frac{\omega_N}{\omega_D} < 1\right)$

Figure 10. System Survey for Control System with Quadratic Dipole

32

suffer a damping decrease, whereas the reverse is true when the numerator, ω_N, is smaller than the denominator, ω_D. The maximum diminution or increase in damping is connected with the maximum phase deviation, due to the dipole, from the phase angle contributed by the rest of the system. This is given by:

$$\Delta\phi(\omega_N, \omega_D)_{max} \doteq -\tan^{-1} \frac{2(\zeta_N + \zeta_D)\left(\sqrt{\frac{\omega_N}{\omega_D}} - \sqrt{\frac{\omega_D}{\omega_N}}\right)}{2 + 4\zeta_N\zeta_D\left(\frac{\omega_N}{\omega_D} - \frac{\omega_D}{\omega_N}\right)} \tag{35}$$

When ω_N/ω_D is near 1, this becomes approximately:

$$\Delta\phi(\omega_N, \omega_D)_{max} \doteq -\tan^{-1} \frac{\zeta_N + \zeta_D}{2\zeta_N\zeta_D}\left(\frac{\omega_N}{\omega_D} - 1\right) \tag{36}$$

When $\omega_N/\omega_D > 1$, the incremental phase is a dip resulting in a decreased phase margin (when crossover occurs in the dipole region) over that which would be present without the dipole. Conversely, $\omega_N/\omega_D < 1$ implies a phase lead blip and an increased phase margin. The greater the blip, the larger the attainable closed-loop damping ratio, ζ_D'.

All of the ramifications implicit in the idealized situations above are exhibited in practical control situations. When $\omega_N/\omega_D > 1$ the presence of the dipole and its associated phase dip is a distinct nuisance, often causing instability or marginally stable operation. Conversely, the presence of the dipole is advantageous in that the phase blip connected with $\omega_N/\omega_D < 1$ situations permits the closed-loop damping to be increased over that available open-loop.

When applied to a single isolated structural mode the same phenomenon will occur. This is developed in Fig. 11, for the case of an idealized longitudinal control system involving the short period and first fuselage bending modes, with a pitch rate gyro as the controller sensor. The analysis there is very elementary, resulting in the simple rule of thumb that rate gyro locations with positive mode shape slopes, ϕ_1', will create the proper conditions for phase stabilization of the mode being considered.

33

RIGID BODY

$$\frac{q}{\delta_e} = \frac{M_{\delta_e}(s + 1/T_{\theta_2})}{\left[s^2 + 2(\zeta\omega)_{sp}\, s + \omega_{sp}^2\right]}$$

$$+ \frac{M_{\delta_e}}{s} \sim \frac{\phi_0'}{s} \quad , \quad \text{for } |s| > \omega_{sp}$$

FLEXIBLE MODE (Rate Gyro at Station x)

$$\frac{q_{flex}}{\delta_e} \sim \frac{\phi_1'(x)\, s}{s^2 + 2\zeta_D\omega_D s + \omega_D^2}$$

COMBINATION

$$\frac{q}{\delta_e} \sim \frac{\phi_0'}{s} + \frac{\phi_1'\, s}{\left[s^2 + 2\zeta_D\omega_D s + \omega_D^2\right]}$$

$$= \frac{(\phi_0' + \phi_1')\left[s^2 + \dfrac{\phi_0'}{\phi_0' + \phi_1'}\, 2\zeta_D\omega_D s + \dfrac{\phi_0'}{\phi_0' + \phi_1'}\, \omega_D^2\right]}{s\left[s^2 + 2\zeta_D\omega_D s + \omega_D^2\right]}$$

$$= \frac{K\left[s^2 + 2\zeta_N\omega_N s + \omega_N^2\right]}{s\left[s^2 + 2\zeta_D\omega_D s + \omega_D^2\right]}$$

where

$$\frac{\omega_N}{\omega_D} = \sqrt{\frac{\phi_0'}{\phi_0' + \phi_1'}} = \frac{\zeta_N}{\zeta_D}$$

PHASE STABILIZATION

$$\frac{\omega_N}{\omega_D} < 1 \quad ; \quad \text{so want } \phi_1' > 0$$

Figure 11. Application to Structural Mode Stabilization

This is one special case of the old rubric used by flight control designer's for decades. In the words of Ref. 8, for example, "If only one set of instruments is used in one plane for several bending modes the location of the sensing instruments ... has to be selected so that the [mode shape] slopes of all the bending modes have the same [and appropriate] sign."

In general, regardless of whether rate gyros, accelerometers or combinations are being considered as the sensors, the key to stabilization possibilities is the presence of a positive phase blip in transfer functions relating the sensed quantity to the control effector to be used. The wider and larger this blip is, the better the attainable closed-loop damping ratio will be. Conversely, the presence of a marked phase dip can often be the indication of either a nuisance or more serious instability problem.

SECTION III

HYBRID FREQUENCY RESPONSE CASE STUDY

In the last section the fundamentals of flexible mode control and of the hybrid frequency response were reviewed as separate entities. In this section the two topics will be brought together to explore the hybrid frequency response concept more fully for a system which contains terms representing flexible modes. The example problem will still be somewhat idealized to permit a clearcut illustration of some of the more interesting phenomena. To provide an easy to follow treatment through the many graphical representations, the section is laid out so that text presented, faces the figures being described.

A. THE EXAMPLE SYSTEM

The open-loop effective vehicle characteristics relating pitching velocity to elevator deflection for the example are given by the transfer function,

$$G(s) = \frac{q}{\delta_e} = \frac{K\left[s^2 + (8)^2\right]\left[s^2 + (80)^2\right]}{s\left[s^2 + (10)^2\right]\left[s^2 + (100)^2\right]} \tag{37}$$

The free s in the denominator represents a high frequency approximation to the rigid body characteristics, and two flexible modes are present at 10 and 100 rad/sec, respectively. This transfer function would be typical of that achieved with an appropriate rate gyro location such that the numerator quadratics for the first two sensible modes, at 8 and 80 rad/sec, are both less than their associated eigenfrequencies. With this pole-zero configuration a simple pure gain controller yields a highly robust and effective control over the damping of the flexible modes. That is, as the loop gain of the continuous controller is increased the root locus from both the poles (with undamped natural frequency at 10 and 100) depart into the left half plane and proceed in nearly semi-circular segments toward their respective zeros. The attainable damping in either mode depends primarily on the pole-zero separation associated with that mode.

36

A typical example of a closed frequency response for a continuous design is shown in Fig. 12 for K = 10. Closing the loop has greatly increased the damping of the first flexible mode (10 rad/sec), whereas the second mode is hardly affected. The phase between phase blips always approaches -90 deg. The high frequency amplitude ratio of the second flexible mode decreases uniformly with a slope of -20 dB per decade. Thus there are no disruptions in the smooth, ever decreasing amplitude ratio and essentially constant phase above the second mode.

A block diagram and "hybrid" frequency response for a sampled data control with 1/T = 50 Hz and zero order hold is shown in Fig. 13. This frequency response is computed using the Ref. 4 techniques reviewed in Section II. As noted there, the amplitude ratio and phase of an output sinusoid generated by a sinusoid inserted at the q_c command point can be read from this response function as well as the infinity of modulation products also present. Construction of the actual continuous system output time response requires consideration of all of the output power.

When constrasted with the frequency response for the system with the continuous controller the hybrid frequency response is very similar at frequencies up to and just beyond the second flexible mode. As antici-pated in Section II (Eq. 28) there is a difference in the low frequency phase. The discrete system phase includes an incremental lag which is approximated by

$$\Delta\phi \doteq \frac{\omega T}{2}$$

The phase increment is approximately 45 deg at ω = 80 for the 0.02 sec sample period (i.e., T/2 $\doteq$ 0.01 second). It indicates the low frequency effect of sampling, and corresponds to an effective time delay of 1/2 the sampling interval.

The higher frequency effects begin to show up at approximately 210 rad/sec and even more so at approximately 300 rad/sec with other fluctuations at higher frequencies. Both the amplitude ratio and phase are in marked contrast with those of the continuous system (c.f.

37
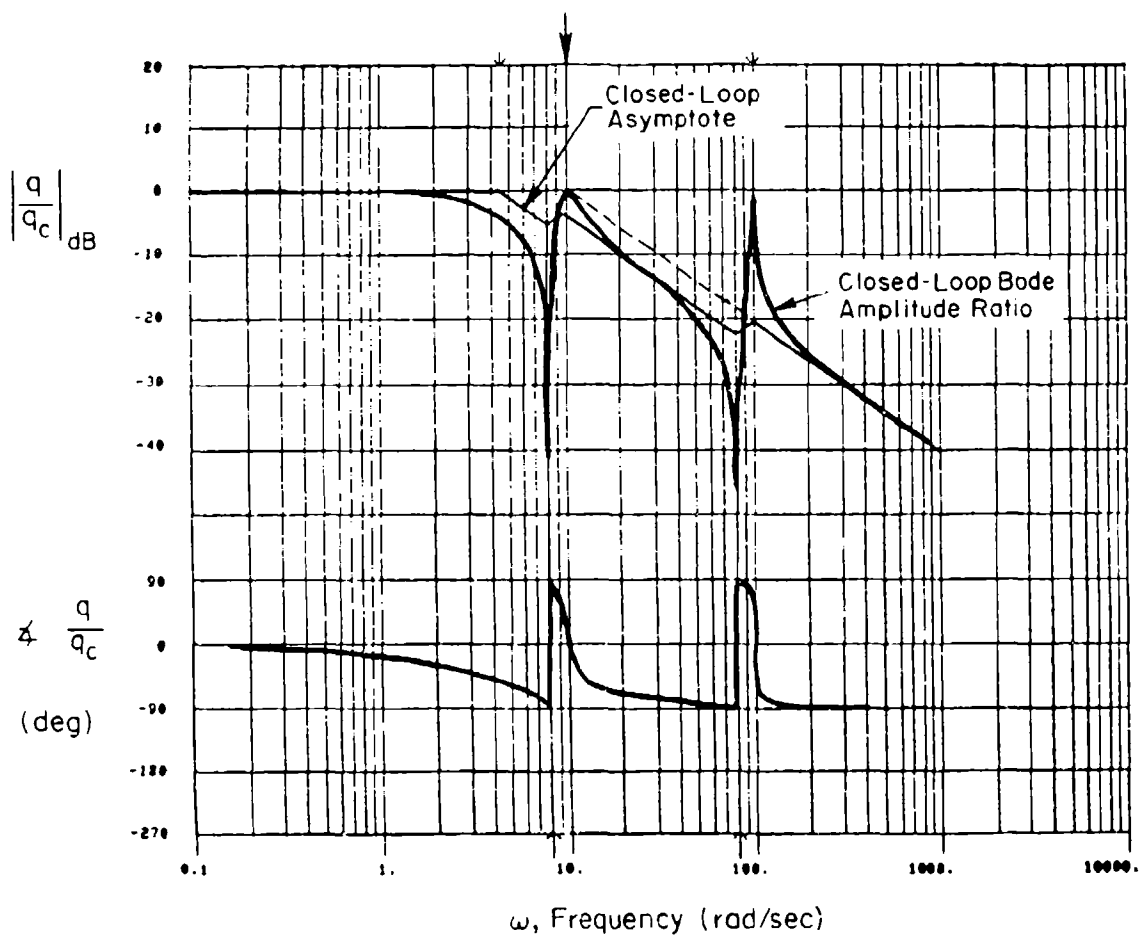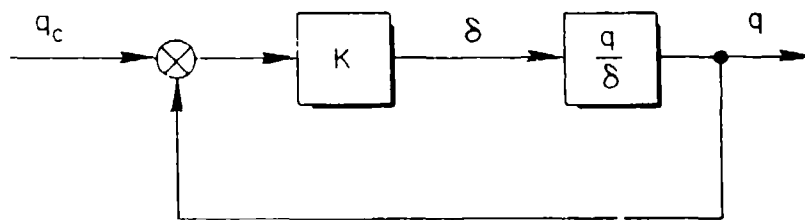
Figure 12. Block Diagram and Closed-Loop Frequency Response for
Flexible Vehicle System with a Continuous Controller, K = 10
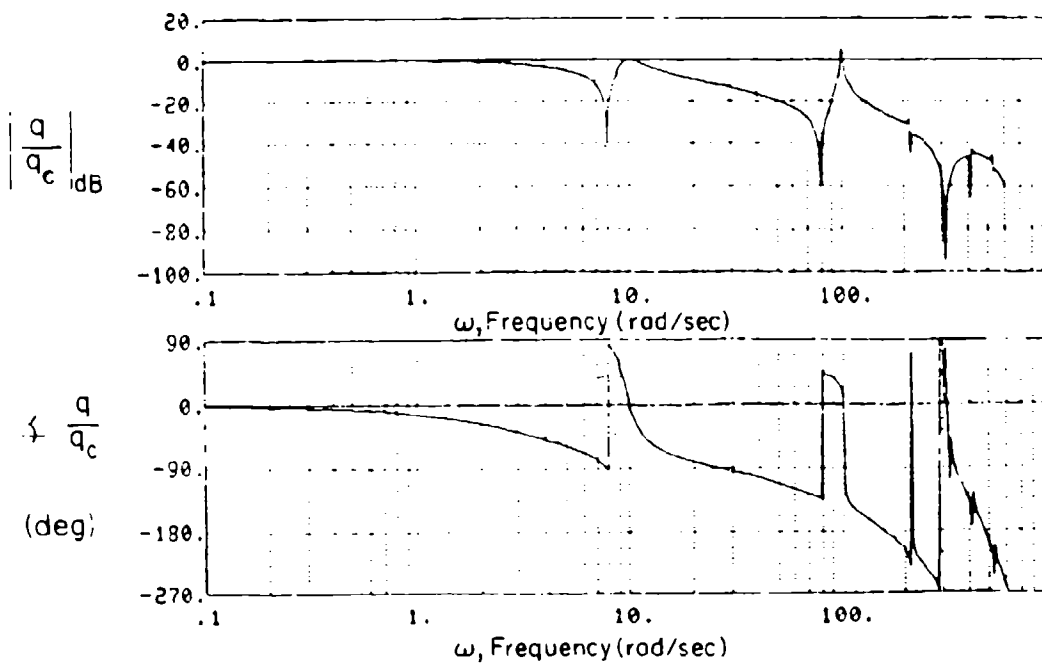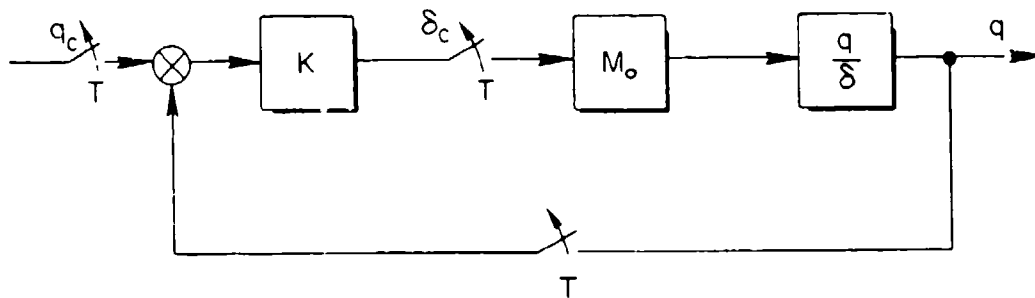
Figure 13. Block Diagram and Closed-Loop Hybrid Frequency
Response for Flexible Vehicle System with a Discrete
Controller, K = 10 and T = 0.02 sec (ω_s = 314 rad/sec)

Fig. 12) at these frequencies and represent the folding consequences of sampling. As anticipated by considering Eq. 33, there is a major notch in the amplitude ratio at the sampling frequency, 314 rad/sec. All of these high frequency effects are typical of sampled data phenomena.

B. OUTPUT RESPONSE FOR SINUSOIDAL INPUTS

While periodic sampling is a linear operation it does introduce peculiar consequences when contrasted with a constant coefficient system. As reviewed in Section II, in a sampled system a sinusoidal input will beget an output component at the same frequency plus an infinity of frequencies which are sums and differences of the forcing and integral multiples of the sampling frequencies. In general, the output may not even be periodic. To illustrate some of these points the system shown in the block diagram of Fig. 13 will be used as a test case for several different input sinusoids. First, in order to provide somewhat more damping on the second flexible mode, the open-loop gain will be increased by a factor of 4. The closed-loop system hybrid frequency response for this system is shown in Fig. 14, again for a sampling time of 0.02 sec (50 Hz sampling frequency). On these scales the modulation products at about 210 rad/sec and the sampled notch at 314 rad/sec, as well as the higher frequency modulation effects, show up more dramatically than on Fig. 13. The first-order effect of the lag underlying the effective delay is also plainly evident when contrasted with Fig. 12.

Figure 15 shows two output waveforms in response to a sinusoidal forcing function. In both cases the frequency of the input sinusoid is less than the sampling frequency. In Fig. 15a the input frequency is $\omega_s/30$. The output appears to be essentially sinusoidal with just a small delay, as would be expected. It is very similar to the output of a constant coefficient continuous system with an incremental effective delay.

The output waveform for an input frequency much closer to the sampling frequency ($\omega_i = \omega_s/4$) is shown Fig. 15b. This is an extraordinarily contaminated response and shows no similarity to the single sinusoid that would be expected in the continuous system case.
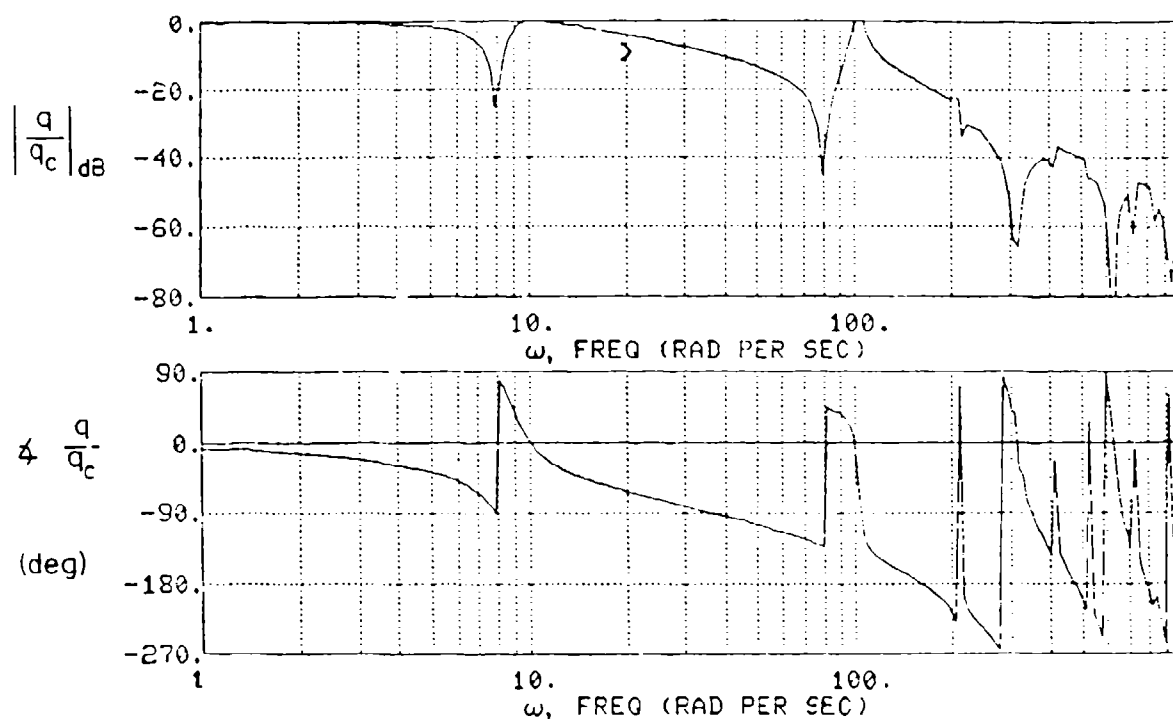
Figure 14. Closed-Loop Hybrid Frequency Response for
Discretely Controlled Flexible Vehicle, K = 40 and
T = 0.02 sec (ω_s = 314 rad/sec)

Both of the responses shown in Fig. 15 are periodic, albeit Fig. 15b is quite complex due to the modulation effects. If the forcing function frequency is incommensurate with the sampling frequency the output waveform will, in general, be non-periodic. As might be expected, the departure from periodicity for a forcing function very low in frequency compared to the sampling frequency will be hardly noticeable.

C. EFFECTS OF SAMPLING INTERVAL ON HYBRID FREQUENCY RESPONSE

We will now examine a cross section of systems as the sampling intervals are modified. The system is still that shown in the block diagram of Fig. 13, but with a loop gain of 40, as applies to the hybrid frequency response of Fig. 14. Figure 16 shows the effects of increasing the sampling period. Figure 16a gives the hybrid frequency response for T = 0.04 sec, Fig. 16b for T = 0.08 sec, and Fig. 16c for T = 0.32 sec. When taken in concert with Fig. 14 (T = 0.02 sec), these frequency responses show the same system for four different sampling intervals.

41
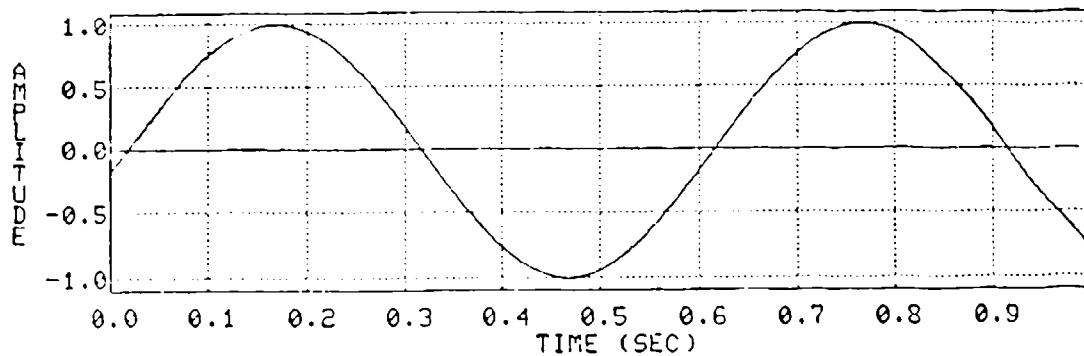
a) Output Waveform for $\omega_i = \omega_s/30$ *;* $(\omega_i = 10.472 \, rad/sec)$
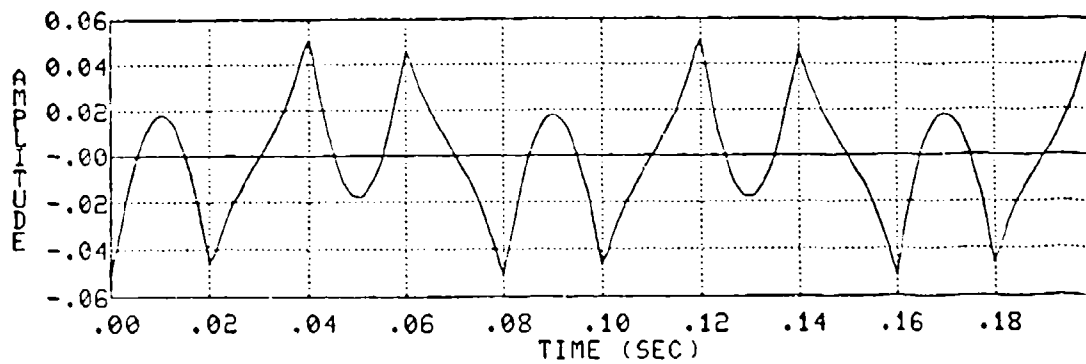
b) Output Waveform for $\omega_i = \omega_s/4$ *;* $(\omega_i = 78.54 \, rad/sec)$

Figure 15. Output Responses for Sinusoidal Forcing Functions which are Commensurate with the Sampling Frequency

42
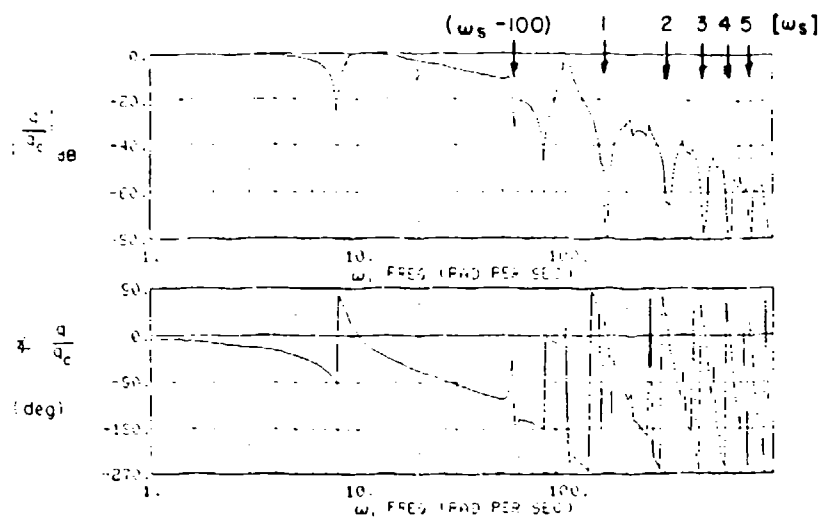
a) $T = 0.04\,sec\,(f_s = 25\,Hz,\ \omega_s = 157\,rad/sec)$
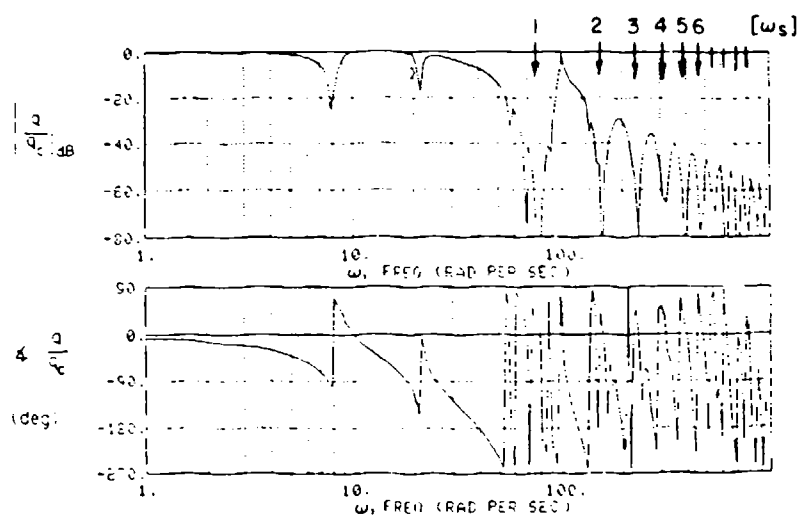
b) $T = 0.08\,sec\,(f_s = 12.5\,Hz,\ \omega_s = 78.5\,rad/sec)$
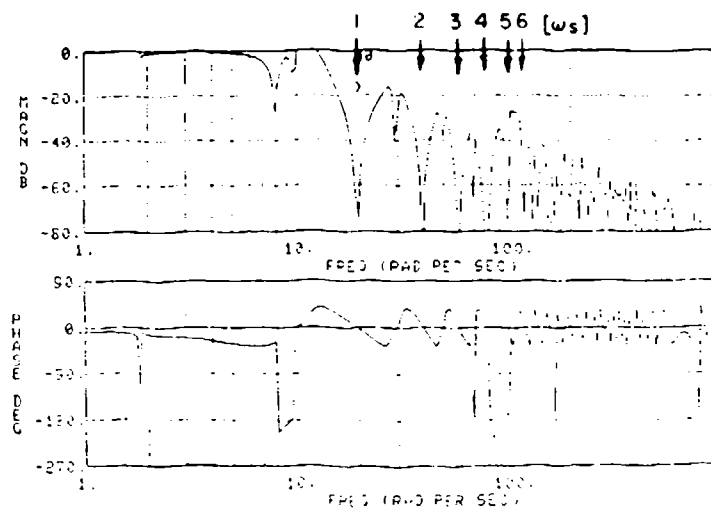
c) $T = 0.32\,sec\,(f_s = 3.13\,Hz,\ \omega_s = 19.63\,rad/sec)$

Figure 16.   Closed-Loop Hybrid Frequency Responses for
Digitally Controlled Flexible Vehicle for
Three Different Sampling Periods

43

The notches in the amplitude ratios at ω_s and its integer multiples $2\omega_s$, $3\omega_s$, etc. are clearly seen in all of the figures.

The differences among the systems are very remarkable. Only the system with $T = 0.02$ sec ($\omega_s = 314$ rad/sec) in Fig. 14 is reasonably close to the continuous system of Fig. 12 over the frequency range containing the flexible modes. Even the system with $T = 0.04$ ($\omega_s = 157$ rad/sec), Fig. 16a, has a different amplitude ratio just before the high frequency flexible mode, which demonstrates some modulation effects. The sampling rates down to 78.5 rad/sec ($0.08 > T > 0$) are suitable for exerting control on the lower frequency flexible mode and have some effect on the high frequency mode. For $T = 0.32$ sec the response is, as might be expected, a hodgepodge.

The novel mixtures of the sampling frequency with the flexible mode frequencies create a large number of peaks in the amplitude ratio which become more confused as T is increased. These peaks are modulation products which reflect difference frequencies between $n\omega_s$ and the flexible modes at 10 and 100 rad/sec. The most easily picked out of these is shown in Fig. 16a at 57 rad/sec, which is $\omega_s - 100$. The introduction of these apparent "resonances" at difference frequencies between sampling and flexible mode frequencies is an interesting feature of systems which contain lightly damped modes. It is a phenomenon which requires special attention for systems where such difference frequencies may reside in the frequency range of control.

Figure 17 gives some additional appreciation for the output responses when the input and sampling frequencies are commensurate. In Fig. 17a the input sinusoid is reflected by the lowest frequency component of the output response. The prominent high frequency waveform superimposed on the large amplitude low frequency component is at approximately 50 rad/sec, which is a difference frequency between the sampling and input frequency. There is, of course, other content present, but these two are by far the most conspicuous. When the ratio of input to sampling is reduced just a bit more, to a factor of 3, the waveform, while periodic, has much less resemblance to a sine wave with some higher frequency deviations. This is indicated in the output
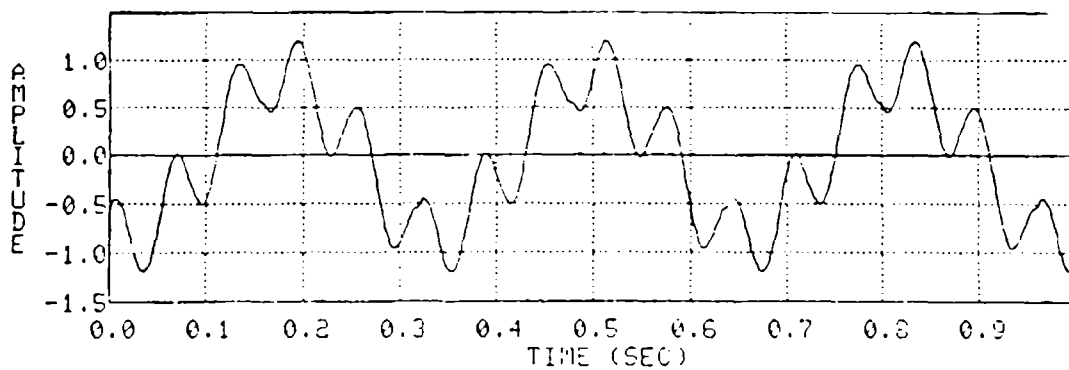
a) $\omega_i = 19.635 = \dfrac{\omega_s}{4}$
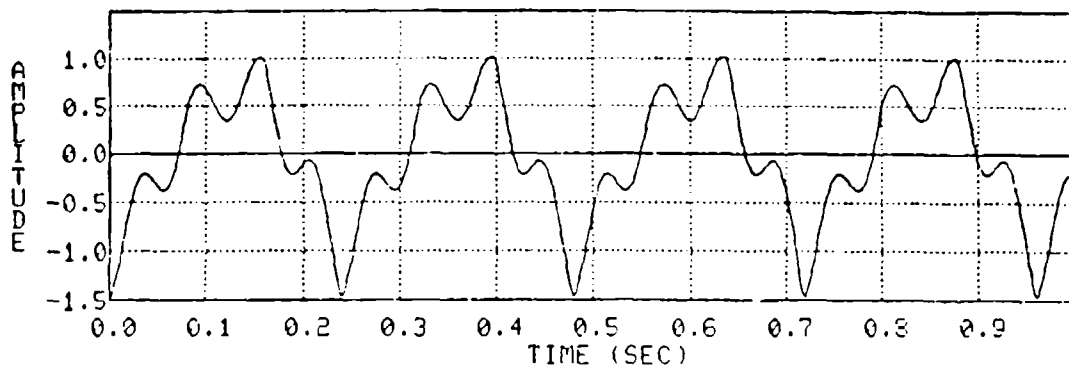
b) $\omega_i = 26.1799 = \dfrac{\omega_s}{3}$

Figure 17. Output Responses for Sinusoidal Forcing Functions
which are Commensurate with the Sampling Frequency,
T = 0.08 (f_s = 12.5 Hz, ω_s = 78.5 rad/sec)

response shown in Fig. 17b which is quite cusp-like in character. The low frequency component representing the principal forcing of the input sinusoid is still there, but is definitely not as evident as in Fig. 17a.

Two waveforms representing output responses with two forcing functions which have frequencies not commensurate with the sampling frequency are illustrated in Fig. 18. Figure 18a shows a response for the system with T = 0.08 sec sampling interval and a forcing function frequency of 30 rad/sec, which is a factor of 2.61799... less than the sampling frequency. Figure 18b shows a similar incommensurate case for the T = 0.32 sec sampling period. Both output waveforms are distinctly nonperiodic functions.

Remarkably the response of Fig. 18b, which has the lowest ω_i/ω_s ratio of any of the output responses shown here, appears to have less distortion than many of the others. This is a consequence of the particular numbers used in the example. Referring to Fig. 16c, it is seen that the 11.424 rad/sec input frequency, which is strongly represented in Fig. 18b, is very close to the resonant peak associated with the open-loop mode at 10 rad/sec. The first difference frequency ($\omega_s - \omega_i$ = 19.635 - 11.424 = 8.211 rad/sec) on the other hand is very close to the notch at 8 rad/sec in the amplitude ratio of Fig. 16c, and is therefore suppressed. The most prominent distorting frequencies are much higher. The situation would be markedly changed with minor modifications to the numerical values. It nonetheless nicely illustrates another of the peculiar features introduced by the combination of sampling and lightly-damped system mode frequencies.
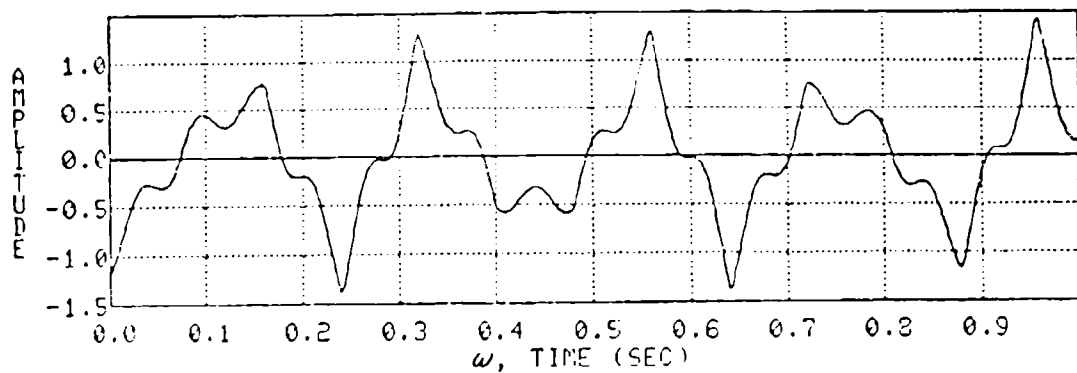
a) $T = 0.08$ (12.5 Hz), $\omega_i = 30 = \dfrac{\omega_s}{2.61799}$
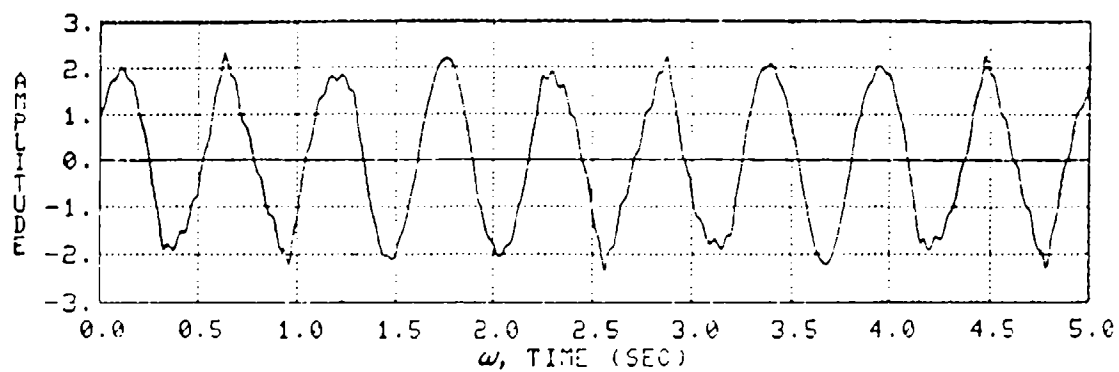
b) $T = 0.32$ sec, $\omega_i = 11.424$ rad/sec $= \dfrac{\omega_s}{1.71875}$

Figure 18. Output Responses for Sinusoidal Forcing Functions
which are Incommensurate with the Sampling Frequency

SECTION IV

FLIGHT CONTROL SYSTEM DESIGN WITH DIGITAL CONTROLLERS

In this section we will present examples illustrating the stabilization of flexible aircraft characteristics. In the process two control system possibilities will be considered -- both continuous and digital controllers. The aircraft selected as the example vehicle is a fighter, and the control problems solved are longitudinal.

In the next subsection a summary of the flexible airplane characteristics will be presented. Some details are relegated to Appendix A. This is followed by the continuous controller preliminary design, which covers topics such as control system architecture, loop closure details, sensitivity and robustness considerations, and assessment of the closed-loop system design. We then turn to the digital system design, which uses the same feedback control architecture as the continuous system -- as is appropriate from the basic physics of the control task. The design is conducted with a w-domain treatment, and emphasizes the effects of sampling rate. The stability limits are explored both in w- and z-domains. Finally, the hybrid frequency response of the digital flight control system is examined over a wide range of sampling conditions. We will continue the practice of showing figures opposite the relevant discussion whenever this is feasible.

The emphasis on sampling rate effects started in Section III is continued here even though many advanced flight control systems are likely to have very high rate systems. The primary reasons are tied in with the flexible modes -- which can cause response peculiarities at quite low frequencies as they interact with the sampling rate as a difference frequency -- and the likely use of relatively low sampling in some development simulations which can give rise to unrealistic anomalies in the simulation.

A. FLEXIBLE AIRCRAFT CHARACTERISTICS AND SURVEY OF FEEDBACK CONTROL POSSIBILITIES

1. Flexible Aircraft Characteristics

The flexible aircraft characteristics to be used for the continuous and digital control examples are given in Ref. 9. Figure 19 shows a three-view of the airplane, which has three possible longitudinal control points -- elevator, flaps, and symmetic ailerons -- available for use in establishing good flying qualities and for flexible mode control. Table 2 gives the available sensor locations and the corresponding mode shape characteristics. In principle either accelerometers or rate gyros could be placed at any or all of the locations.

Table 3 summarizes the aircraft dynamic modes which will be consid-ered, consisting of the short period and five structural modes. As can be seen there the short period characteristics of the airplane are con-ventional, although it has a damping ratio of 0.28 which will result in Level 2 flying qualities. Consequently the pilot-centered requirements, as far as rigid body characteristics are concerned, can be met simply by improving the damping to 0.35 or greater. The flexible modes are less straightforward to correct, and will be considered next.

2. Survey of Feedback Control Possibilities for Flexible Mode Stabilization

A direct approach to the development of feedback system possibili-ties for the fighter flexible mode control is to examine the rate gyro and accelerometer transfer functions which relate these signals at each possible pickup point with the three possible control points (symmetric aileron, flap, and elevator). This is a lot of transfer functions -- [2 sensors] × [4 pickup locations] × [3 control points] = 24 -- yet a trivial computational chore for this case with a limited number of modes.[*] The transfer functions are then examined for the presence of

---

[*]In a more general problem, where specific locations were not fixed and where higher frequency modes were still present in the airplane's mathematical model, several additional steps are needed to get to this point. See, for example, Ref. 6 for more specifics on modal truncation, residualization, etc.
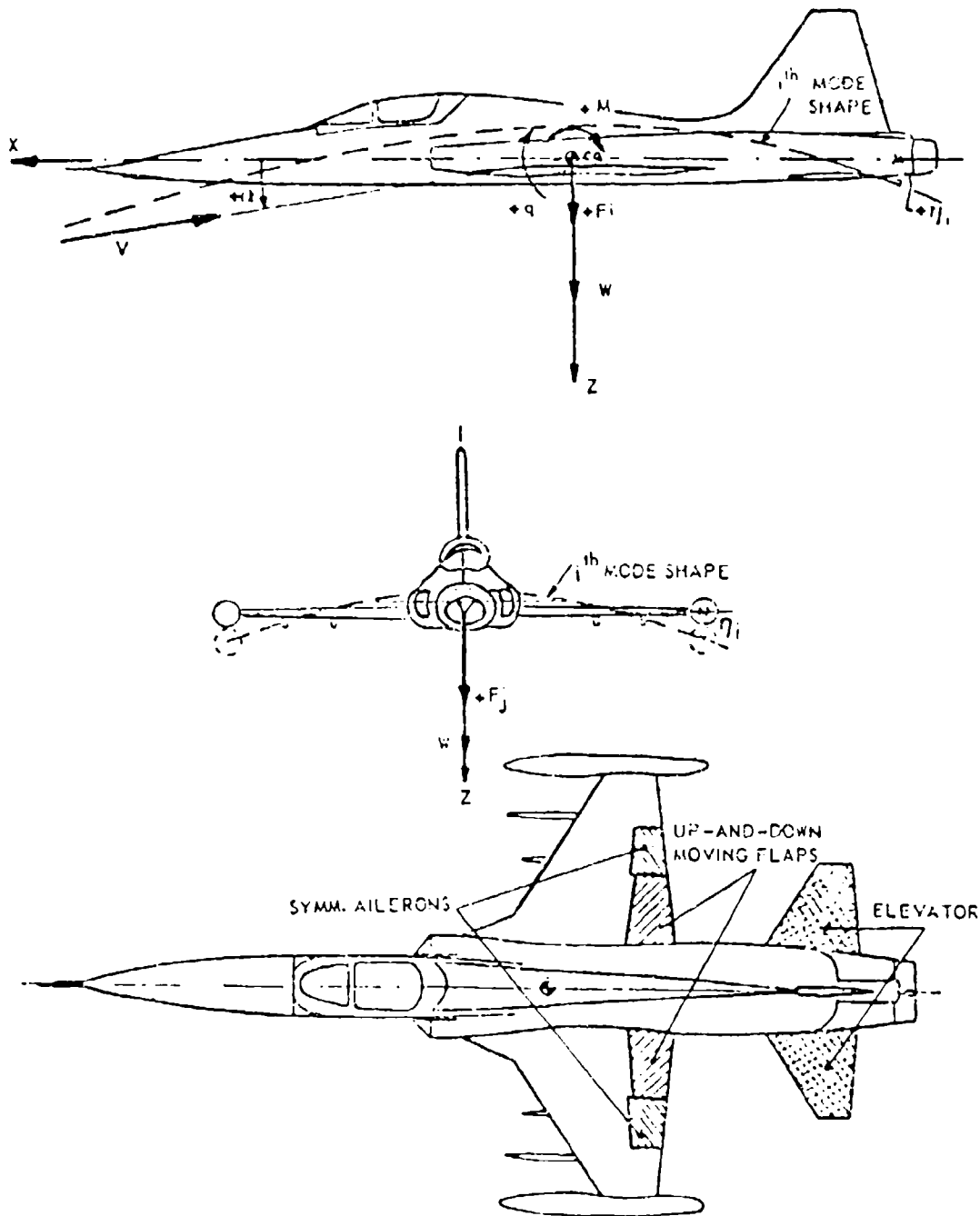
Figure 19. Three View Drawing of the Flexible Aircraft, Including an Explanation of the Motion Parameters, Forces, and Moments (Ref. 9)

TABLE 2.   COEFFICIENTS IN THE FORMULAS OF THE NORMAL
ACCELERATION AND THE PITCH RATE FOR DIFFERENT
AIRCRAFT STATIONS (REF. 9)

normal acceleration at station x:

$$a_{n_x} = \frac{V}{g}\{q - \dot{\alpha}\} + \frac{\ell_x}{g}\dot{q} - \frac{1}{g}\sum_{i=1}^{n}(\phi_i)_x \ddot{n}_i$$

pitch rate at station x:

$$q_x = q - \sum_{i=1}^{n}\{(\frac{\partial\phi_i}{\partial x})_x \dot{n}_i\}$$

Structural mode	Vertical displacement $\frac{\phi_i}{\bar{c}}$ at				Slope $\frac{\partial\phi_i}{\partial x}$ at =			
i	pilot seat p	wing tip w	nose n	tail t	pilot seat p	wing tip w	nose n	tail t
1	-.230	1.0	-.120	-.489	.0004	.007	.001	.001
2	.129	1.0	2.55	-.401	.0044	-.027	.021	.005
3	0	-1.0	0	.455	0	-.039	0	0
4	.542	-1.0	.727	.238	.0096	.068	-.011	-.012
5	.223	-.47	.554	.628	.0017	.039	-.001	-.004

Sensor locations:
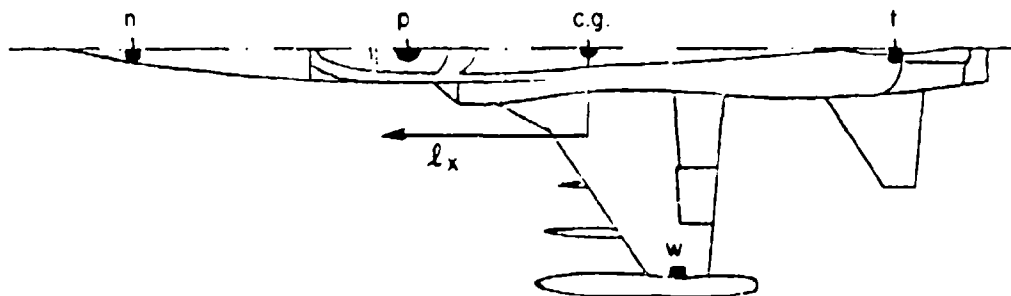
position x	$\ell_x/\bar{c}$
c.g.	0
p	1.13
n	2.96
w	-.55
t	-1.99

51

TABLE 3.   AIRCRAFT DYNAMIC MODES

Short Period: $[\zeta_{sp}, \omega_{sp}] = [0.28, 6.3]$;   Flying Qualities: Level 2

$$1/T_{\theta_2} = 1.097 \qquad (n/\alpha \doteq \frac{U_o}{gT_{\theta_2}} = 32.4)$$

Structural Modes:	Frequency (Hz)/(rad/sec)
1 First Symmetric Wing Bending	2.9/18.2
2 First Symmetric Wing Torsion	3.6/22.6
3 Inboard Store Yaw Mode	4.6/28.9
4 Inboard Store Pitch Mode	5.8/36.5
5 Outboard Store Yaw Mode	6.1/38.3

Control Effectors Available:

Elevator, δ_e

Trailing Edge Flaps, δ_f

Symmetric Ailerons, δ_a

phase blips, phase dips, or near cancellation, for each mode.   The
equalization, if any, needed to adjust the particular transfer function
being considered to an appropriate sawtooth Bode form is also consid-
ered.

Figure 20 illustrates the examination process.   Figure 20a shows the
transfer function relating normal acceleration at the wing tip loca-
tion, a_{n_w}, and the elevator.   First wing bending (Mode 1), first wing
torsion (Mode 2), and the outboard store yaw mode (Mode 5) are all
represented with strong positive phase blips.   Considered in context
with the sawtooth Bode concept described in Section II (Fig. 10), these
phase blips indicate a promising feedback possibility for improving the
damping of those modes.   There is essentially no reflection of the

a) $a_{n_w}/-\delta_e$

b) a_{n_w}/δ_f

c) $q_n/-\delta_e$
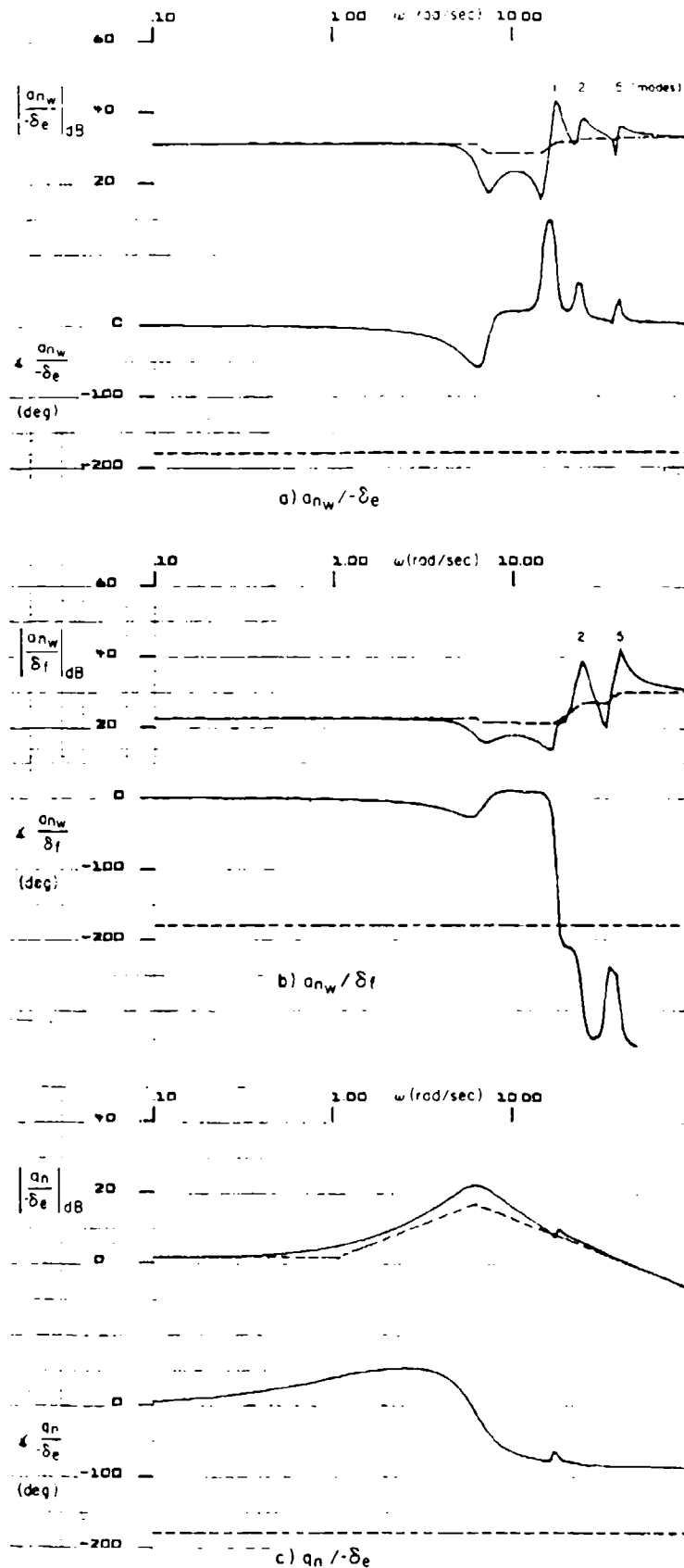
Figure 20. Examples of Survey for Flexible
Mode Control Possibilities

53

inboard store yaw (Mode 3) or pitch (Mode 4) modes in the transfer function, indicating that these are unobservable. Figure 20b, the a_{n_w} to flap, δ_f, transfer function, shows unfavorable phase characteristics for Modes 1 and 2, again nothing for Modes 3 and 4, and a possibly favorable phase blip for Mode 5. In the third example, shown in Fig. 20c, the transfer function for pitching velocity at the nose location, q_n, to elevator, δ_e, has only a tiny phase blip at Mode 1 and nothing at any other. This qualifies for an unusable (or "nil") classification.

The results of the complete survey are given in Table 4. There it is seen immediately that the 3rd (Inboard Store Yaw) and 4th (Inboard Store Pitch) modes show neither blips nor dips. In other words, the transfer function poles corresponding to these modes are essentially cancelled by zeros for all sensor and control effector combinations. The modes are, therefore, neither observable nor controllable from the pickup locations and control effector points available. If their control was essential to the mission some alternative configurations would have to be considered.

On the other hand, there are a number of favorable possibilities for the improvement of short period damping, and for increased stabilization of wing torsion, wing bending, and the outboard store yaw mode. These possibilities are summarized in Table 5.

B. CONTINUOUS CONTROL SYSTEM DESIGN

1. Control System Purposes and Requirements

The fundamental purposes of the system are to:

- Improve the flying qualities (increase short period damping ratio).

- Improve the flexible mode dampings, as feasible.

- Reduce the wing root bending moment.

- Reduce the flexible mode induced vibratory environment at the pilot station.

TABLE 4. SURVEY OF FEEDBACK POSSIBILITIES

	1 1st Wing Bending	2 1st Wing Torsion	3 Inboard Store Yaw Mode	4 Inboard Store Pitch Mode	5 Outboard Store Yaw Mode
	2.9/19.2	3.6/22.6	4.6/28.9	5.8/35.5	6.1/38.3
$q_n \cdot \delta_i$, (i = a, f, e)	Nil	Nil	Nil	Nil	Nil
$q_p \cdot \delta_e$	+	Nil	Nil	Nil	Nil
$\cdot \delta_a$	Nil	+	Nil	Nil	+
$\cdot \delta_F$	Nil	-	Nil	Nil	-
$q_w \cdot \delta_a$	Nil	+	Nil	Nil	+
$\cdot \delta_F$	Nil	-	Nil	Nil	-
$q_w \cdot \delta_e$	+		Nil	Nil	-
$q_T \cdot \delta_a, \delta_e$	Nil	Nil	Nil	Nil	Nil
$\cdot \delta_f$	Nil	-		Nil	Nil
$a_{n_n} \cdot \delta_a$	+	-	Nil	Nil	-
$a_{n_n} \cdot \delta_f, \delta_e$	Nil	Nil	Nil	Nil	Nil
$a_{n_p} \cdot \delta_a$	+	+	Nil	Nil	-
$a_{n_p} \cdot \delta_i$	+	+	Nil	Nil	-
$a_{n_p} \cdot \delta_e$	+	+	Nil	Nil	-
$a_{n_w} \cdot \delta_e$	+	+	Nil	Nil	+
$a_{n_w} \cdot \delta_a$	+	-	Nil	Nil	+
$a_{n_w} \cdot \delta_f$	-	-	Nil	Nil	+
$a_{n_T} \cdot \delta_a$	+	-	Nil	Nil	-
$a_{n_T} \cdot \delta_f$	-	-	Nil	Nil	+
$a_{n_T} \cdot \delta_e$	+	Nil	Nil	Nil	+

CRITERIA FOR SURVEY OF FEEDBACK POSSIBILITIES

Promising (+) -- Positive Phase Blip
                 Adjustable to Appropriate Sawtooth Bode Forms

Unfavorable (-) -- Negative Phase Blips or Excessive Equalization

Unusable ("Nil") -- No Blips at all

TABLE 5. MOST FAVORABLE FEEDBACK POSSIBILITIES

Additional Considerations

Short Period Damping:

q_p ---> Elevator   Positive Effect on 1st Wing Bending.

q_w ---> Symmetric Aileron $Z_{\delta_a}/M_{\delta_a} = 15.4$; $Z_{\delta_e}/M_{\delta_e} = 4.6$ Therefore, $q_w \rightarrow \delta_a$ produces 3.36 times more lift due to δ than $q_p \rightarrow \delta_e$.

Wing Torsion:

q_w ---> Symmetric Aileron $q_w \rightarrow \delta_a$ increases Wing Root Bending Moment.

a_{n_w} ---> Elevator   Tends to degrade short period damping; small pole-zero separations for torsion.

Wing Bending:

a_{n_w} ---> Elevator   Tends to degrade short period damping; small pole-zero separations for torsion.

a_{n_w} ---> Symmetric Aileron   Short period damping degradation. Pole-zero separation for torsion less than for $a_{n_w} \rightarrow \delta_e$.

The survey results summarized in Table 5 provide the implied requirements that an accelerometer at the wing location and a pitch rate gyro at the pilot station are well constituted to satisfy the various damping requirements.

2. Control System Architecture (Figure 21)

The closed-loop system involves only the elevator. Remarkably, this selection, while demonstrably the best in performance potential, is also probably the simplest since it does not require specialized high bandwidth actuation for the symmetric aileron and/or flap effectors. The
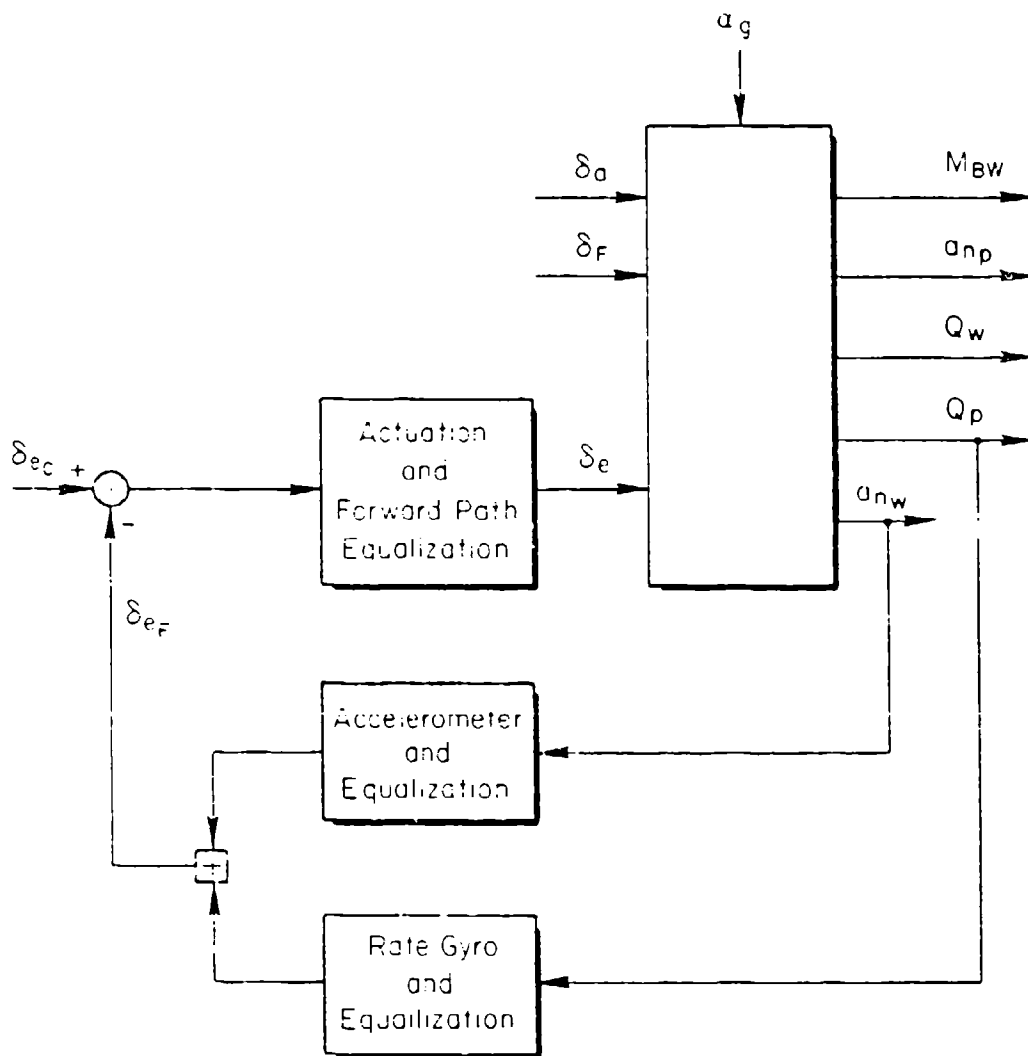
Figure 21. Closed-Loop System for Flexible Mode
and Short-Period Damping Augmentation

control system involves two loop closures which naturally operate primarily in two frequency ranges. Thus, successive stable loop closures using the higher bandwidth closure as an inner-loop is appropriate to assure a robust design. If the lower bandwidth outer-loop pathway is lost the system will still be stable and will still accomplish its primary flexible mode stabilizing functions. The appropriate inner-loop is the $a_{n_w} \rightarrow$ elevator feedback.

The most desirable feedback for flexible mode damping augmentation is one proportional to the velocity of the modal deflection. This is most easily approximated with the accelerometer by using a low frequency lag equalization on the accelerometer signals. This will establish a -20 dB/decade slope in the frequency regions above 10-15 rad/sec where the positive phase blips occur and will thereby assure stable and effective loop closure conditions. In terms of the root loci for the bending and torsion modes this shaping will pull the loci further into the left-half plane thereby increasing the closed-loop damping and damping ratios. Because the pole-zero pairs will be closer together in the closed-loop system than they are in the open loop, the near-cancellation tendencies will further reduce the excitation of these modes by control system inputs. So both the damping augmentation and improved pole/zero cancellation effects are favorable.

A typical elevator actuator will have a bandwidth which can be approximated by a first-order lag at about 20 rad/sec. This lag will be very detrimental to the stabilization process for the higher order modes, destroying the -20 dB/decade slope just where it is most needed. Therefore it will be necessary to compensate for the actuation dynamics. This can be done by using a lag-lead equalization for the accelerometer. Thus, the acceleration loop feedback (including actuator) component, δ_{e_a}, of the total elevator deflection δ_e, will be

$$\delta_{e_a} = a \frac{(s + 20)}{(s + a)} \frac{1}{(s + 20)} a_{n_w}$$

$$= \frac{a}{(s + a)} a_{n_w}$$

(38)

58

3. Inner and Outer Loop Closure Characteristics

a. Inner [Accelerometer] Loop Closure (Figure 22)

Figure 22 shows the open-loop frequency response and the system root locus when the first order lag $\omega = 5$ rad/sec is used for the equalization. It is seen there that a gain of 0.1 rad/g provides maximum damping in the wing bending and torsion modes and some damping improvement for the outboard store yaw mode. The other two flexible modes are essentially unaffected as they are scarcely observable. The short period is somewhat destabilized as it progresses toward its nearby zero. This zero is, however, in the left-half plane so the system is assured of stability even without an outer loop. The flying qualities would, of course, be very poor because of this short period damping ratio ($\zeta_{sp}' = 0.0107$).

b. Outer [Pitch Rate Gyro] Loop Closure (Figure 23)

The fundamental purpose of the pitching velocity feedback is to improve the short period damping while not degrading the flexible mode improvements due to the inner loop. This is most easily accomplished by low pass filtering the rate gyro signal at frequencies above about 10 rad/sec. A first-order filter at 10 when combined with the actuator dynamics at 20 rad/sec, readily satisfies this regimen. The frequency response and closed-loop system root locus for this loop, with the aircraft characteristics modified by the acceleration loop closure, are shown in Fig. 23. It is seen there that with a very low gain of 0.2 rad/rad/sec the short period damping ratio is improved to a Level 1 value of $\zeta = 0.35$. The gain margin G_M for this is 12 dB. The root locus shows the roots at ±6 dB from this Level 1 value by + markings. It is easy to appreciate from the short period locus that damping ratios below Level 2 minimums are excluded even with a 5 dB gain reduction. Higher gains are appropriate for the final setting.

At the gain levels considered here the effects of the pitching velocity feedback on the flexible modes is nil. The relatively heavy filtering of the pitching velocity feedback assures that the system will be robust if the accelerometer loop is opened.
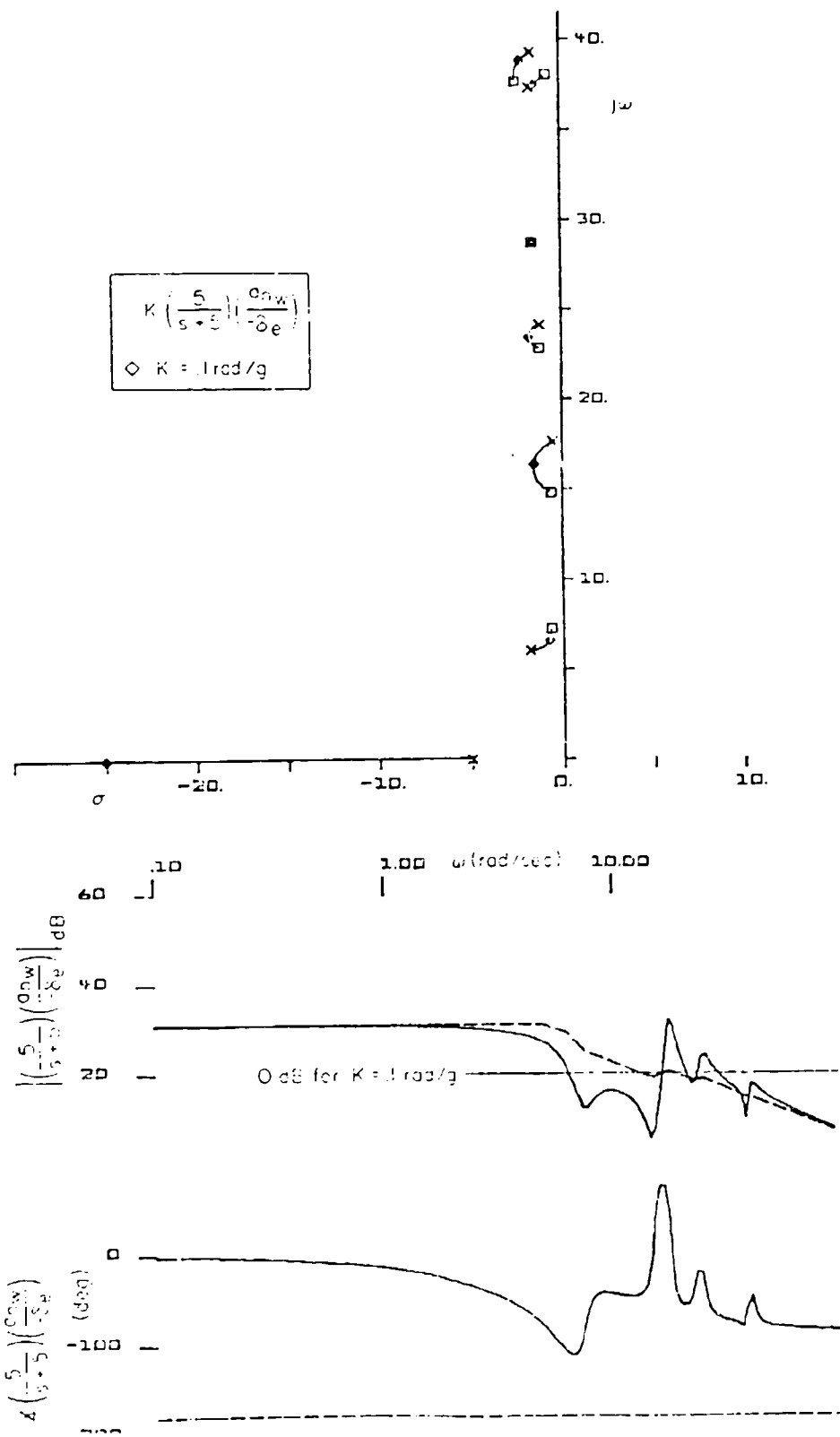
Figure 22. Inner Loop Closure of $a_{nw} \left(\dfrac{5}{s+5}\right) \rightarrow \delta_e$
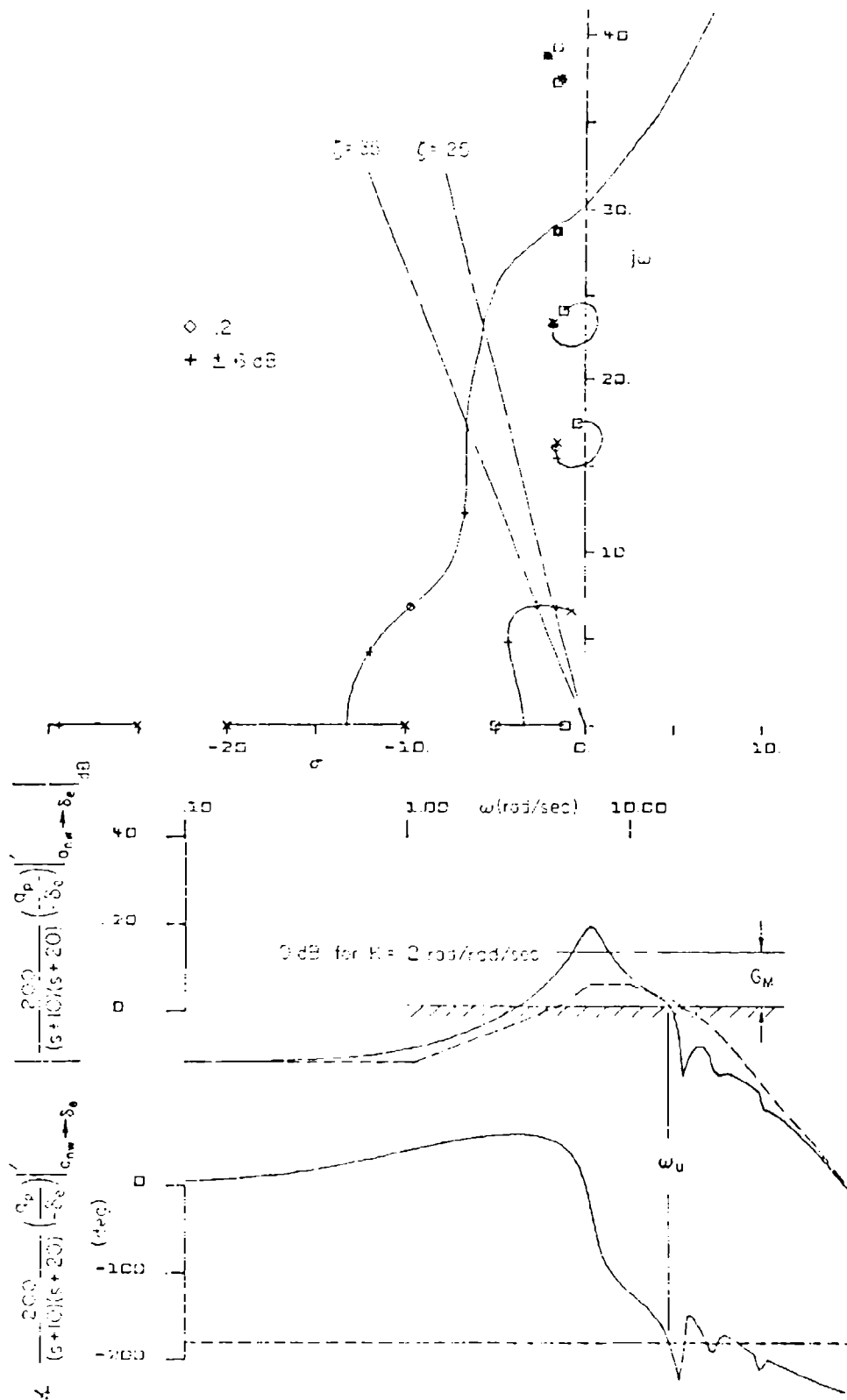
Figure 23. Outer Loop Closure of $q_p \dfrac{200}{(s + 10)\ (s + 20)} \rightarrow \delta_e$

4. Sensitivity and Robustness

With the design as developed above a zero signal in either the accelerometer or rate gyro loops will not result in an unstable system. The degraded aircraft dynamics with the pitch rate gyro loop open are quite undesirable from a flying qualities standpoint, although the flexible modes are stabilized as well as can be accomplished with available effectors and instrument sites. Loss of the accelerometer loop is not in itself crucial, as the flexible modes are all still stable; they will, however, suffer from significantly decreased damping.

Another sensitivity assessment is to consider the effects of change in the composite loop gain. In this instance the equalized accelerometer and rate gyro signals are first summed and the composite is then presumed to share a common changeable loop gain. These changes physically could occur in the forward path of Fig. 21 and could be the result of uncertainties in surface effectiveness, less than ideal gain compensation, actuator gain changes, etc.

The frequency response and root locus for these combined loops is shown in Fig. 24. The composite loop gain margin is 16 dB and the phase margin about 80 deg. For this system there are several phase margins because there are several crossover frequencies. There will also be a corresponding set of delay margins given by $T_M = \phi_m/\omega_c$. The phase and delay margins of major interest are given in the table.

Crossover Frequency, ω_c (rad/sec)	Phase Margin, ϕ_m (degs)	Delay Margin, T_M (secs)
9.8	80	0.14
16	90	0.10
23.5	160	0.12

Thus, while the gain and phase margin values seem large, the delay margins may at first glance appear quite small. They imply that the insertion of an effective pure time delay of 0.1 to 0.14 sec (which can be

Elevator Loop Root Locus

$$\frac{\delta_{er}}{\delta_e} = G^{\delta_{er}}_{\delta_{nw}} N^{\delta_{nw}}_{\delta_e} + G^{\delta_{er}}_{\delta_p} N^{\delta_p}_{\delta_e}$$

$$-1\left(\frac{5}{(s+5)}\right) -2\left(\frac{200}{(s+10)(s+20)}\right)$$

○ Nominal
× ± 6 dB
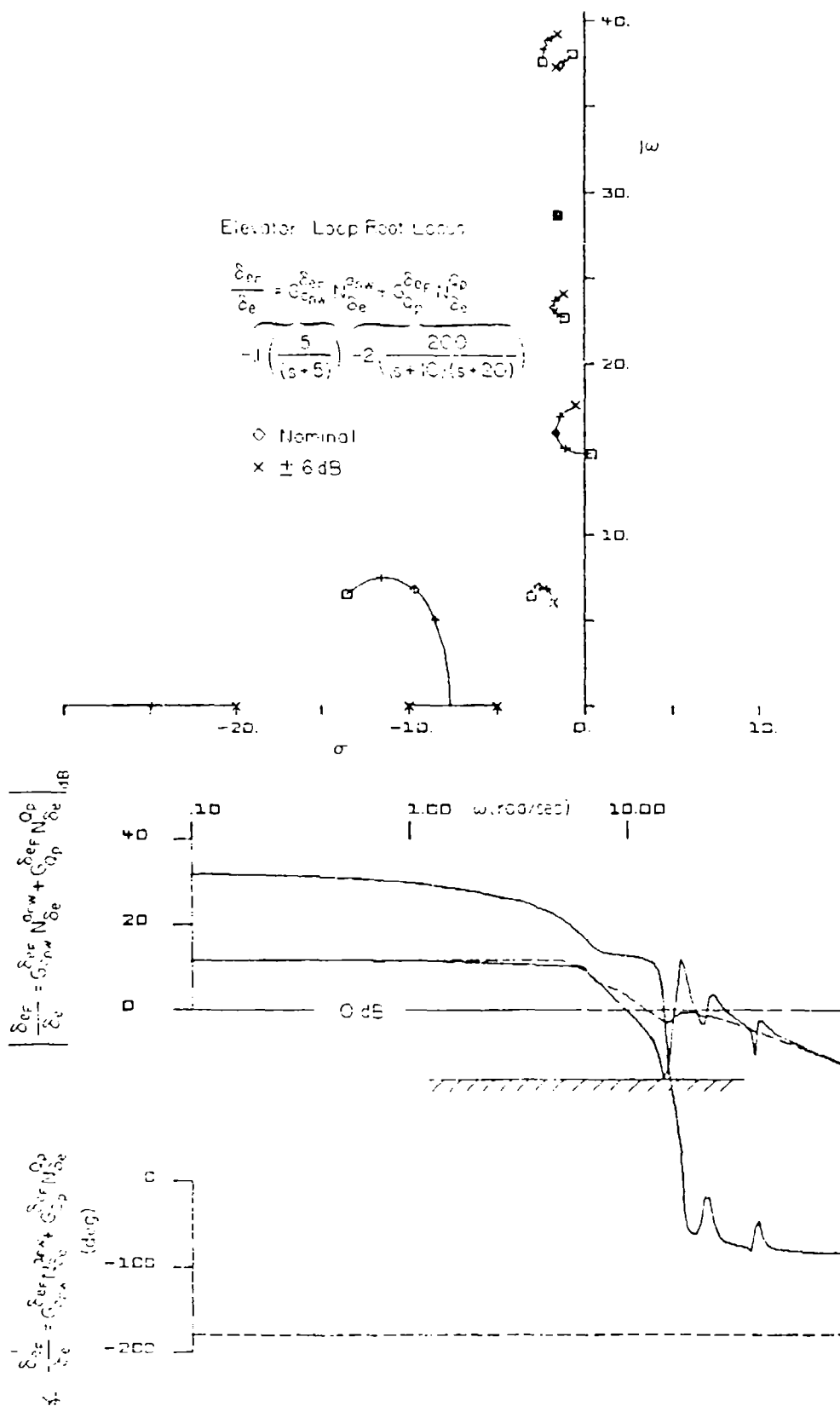
Figure 24. Sensitivity of Design to a Change in Composite Gain

63

made up of a combination of high frequency lags and delays not included in the analysis) would result in a system instability. These small values must be viewed in perspective with the potential instability, which will be the wing bending mode at approximately 15 rad/sec. At these frequencies an effective pure delay of 0.10 (as needed to develop a 90 deg phase loss) is quite large indeed.

The other modes are typically somewhat improved when gain is increased over the nominal and somewhat degraded with gain decreases. Consequently, the system can be considered quite insensitive and highly robust to even major changes in the system gains and even loop removal.

5. Assessment of the Closed-Loop System Design

The fundamental purposes of the system were to

- Improve the flying qualities (increase short period damping ratio)

- Improve the flexible mode dampings

- Reduce the wing root bending moment

- Reduce the flexible mode induced vibratory environment at the pilot station

The first two of these purposes have already been achieved as described above. Figures 25, 26, and 27 show that the wing root bending moment and acceleration at the pilot station are also significantly modified and improved.

Figure 25 shows the asymptotic and total frequency responses for pilot location acceleration and wing root bending moment in response to an angle-of-attack gust, α_g, input. Peak bending moment amplitude ratios of about 130 dB are indicated for the wing bending and outboard store yaw modes. Figure 26 shows that these are reduced significantly to 122 dB for wing bending and 126 dB for the outboard store. The cost of this is an increase in the wing bending at short period frequencies of approximately 6 dB. This stems, of course, from the reduced short period damping ratio with just the accelerometer loop closed. The final system closure of the pitch rate gyro (Fig. 27) removes this defect and,
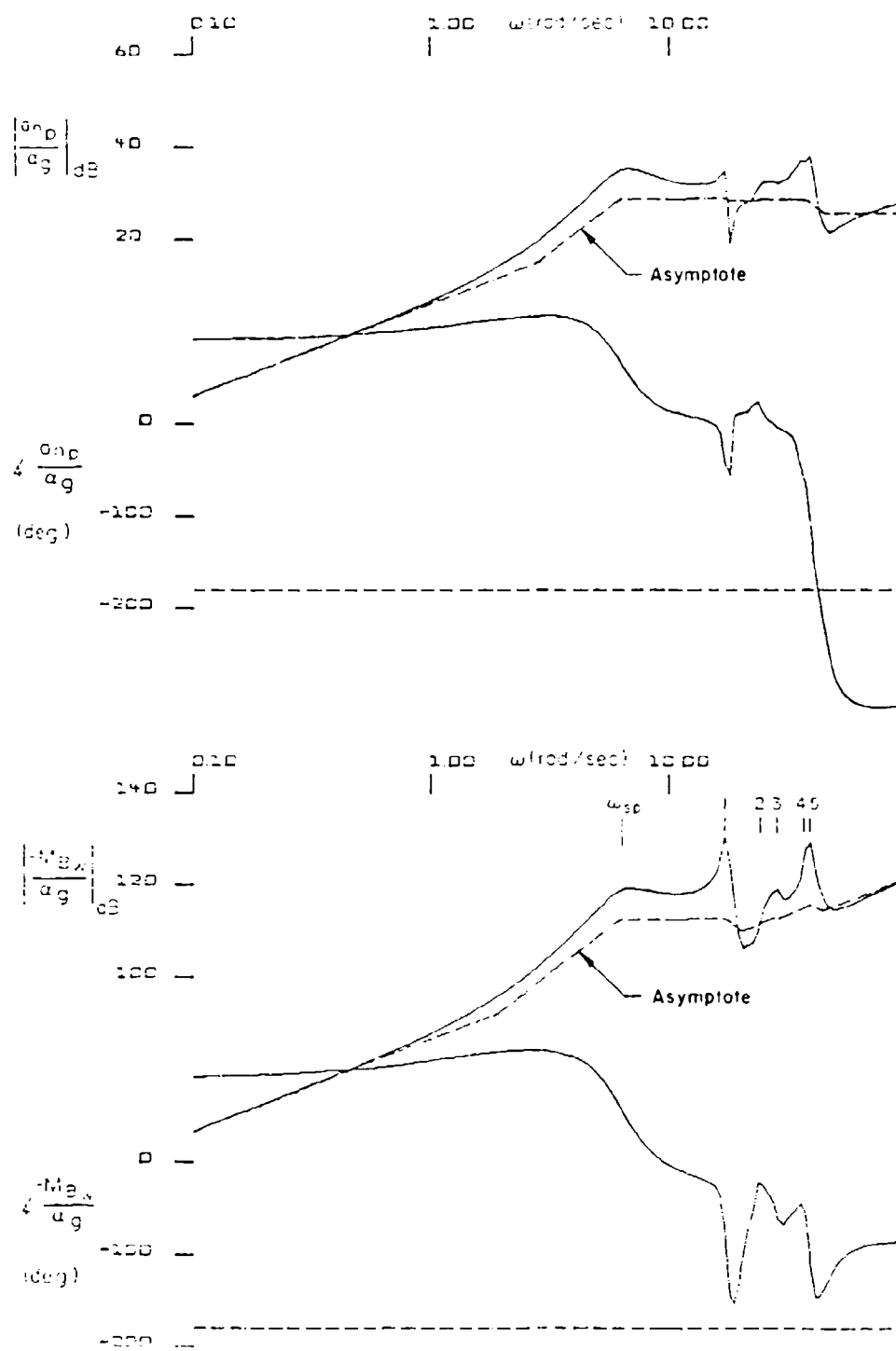
Figure 25. Baseline (Open-Loop) $\frac{a_{n_p}}{\alpha_g}$ and $\frac{M_{B_w}}{\alpha_g}$ Frequency Response

65

Figure 26. Effects of Acceleration Loop Closure on $\dfrac{a_{n_p}}{a_g}$ and $\dfrac{M_{B_w}}{a_g}$ Frequency Responses

Figure 27. $\dfrac{a_{n_p}}{\alpha_g}$ and $\dfrac{M_{B_w}}{\alpha_g}$ Frequency Responses with the Closed-Loop Control System

in fact, improves the wing root bending moment at and near short period frequencies over that of the aircraft without control. There is an additional very small improvement at wing bending frequencies and little or no effect at still higher frequencies.

Comparison of the acceleration at the pilot station of the total closed-loop system with that of the open-loop indicates only very minor changes. It should be recalled, however, that the rate gyro gain is set at the Level 1 lower boundary for these calculations merely to illustrate what was required to change the short period to a Level 1 status. When full advantage is taken of the augmentation system the pitching velocity gain will be increased somewhat so that the gust induced acceleration in the short period at the pilot station will be reduced from that shown.

These considerations indicate that the closed-loop system design has accomplished its desired purposes.

C. DIGITAL SYSTEM DESIGN

The system architectural configuration for the digital controller is the same as that for the continuous control case. Accordingly the system block diagram, as shown in Fig. 28, is similar except for the samplers and zero-order holds.

As already noted, there are two very instructive approaches to the direct digital design problem. In the first, the s-domain transfer characteristics, including those of samplers and holds, are converted to the w-domain. The design is then carried out in a fashion directly analogous to that for continuous controls. The design data presentations and techniques used are essentially those transferred from continuous analysis in which w replaces s as the complex variable. The results of such procedures are precise for stability margins, etc., but may leave something to be desired as far as full appreciation of the response artifacts associated with discrete systems are concerned. These response considerations are very effectively treated using the

δ_{e_c} + δ_e Y

1.   ZOH   Aircraft

$-\dfrac{.5}{s+5}$ ZOH a_{n_w}

$\dfrac{-40}{s^2+30s+200}$ ZOH Q_p
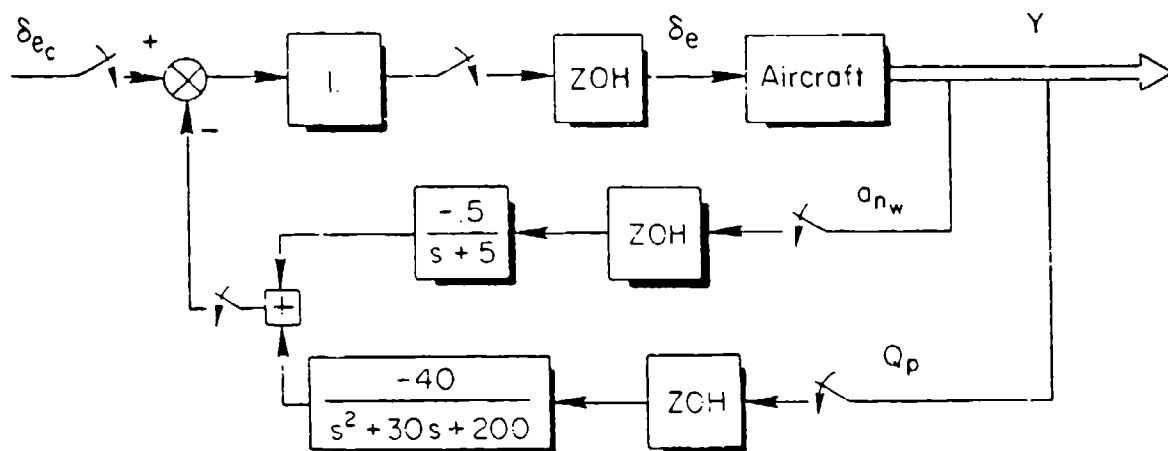
All Samplers Operate With Period T

Figure 28. Aircraft Plus Discrete Controller

second direct digital design technique associated with the hybrid spectrum of the digital controller. These two complementary approaches are illustrated in the following articles.

1. Direct Digital Design Using w-Domain Transfer Functions

The w-domain is the natural extension to use in accomplishing a direct digital design analysis of the system. The graphical presentation of results use the same forms as for the continuous control case, i.e., system surveys showing w-plane root loci, "ordinary" Bode plots, and w-plane Bode root loci. The root loci are directly comparable to those in the continuous domain in that they are true root plots. They do not compare in the sense that the w-plane roots necessarily imply a corresponding time domain mode damping and undamped natural frequency. The results approximate this for modes much lower in "w frequency" than 2/T, but will depart markedly as the modes approach the sampling rate (see, e.g., Fig. 2). One can, of course, convert back to the s-domain to find the true (as contrasted with the "w-domain") dampings and natural frequencies. The "ordinary" Bode diagram, for which an imaginary variable replaces w (just as $j\omega$ replaces s for continuous systems), does not correspond to a true frequency response in the same sense as

for the continuous case. Yet, the limiting characteristics, as T → 0, provides, by analogy, a significant amount of insight if not exact interpretations.

In the following treatment system surveys are presented for four values of sampling, $1/T$ = 100, 50, 25, and 14 Hz. The actual open-loop transfer functions used in the surveys are for the composite form wherein the accelerometer and rate gyro signals are combined. The appropriate comparison for the continuous case is with Fig. 24. [On the w-plane Bode plots which follow the real roots (w = σ) are shown as solid lines, and the complex roots as crosses (+). The asymptotes shared by both the Bode "frequency response" and root loci are dashed lines.]

Figure 29, for a sampling rate of $1/T$ = 100 Hz, is virtually indistinguishable from Fig. 24 except for the appearance of the non-minimum phase w-plane lead at 200 rad/sec and the continuing decrease in the high frequency phase associated with the same right half plane zero.

Essentially the same statements can be made for the sampling rate at $1/T$ = 50 Hz (Fig. 30) except for a major change in the low frequency phase. This is due to a tiny shift in the zero (at approximately 1⅄ rad/sec) associated with the wing bending mode (at 17.6 rad/sec). For the continuous case and $1/T$ = 100 Hz cases this zero is just very slightly in the right half plane, whereas for $1/T$ = 50 Hz it has moved into the stable region of the w-plane.

For the much lower frequency sampling rates of $1/T$ = 25 (Fig. 31) and 14 Hz (Fig. 32), there are some major shifts in the high "frequency" amplitude ratio high gain asymptote as it approaches closer to the level of the very-low "frequency" asymptote. The phase blips for $1/T$ = 50 and $1/T$ = 25 are very similar. But there is a major change in the highest frequency blip for $1/T$ = 14 Hz (Fig. 32) as the magnitude of the rhp zero becomes less than the highest frequency mode. This is also reflected in the Bode root locus shift in the undamped natural frequencies of the higher frequency modes for $1/T$ = 14 Hz.
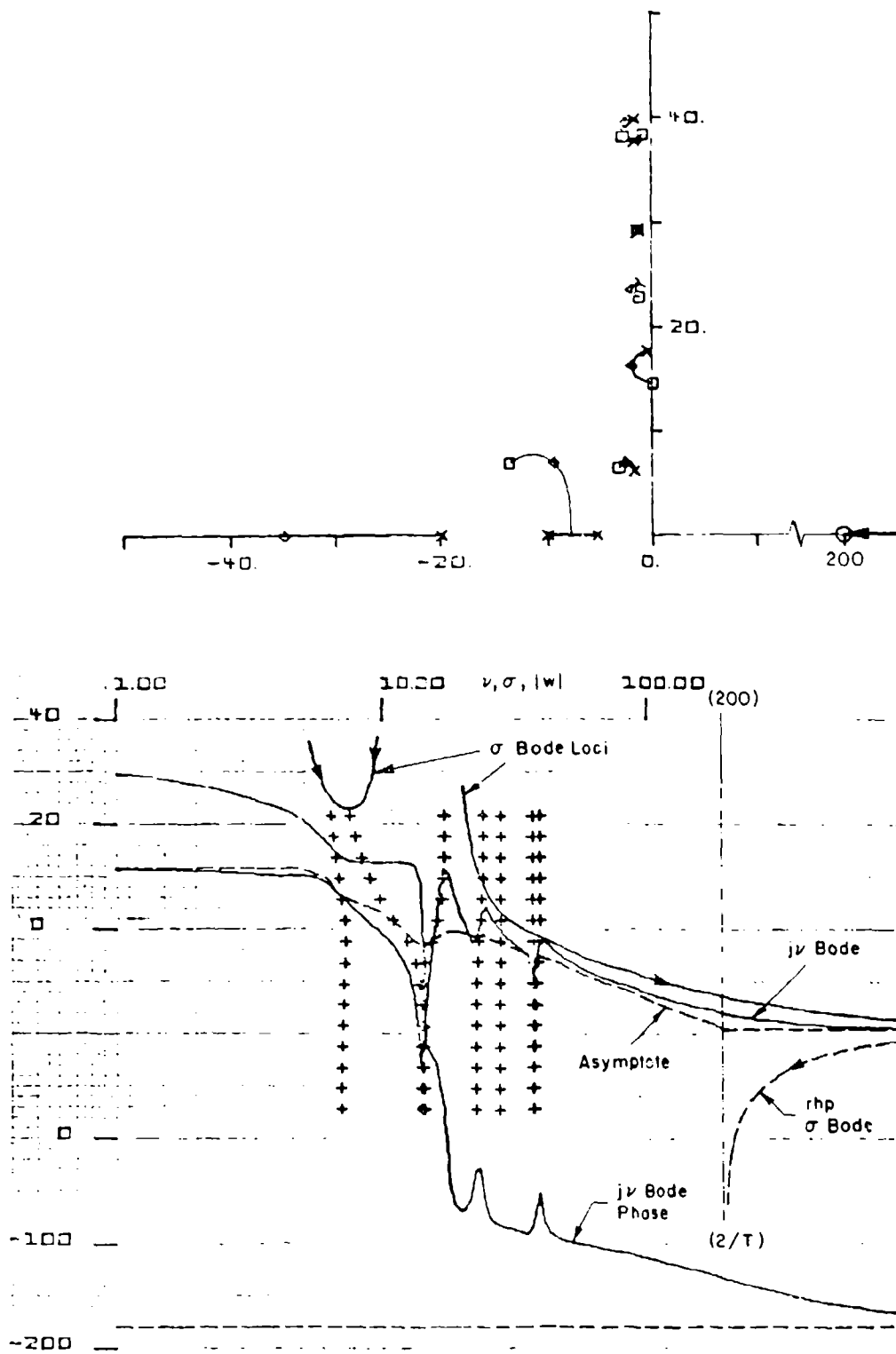
Figure 29.   System Survey for Digital Flexible
Aircraft Control System, 1/T = 100 Hz

71
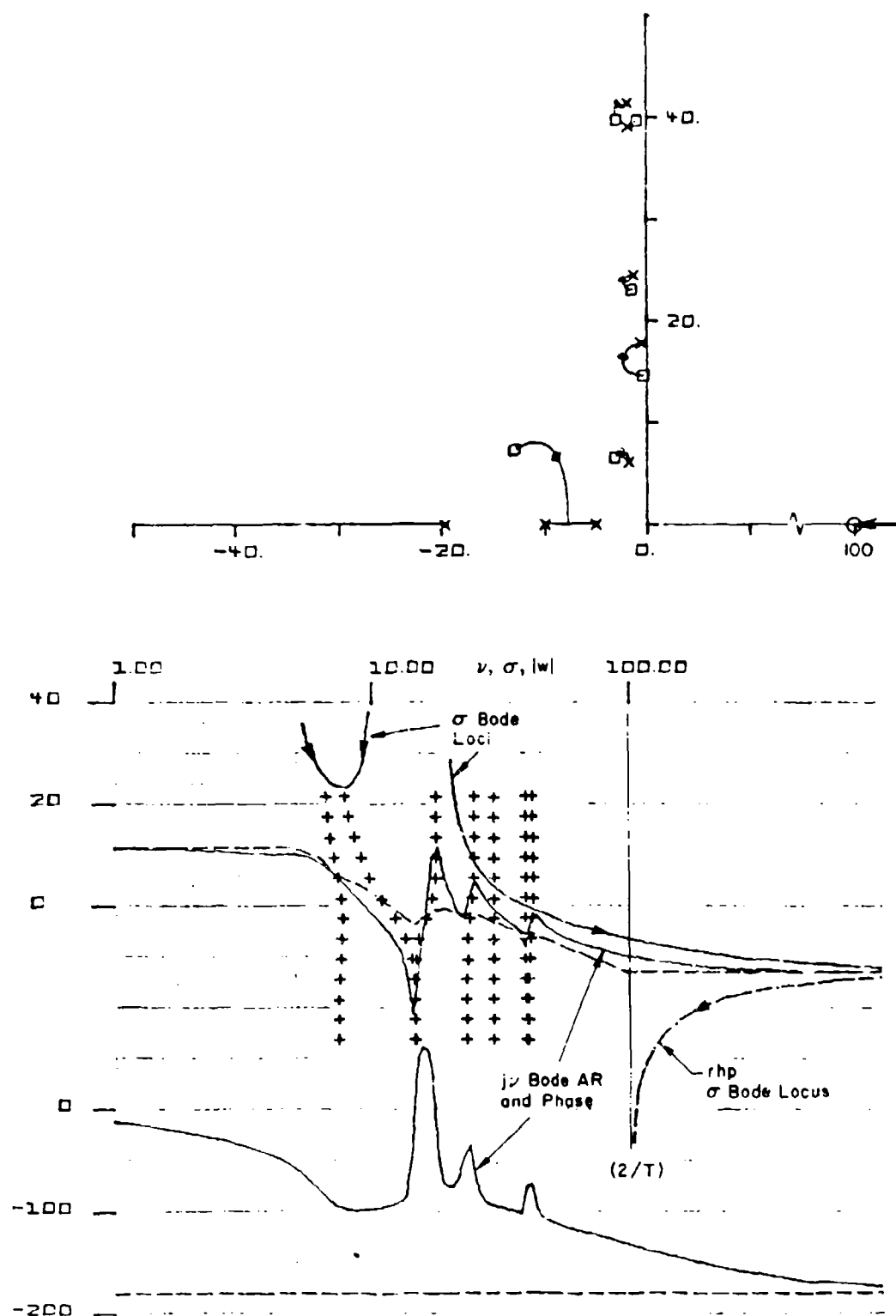
Figure 30. System Survey for Digital Flexible
Aircraft Control System, 1/T = 50 Hz
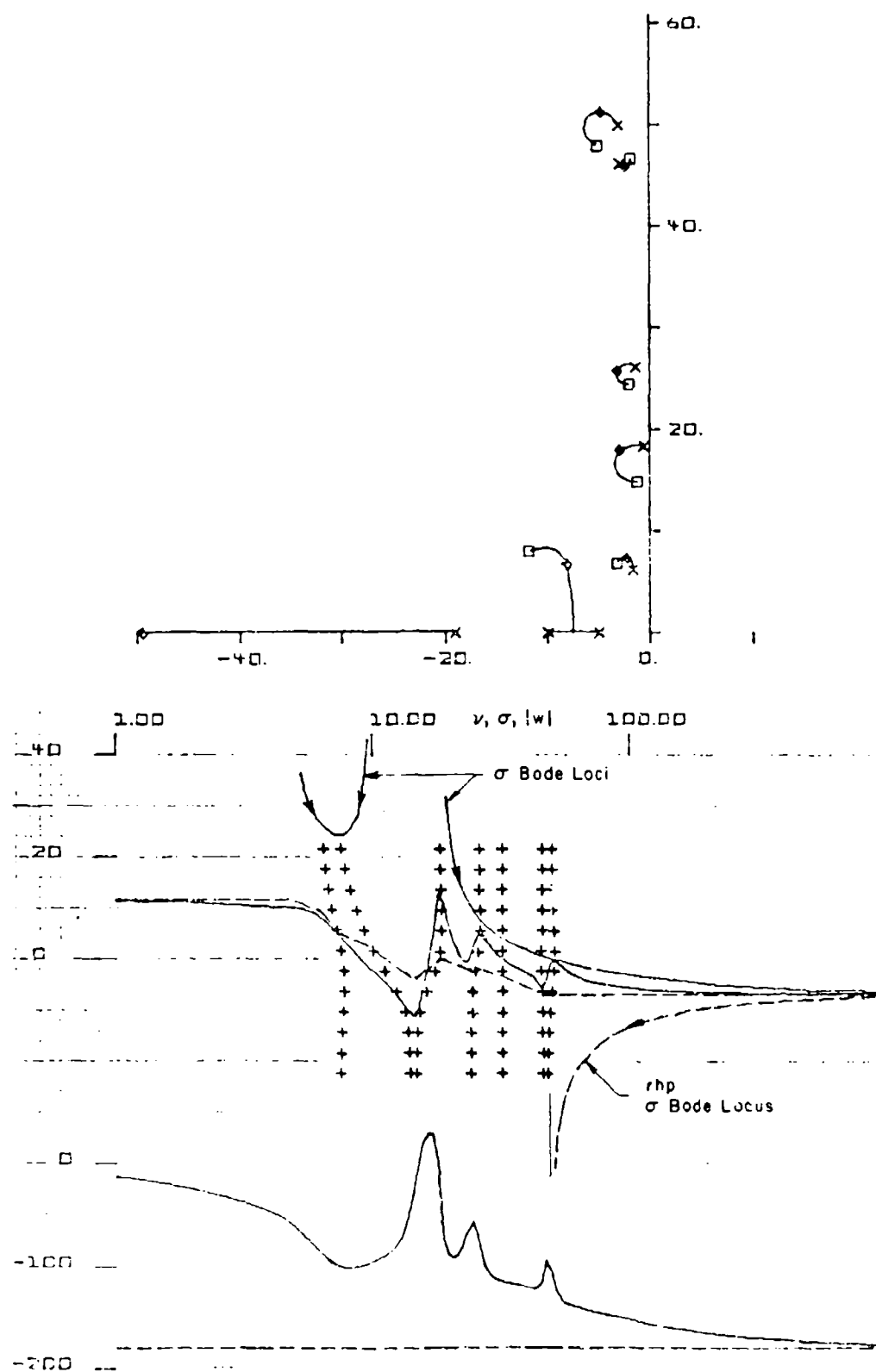
Figure 31. System Survey for Digital Flexible
Aircraft Control System, √/T = 25 Hz

73
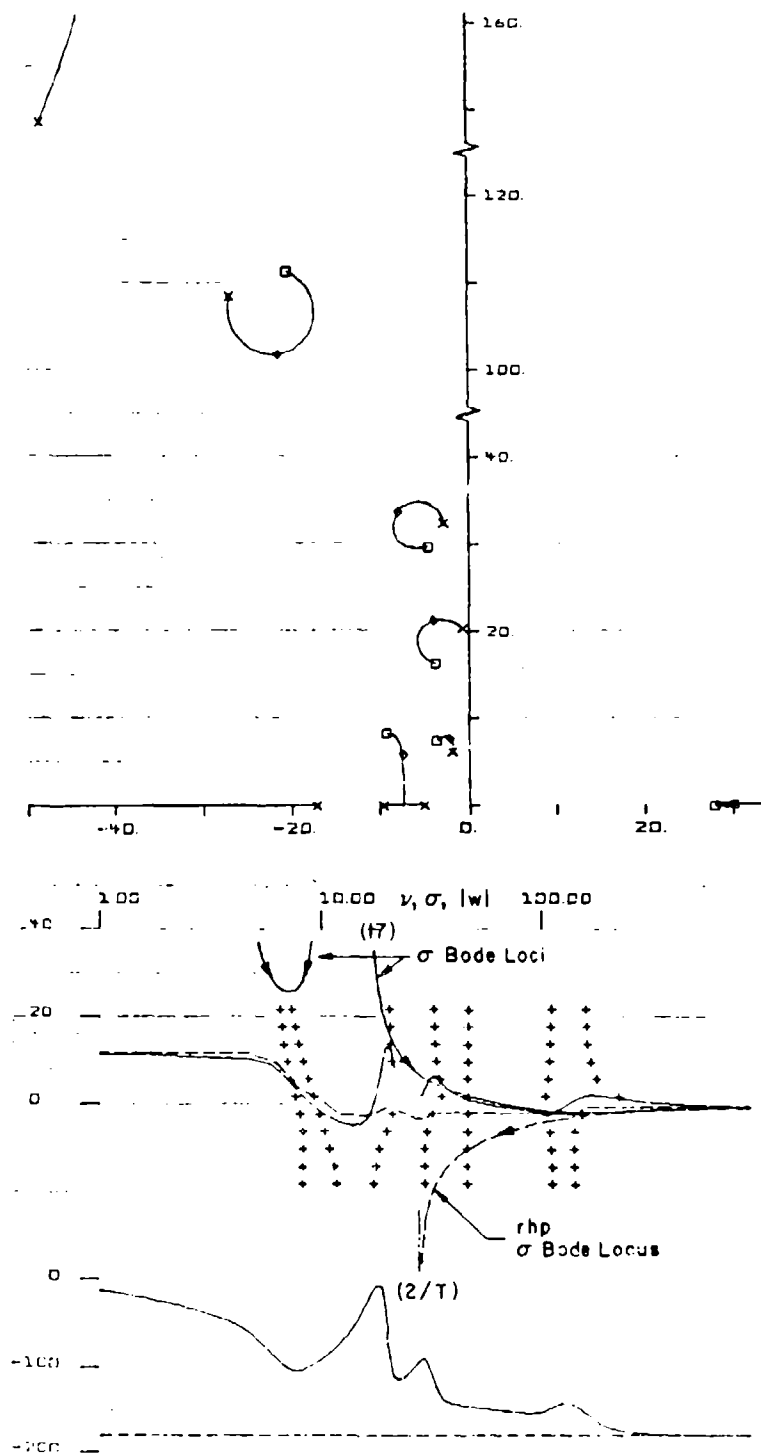
Figure 32. System Survey for Digital Flexible
Aircraft Control System, 1/T = 14 Hz

The conventional root loci for the two lower sampling frequencies also illustrate the marked shifts in w-plane location as sampling rate is reduced. Not only are the "natural frequencies" increased, but the apparent attainable "damping ratios" are also. These appearances are not "real" in terms of the time domain, but occur because of the w-plane distortion when contrasted with the s-plane.

Examination of the real portion of the Bode root locus of Fig. 32 shows the real root starting at $w = -17$ sec^{-1} (the value of the w-plane root which, in this case, corresponds to the s-plane real axis root at -20 1/sec in Fig. 24) is driven to infinity, and then around the Riemann surface to plunge into the sampling zero at $2/T = 28$ sec^{-1}. The system at nominal gain is thus unstable, due to this feature. The instability is caused by the sampling zero being reduced to the point that the high frequency asymptote coincides with the zero dB line. This is very easy to see, and track, on the Bode root locus presentations. In fact, the "gain margins" throughout the system surveys can be assessed directly by the distance between the zero dB line and the high frequency horizontal asymptote.

The instability for nominal system gain is also readily found using z-transform analysis. It is, however, more difficult to interpret than the w-domain results. The z-transform root locus for the $1/T = 14$ Hz condition is given in Fig. 33. The poles and zeros in this domain are, of course, extremely distorted when compared with the s- or w-domains. With considerable effort they can be identified and traced as sampling rates are changed, but very little insight is available as to what is crucial. Figure 33 is a good example. There it is seen that many of the poles and zeros are relatively close to the unit circle, with little to indicate that the pole originally at -20 sec^{-1} in the continuous system is the one that ultimately goes unstable first. The degree of stability, and hence any estimates of robustness, are difficult to appreciate in this format as well.

Figure 3?   z-Transform Root Locus for $1/T = 14$ Hz

76

2. Hybrid Frequency Response of Flexible Vehicle Digital Controller for Various Sample Rates

The digitally controlled system will now be considered using the so-called Hybrid Frequency Response. As reviewed in Section II, the hybrid or "generalized frequency response" gives all of the output components for a sine wave input as values on a frequency response plot of amplitude ratio and phase. In a continuous system the frequency response is interpreted as the output/input amplitude ratio and phase at a specific frequency which is the same in both the input and the output. Thus, a particular sine wave input gives rise to a similar sine wave output at the same frequency. When applied to the discrete system the amplitude ratio and phase curves in the generalized frequency response appear somewhat similar at low frequencies (well below the sampling frequency) but markedly different at high frequencies. The interpretation of the frequency response is also somewhat different in that a particular sine wave input begets an infinity of output components. The first is at the same frequency as the input. The rest are at an infinity of sum and difference frequencies involving integers (n = 1, 2, 3 ...) times the sampling frequency plus the input frequency and n times the sampling frequency minus the input frequency. As exemplified by Fig. 8 all of these points, for a given frequency input, can also be seen in the generalized frequency response. Then, when computing the actual output response to a sinusoidal input, all of the higher frequency terms must be included along with the fundamental. Because of the sum and difference rather than harmonic character of the modulation products, the output wave is, in general, not periodic. An important feature of the hybrid frequency response, and of the method reported in Refs. 3 and 4, is that it is applicable to both single and multiple rate sampled-data systems. Since the w- and z-transform methods do not directly apply to the multiple rate situation, the hybrid frequency response becomes a primary tool for these situations.

In the following discussion the hybrid frequency responses for the flexible mode FCS will be considered for a number of sampling rates. As a practical matter only the higher rates are likely candidates for the

77

actual flight control system. The other rates considered are, however, instructive and thought-provoking when simulations using a "digital airplane" are considered. In these cases some of the phenomena introduced by the artificial digitization of the aircraft equations of motion will be similar to the characteristics shown for the lower sampling rates for the controller.

To establish a basis for comparison the closed-loop frequency response functions for the continuous system are given in Fig. 34. The acceleration and pitching velocity at the pilot station and the wing root bending moment are the frequency response functions represented. Figure 35 shows the same responses for a sample period of 0.01 sec corresponding to 100 Hz sampling frequency. The two figures show essentially identical characteristics up to approximately 100 rad/sec. At and above this frequency the effect of the small incremental phase lag, $\Delta\phi$, due to sampling, i.e., $\omega T/2$, becomes apparent in the phase for the sampled system. Then at $\omega = 628$ rad/sec $(2\pi/0.01)$ the first distinctive notch due to sampling occurs.

Figure 36 shows the same responses for a 50 Hz sample rate. The trends are similar to those for the 100 Hz case at frequencies below about 100 rad/sec, although the incremental phase is twice as large because the sampling frequency is just half that of the previous case. The first notch due to sampling appears at 314 rad/sec $(2\pi/0.02)$. The second notch appears at 628 rad/sec, and a third at 942 rad/sec. But the important thing is that the low frequency system characteristics (below 100 rad/sec) are nearly identical to those of the 100 Hz sampled and the continuous system except for the small phase shift traceable to the sample and hold operations.

For a sample rate of 25 Hz (Fig. 37) the frequency range over which the continuous and sampled system responses are very close, except for the additional phase lag, is reduced to about 70 rad/sec. The sampling notches now occur at values of 157 n rad/sec $(2\pi n/0.04)$, n = 1, 2, 3, ... Also, the higher frequency flexible modes are beginning to have their impact on the frequency response amplitude just prior to the first notch. This is seen on all three response functions but is perhaps most

78
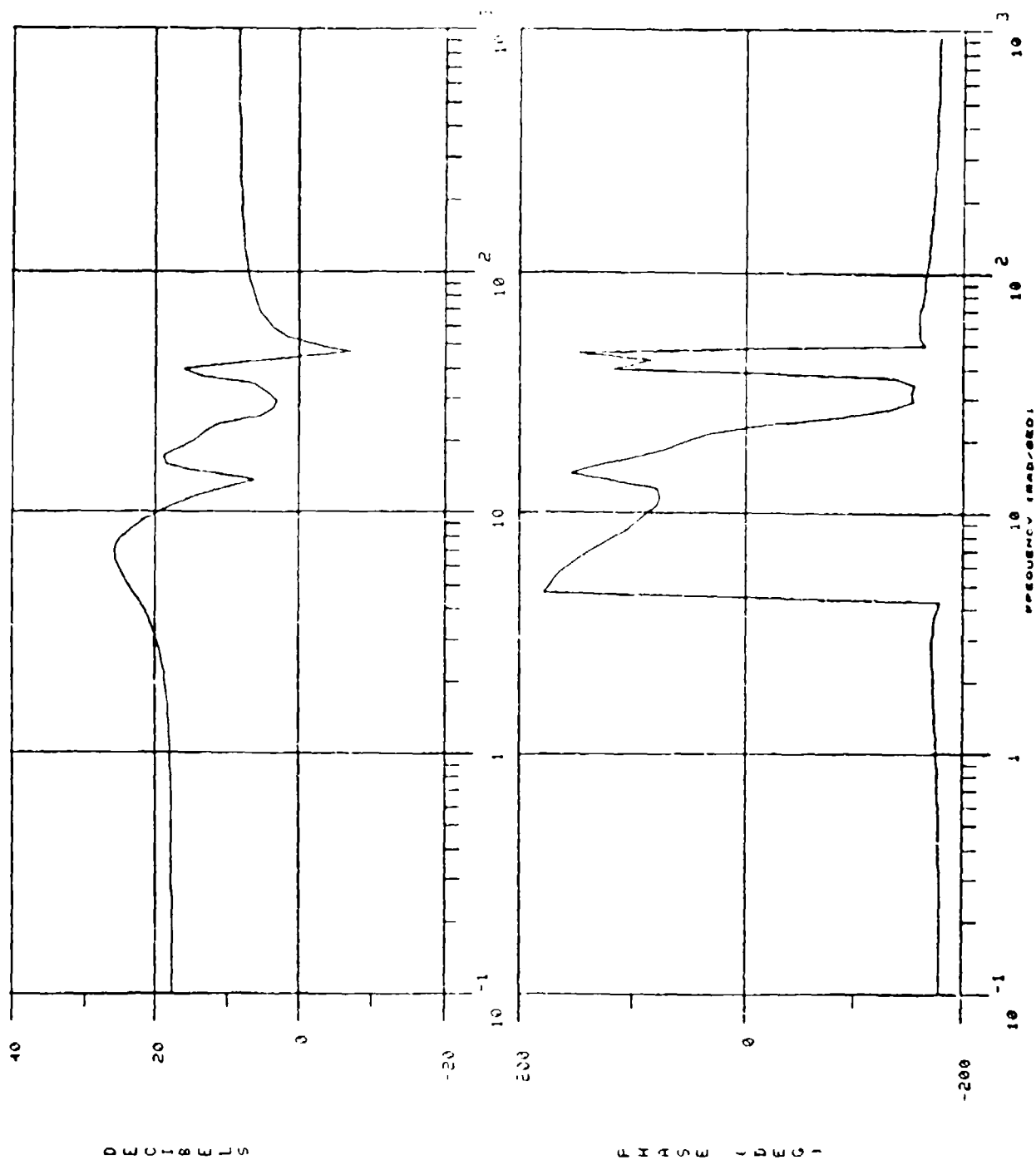
Figure 34. Closed-Loop Frequency Response for Continuous System

a) $\sigma_{n_p}/\delta_{e_c}$

79

b) q_p/δ_{e_c} (Continued)

Figure 34.

80
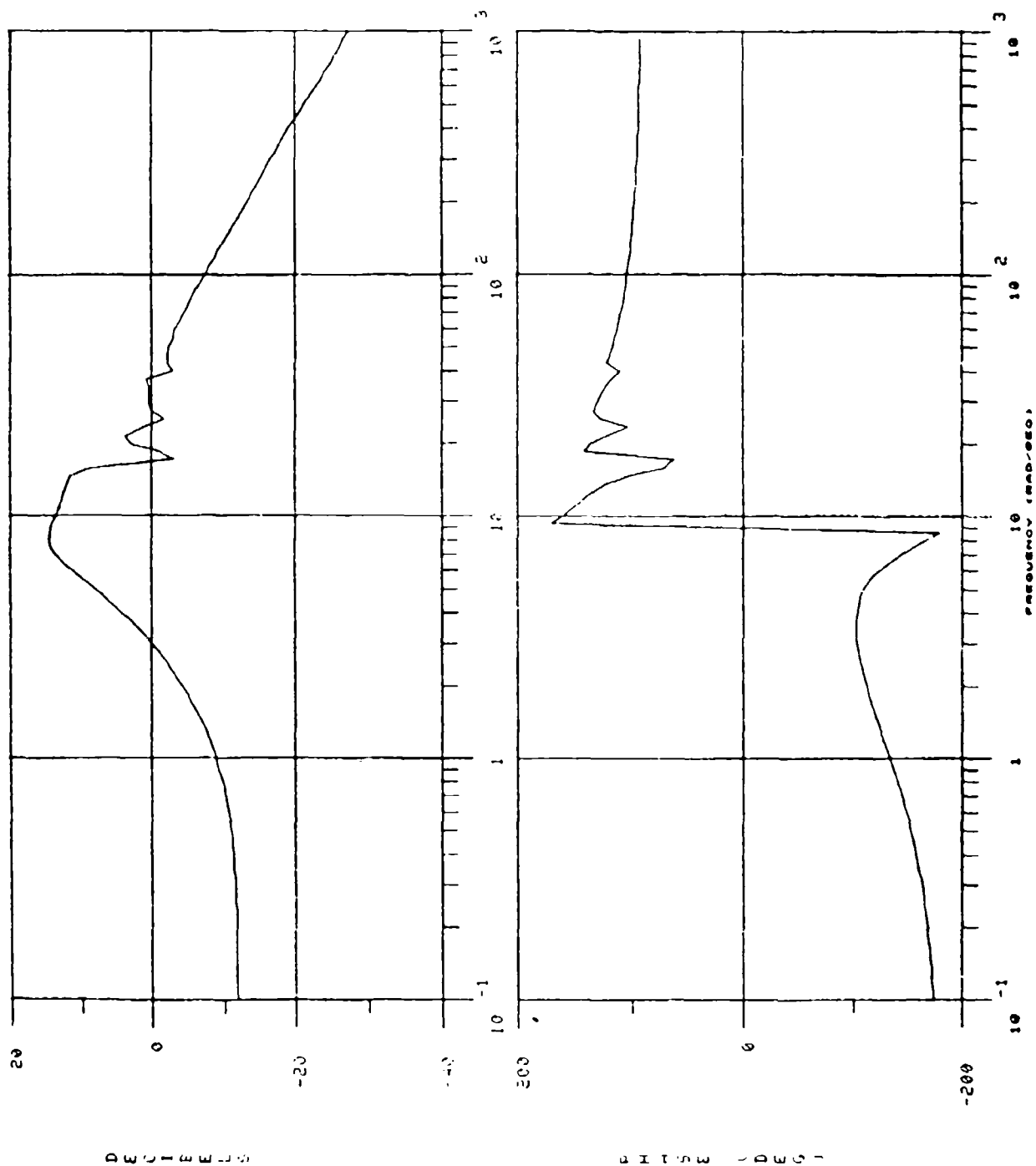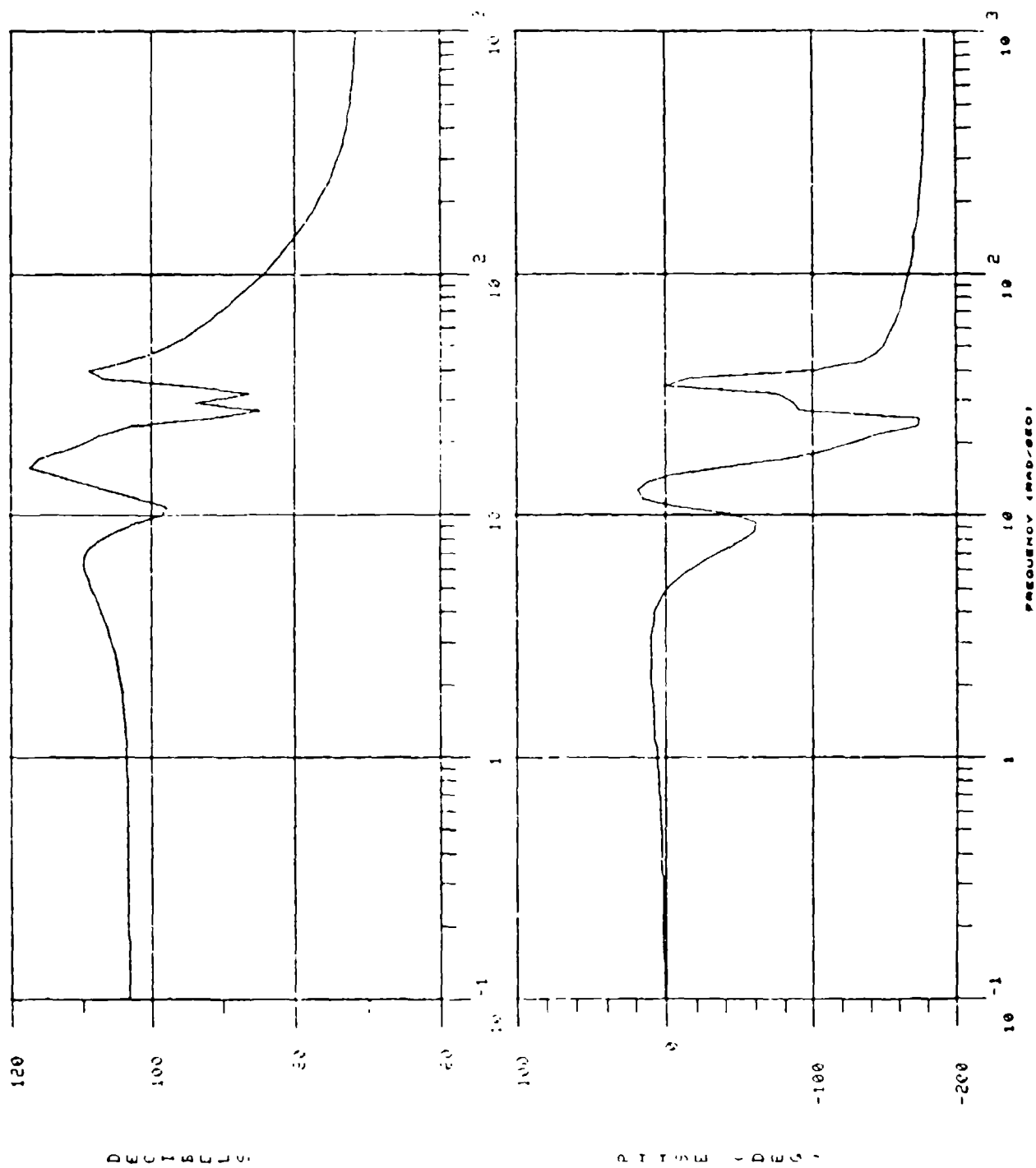
c) M_{BW}/δ_{e_c}

Figure 34. (Concluded)

81
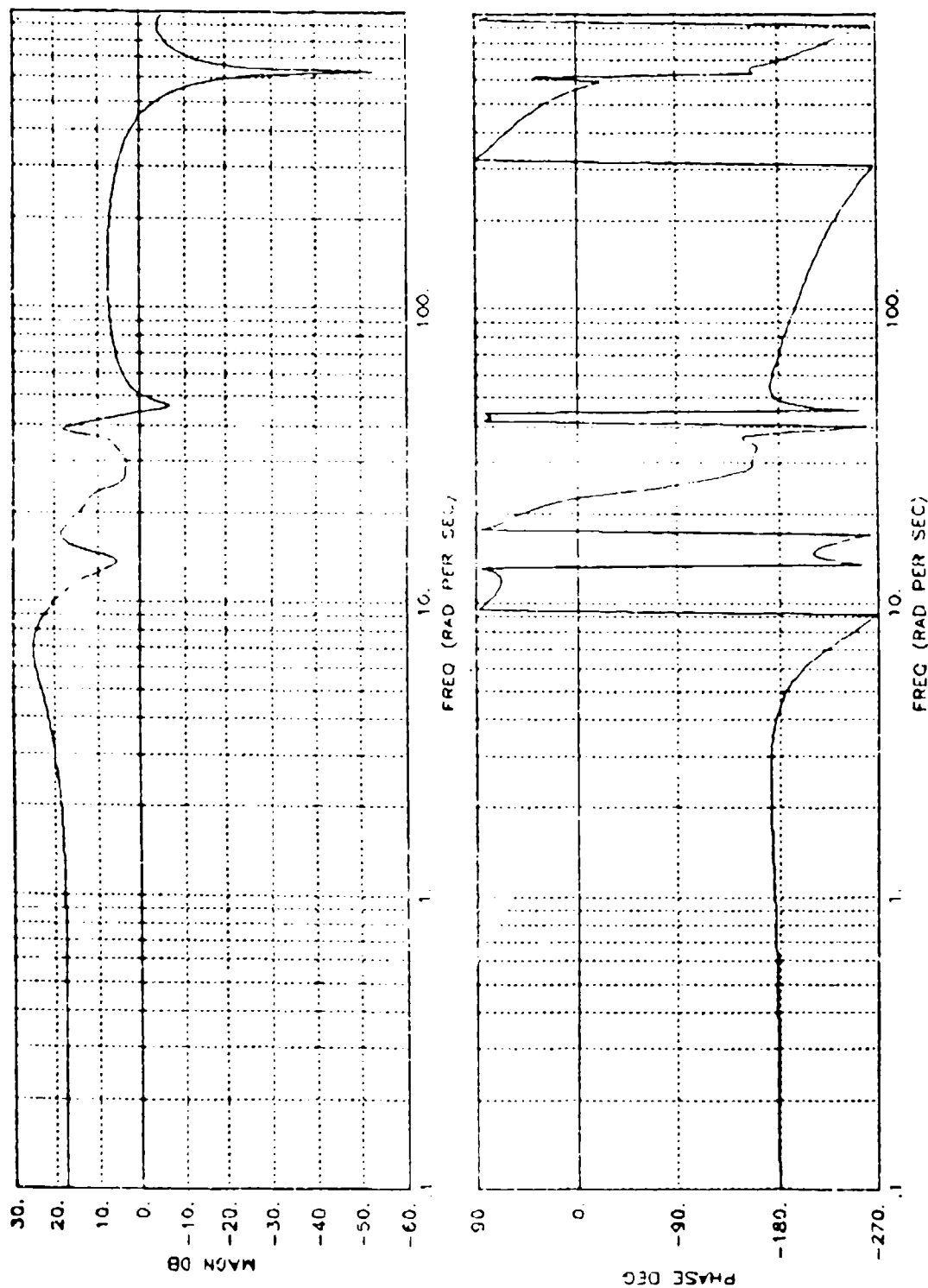
Figure 35. Closed-Loop Generalized Frequency Response Functions for Discrete System, 1/T = 100 Hz

a) σ_{np}/δ_{ec}

82
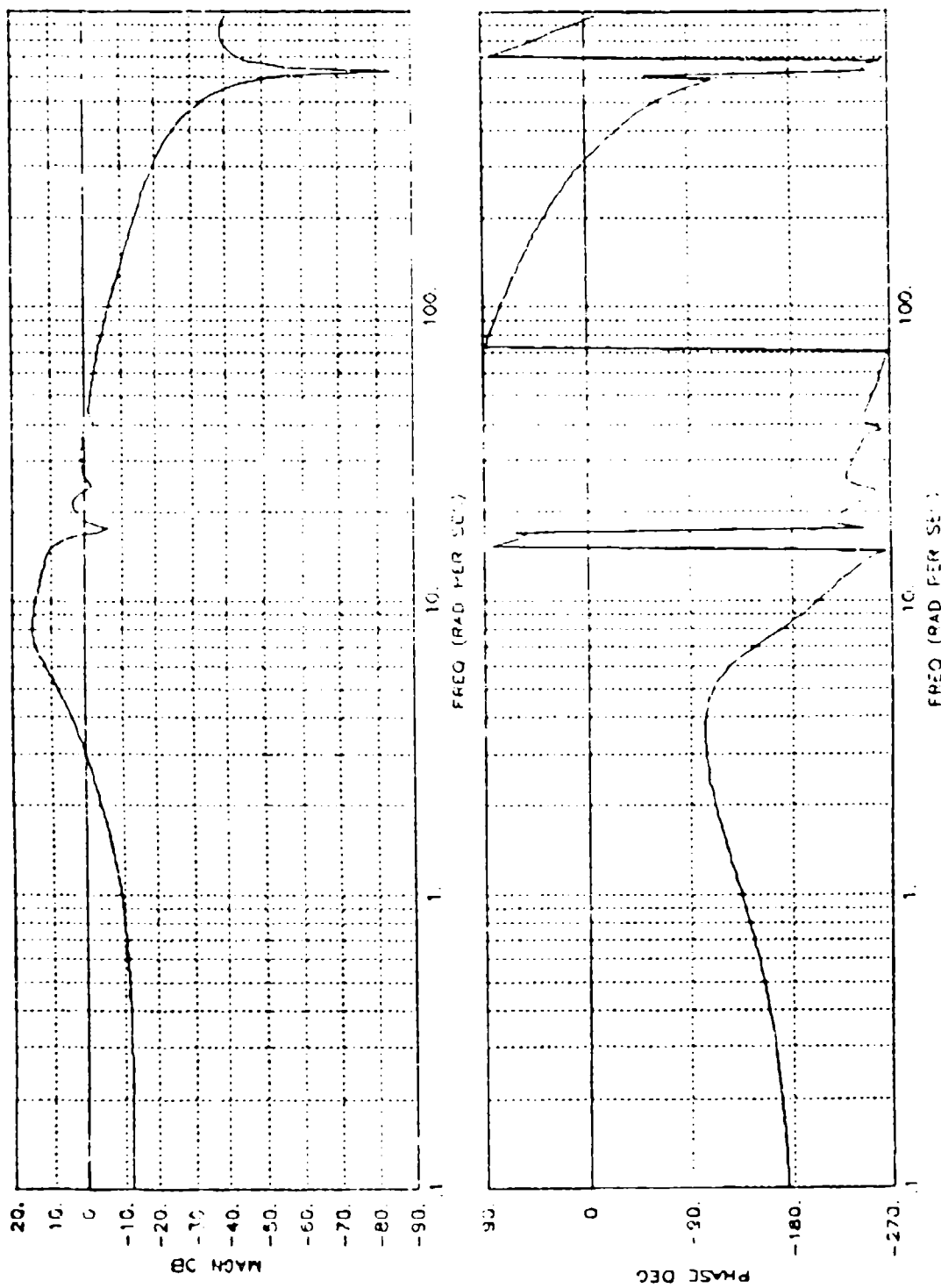
b) q_p / δ_{e_c}

Figure 35. (Continued)

83
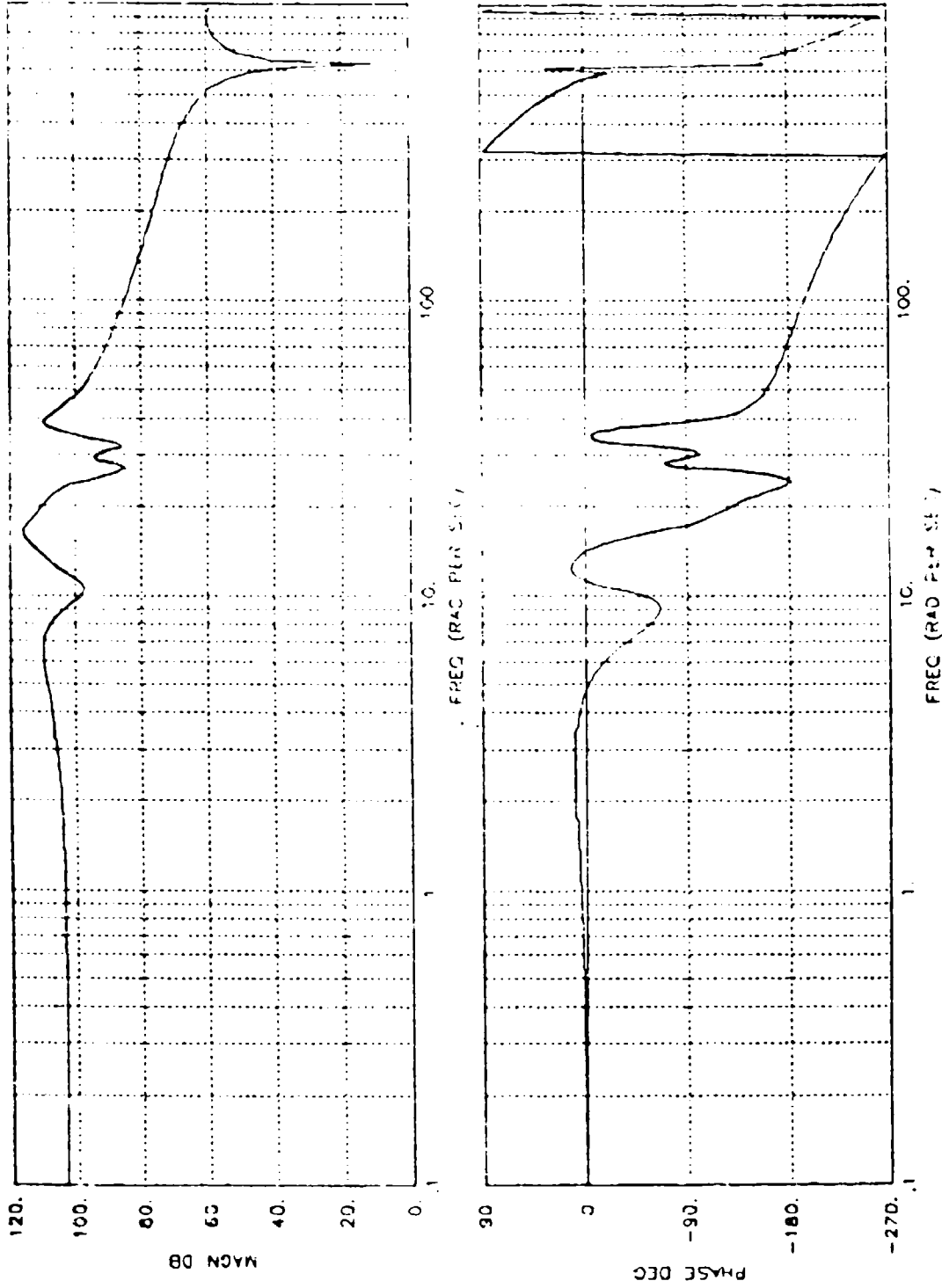
c) M_{BW}/δ_{e_c}

Figure 35. (Concluded)
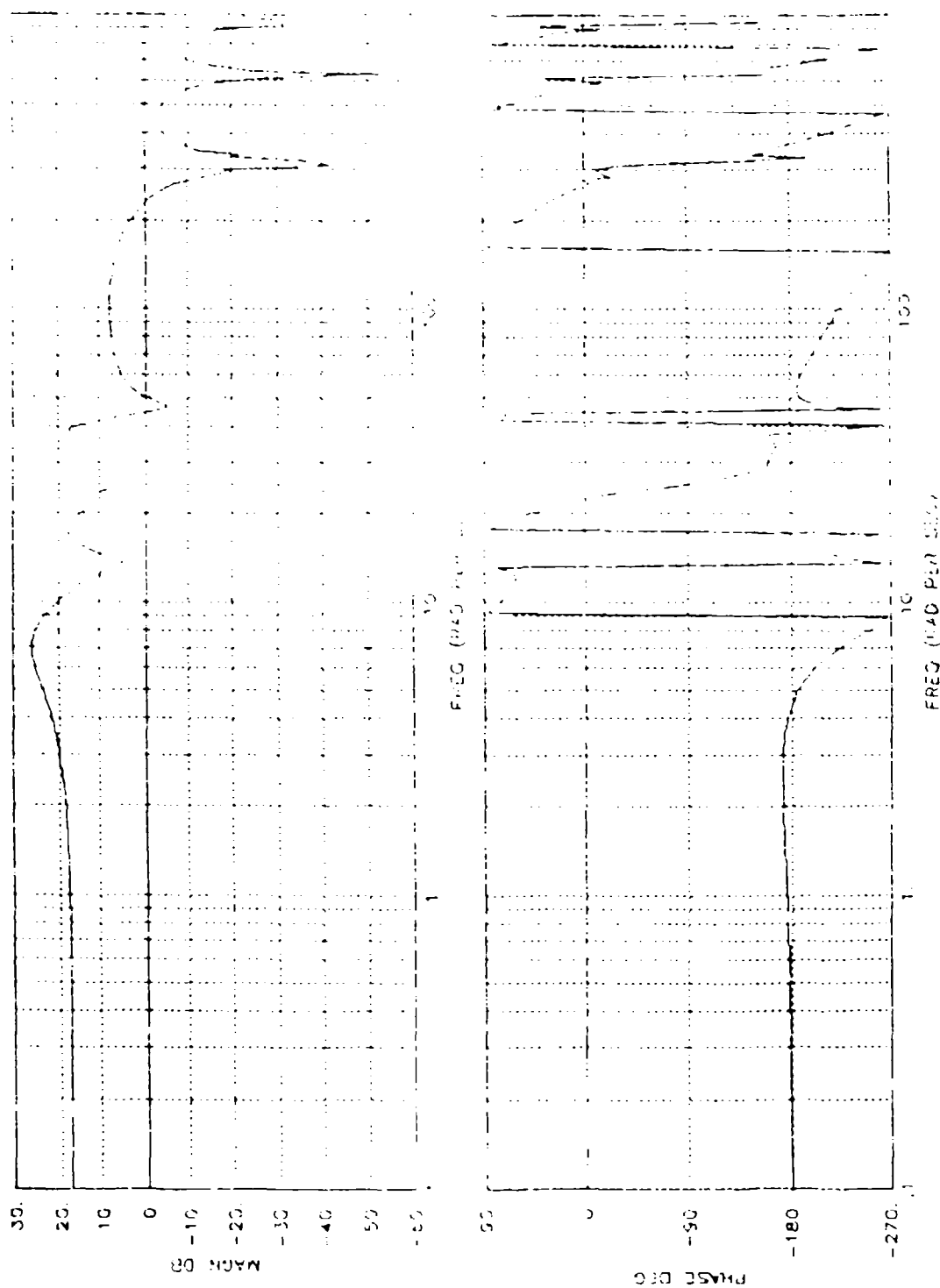
Figure 36. Closed-Loop Generalized Frequency Response Functions for Discrete System, 1/T = 50 Hz

a) a_{n_p} / δ_{e_c}
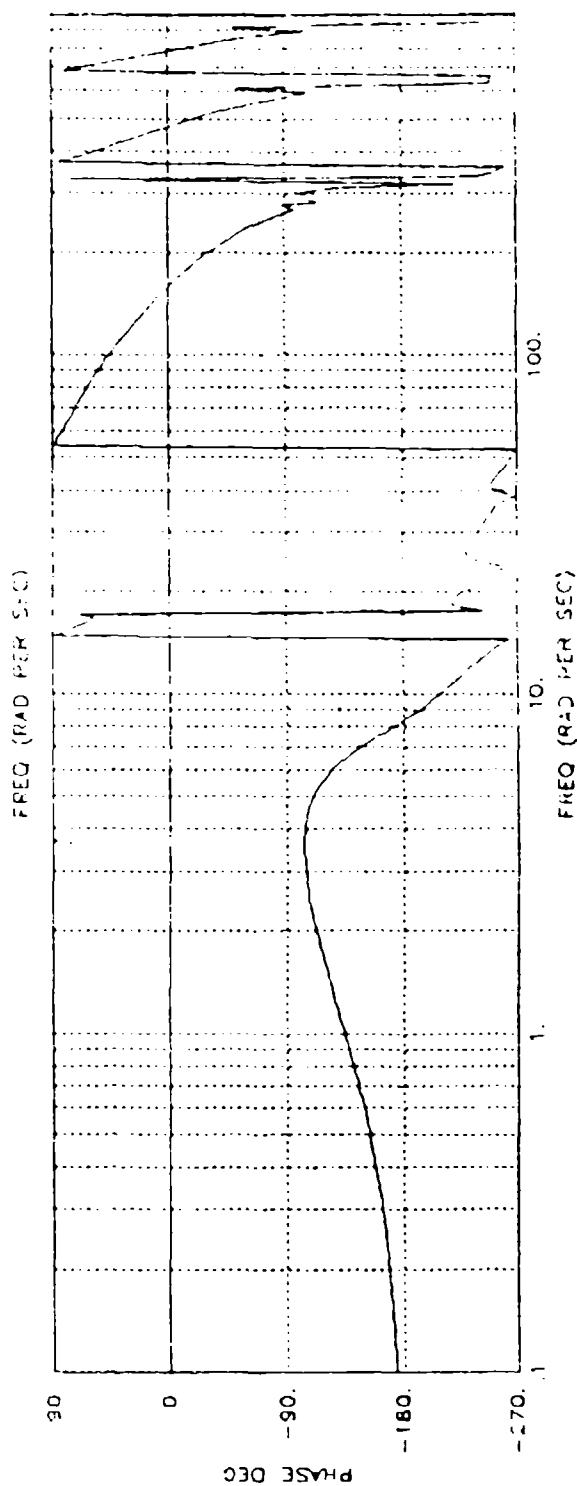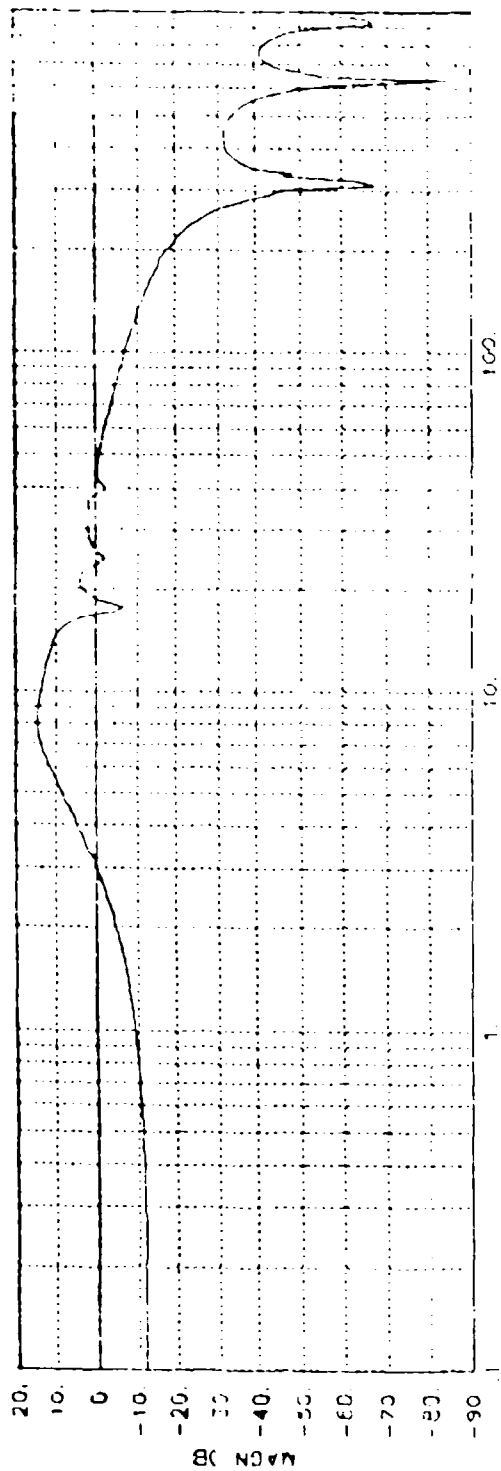
b) q_p / δ_{ec}

Figure 36. (Continued)

86

c) $M_{BW}/\delta e_c$

Figure 36. (Concluded)

87
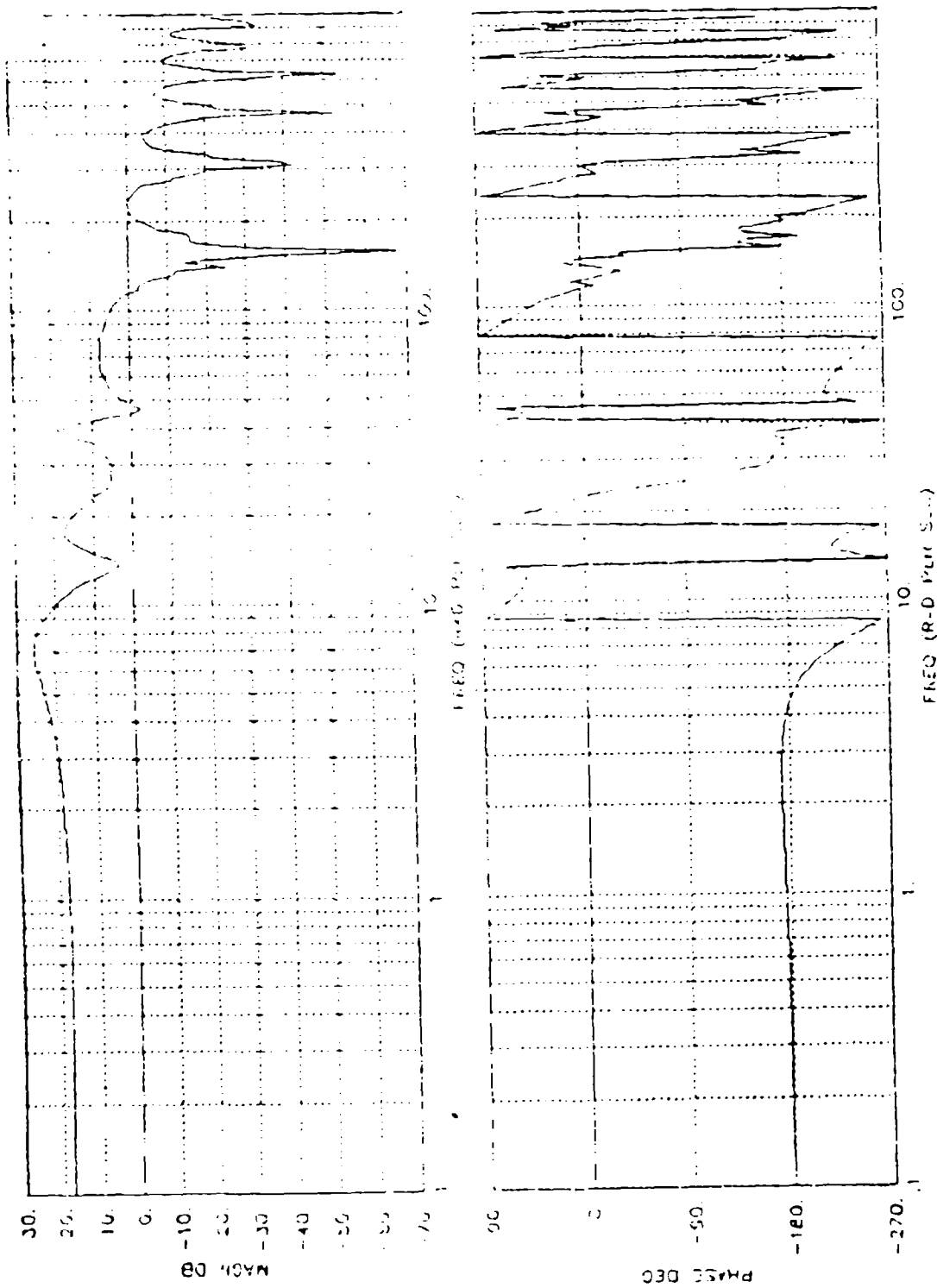
Figure 37. Closed-Loop Generalized Frequency Response Functions for Discrete System, $1/T = 25$ Hz
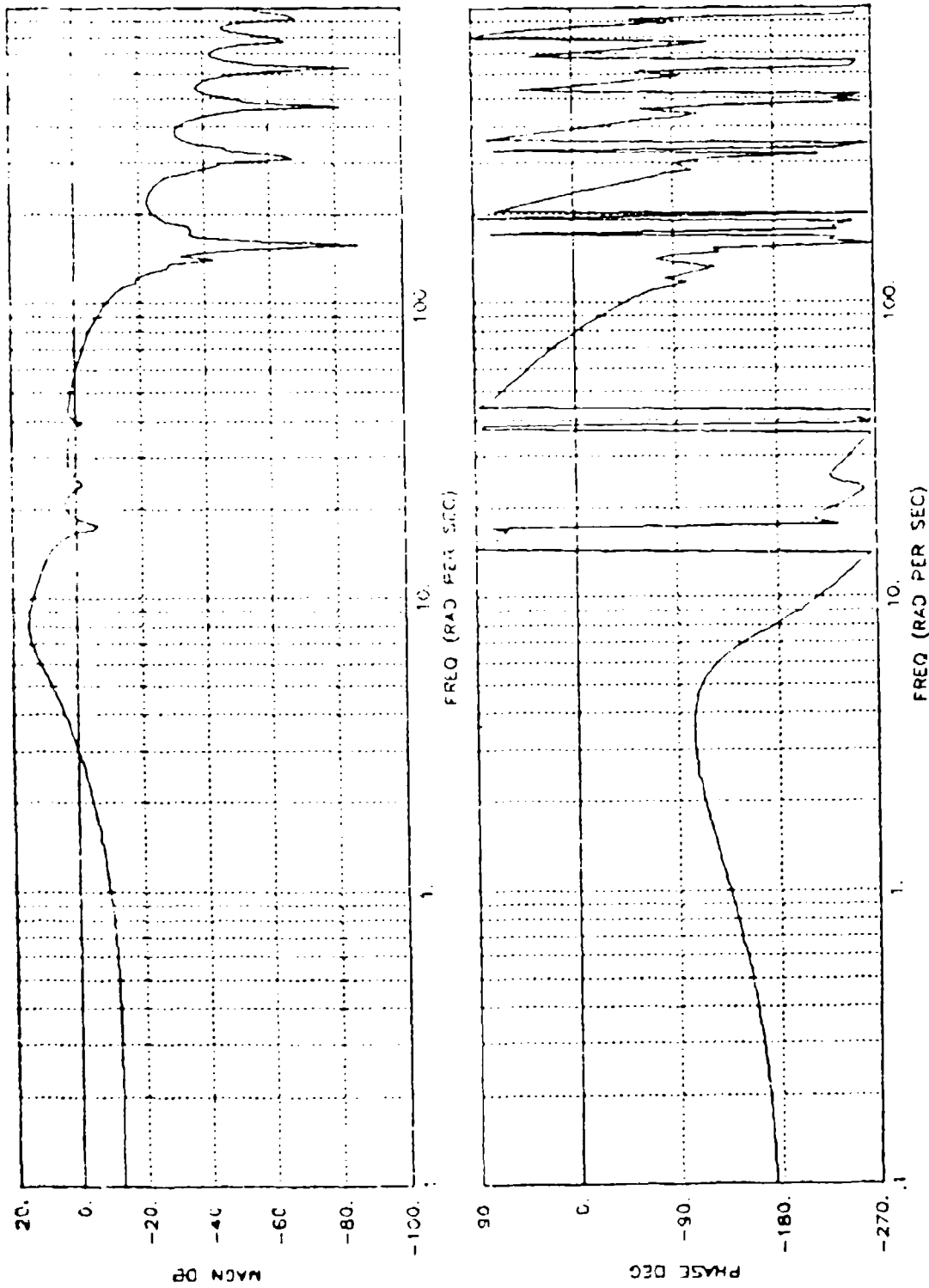
a) $\sigma_{n_p}/\delta_{e_c}$

b) q_p/δ_{ec}

Figure 37. (Continued)

89
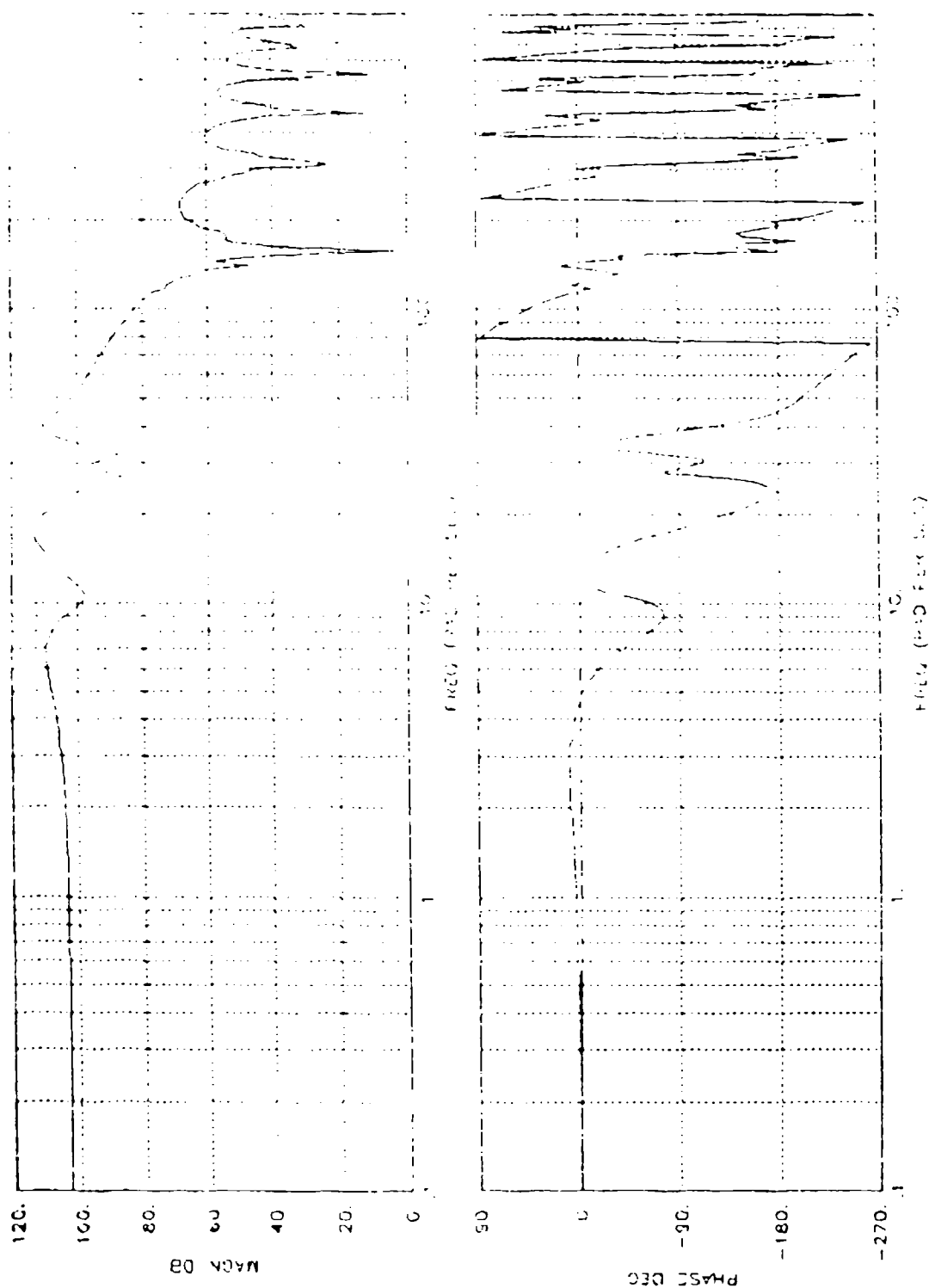
c) M_{bw}/δ_{cc}

Figure 37. (Concluded)

90

noticeable for a_{np}/δ_{ec}. The difference frequency involving wing bending is the most prominent at approximately 140 rad/sec ($2\pi/0.04 - 18$). The effects of the flexible modes (ω_s + modal frequencies) are also beginning to show up on the high frequency side of the first notch especially. Nonetheless, the system is still effective in the basic task of flexible mode and short period control with this sampling rate.

In the w- and z-domain study of the closed-loop system it was found that the system will go unstable for a sampling frequency between 13 and 14 Hz. Thus, the most extreme changes in the generalized frequency response that can be observed in this stable system will occur for a discrete system where $1/T$ = 14 Hz (0.0714 sec). The closed-loop frequency responses are illustrated in Fig. 38. The sampling notch at 88 rad/sec and its successors at 176, 263,... rad/sec all show up well. The short period and the first two flexible modes are still essentially uneffected by the sampling, but the high frequency characteristics from about 35 rad/sec on up are very dramatically affected. The most important effect is the neutral stability of the highest frequency flexible mode at about 40 rad/sec. The frequency response between there and the first notch also exhibits a number of the difference frequencies between the sampling and the several modes. The amplitude ratios on the high side of the 40 rad/sec mode and on either side of the sampling notches as well, reflect the $n\omega_s$ and flexible mode sum and difference characteristics.

3. Response Characteristics for Sinusoidal Inputs

A very graphic way to show the effects of the modulation products, is to examine sample outputs derived from the generalized frequency response functions. These are illustrated in Fig. 39 which shows the bending moment response to a 5 Hz sinusoidal input applied at the pilot command point. Figures 39a and 39b, for 100 Hz and 50 Hz sampling rates respectively, show outputs that are essentially sinusoidal. Low frequency lags due to the zero-order hold sample data for these two responses would only be 0.005 and 0.01 seconds, and could hardly be read

91
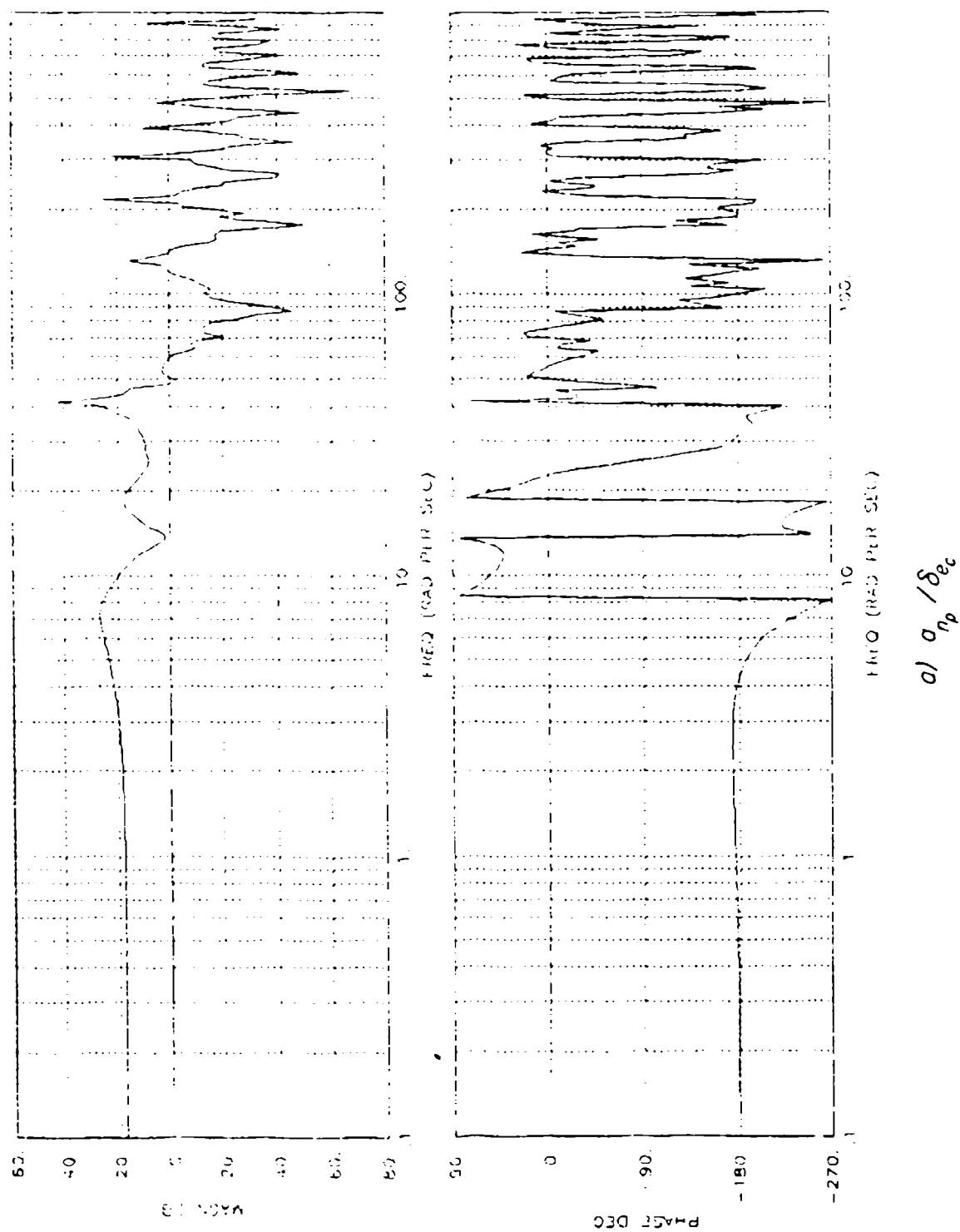
Figure 38. Closed-Loop Generalized Frequency Response Function for Discrete System, $1/T = 14$ Hz

a) a_{np}/δ_{ec}

92

b) q_p / δ_{e_c}
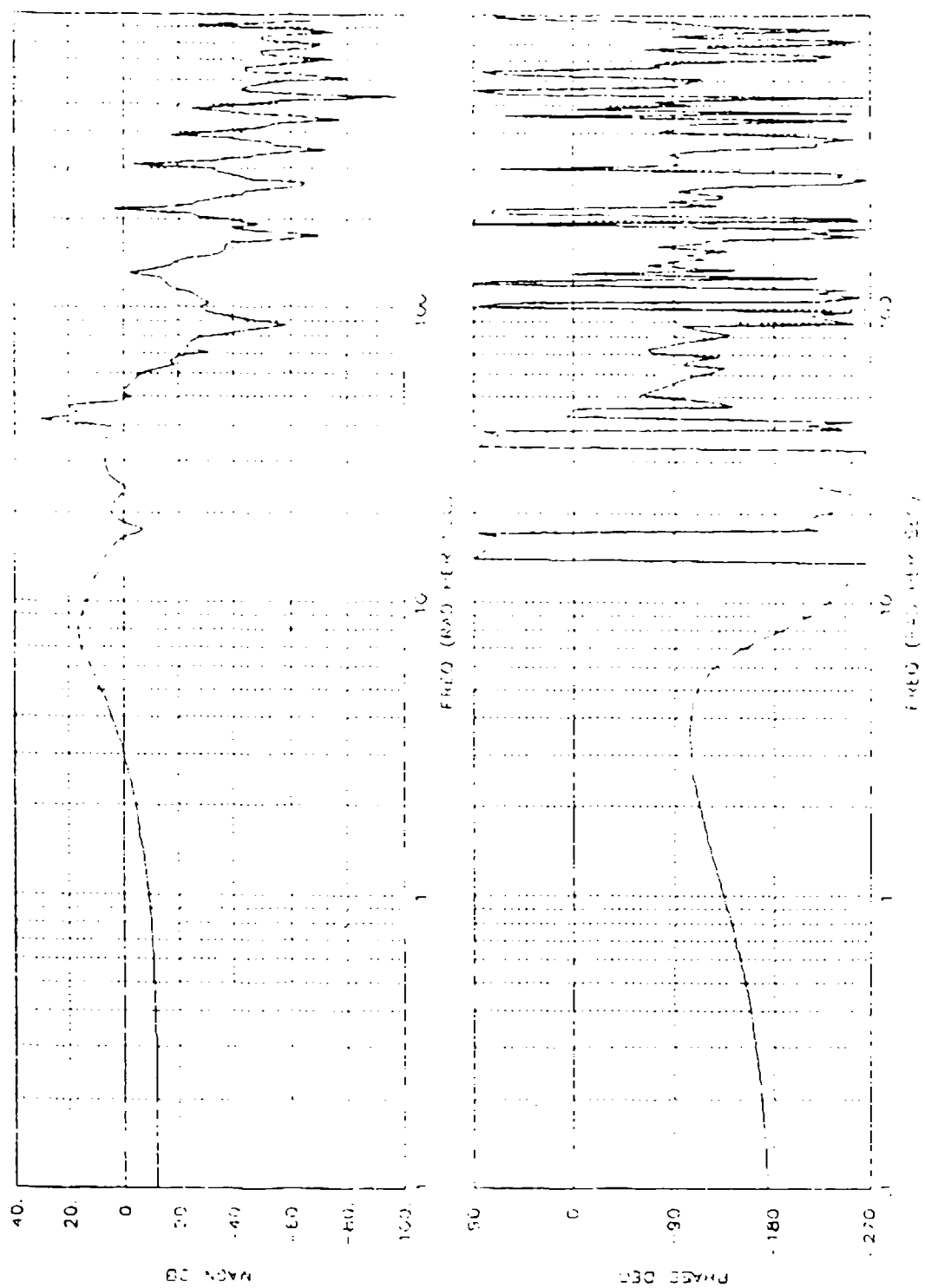
Figure 38. (Continued)

93
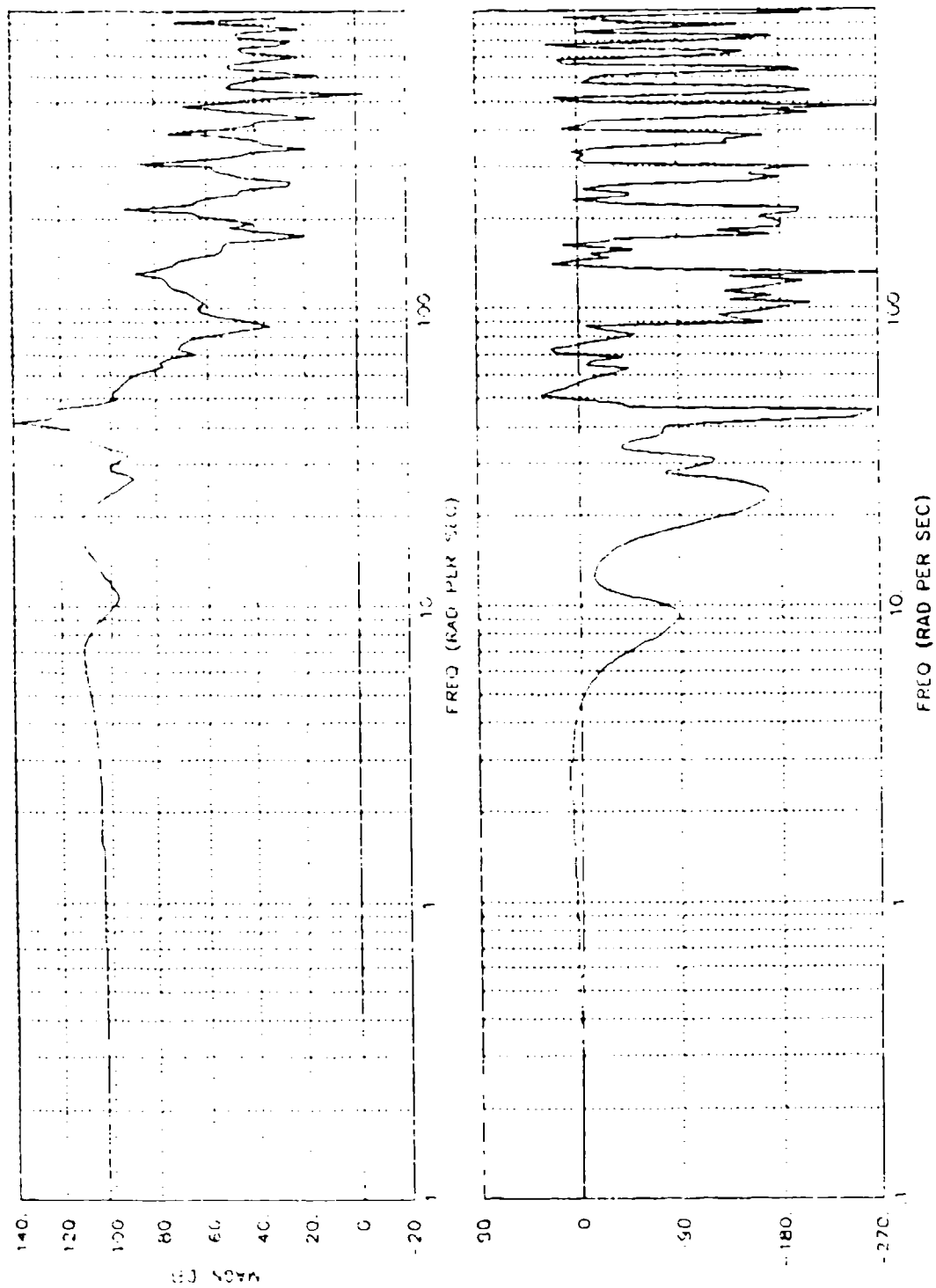
c) M_{BW}/δ_{e_c}

Figure 38. (Concluded)
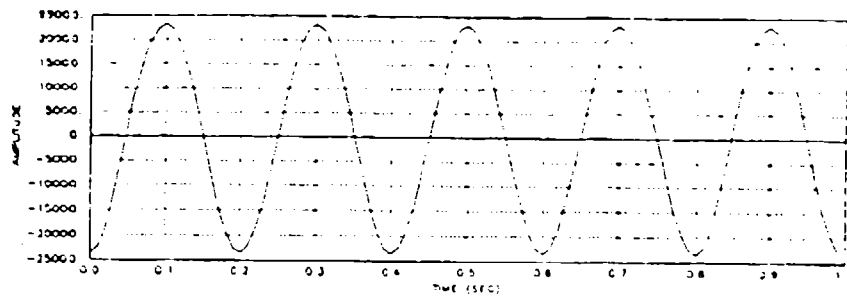
a) 1/T = 100 Hz
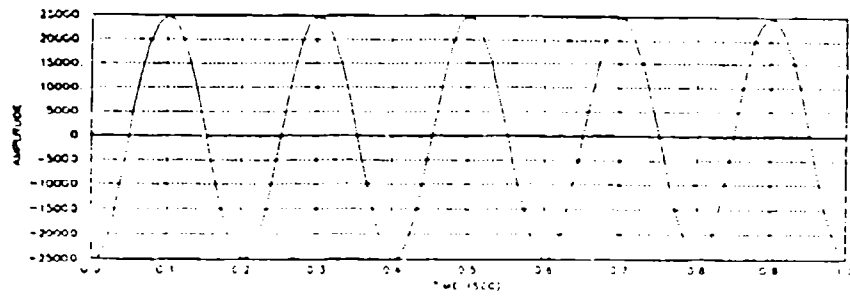
b) 1/T = 50 Hz
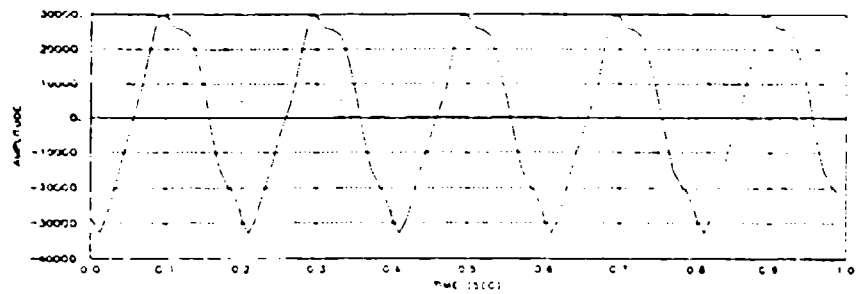
c) 1/T = 25 Hz
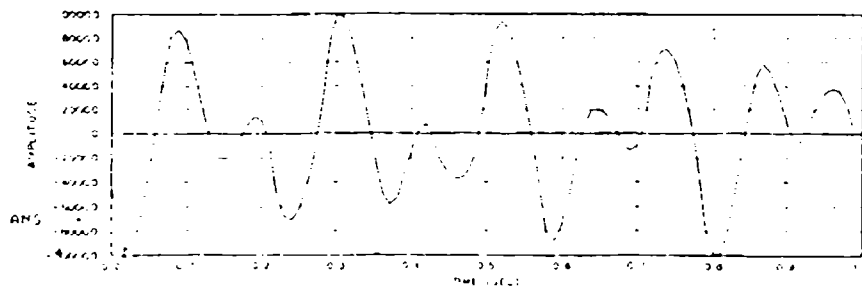
d) 1/T = 12 Hz

Figure 39. Bending Moment, M_{B_w}, Response to a 5 Hz
(31.4 rad/sec) Sinusoidal δ_{e_c} Input

95

on the scale. For the 25 Hz sampling rate, however, (Fig. 39c) the output waveform is quite distorted and the delay is easily seen. Finally, for the lowest sampling frequency for which stability is just barely retained (1/T = 14 Hz) the output waveform is asymmetric and, indeed, is non-periodic. The amplitude ratios of Fig. 38 for 5 Hz (31.4 rad/sec) are not too different from those for higher sampling frequencies, so the extraordinarily distorted waveform shown in Fig. 39d is a dramatic demonstration of the extreme response distortion due to the high frequency power in the modulation products.

Because the sampling rate for instability (approximately 14 Hz, 88 rad/sec) is relatively high compared to the flexible modes (symmetric wing bending at 2.9 Hz, 18.2 rad/sec and symmetric wing torsion at 3.6 Hz, 22.6 rad/sec), actually being controlled, the sum-difference effects illustrated in Section III are not as apparent for this aircraft example. However, the modulation products for a 5 Hz input are quite important at 1/T = 25 Hz, (e.g., Fig. 39c), and the Mode 5 impact on the hybrid frequency response is an important effect for 1/T = 14 Hz. Thus the phenomena illustrated in Section III have their parallels for the practical example presented here. The differences that exist are more in degree than in kind.

SECTION V

SOME COMPARISONS WITH OPTIMAL CONTROL RESULTS
AND A NEW OPTIMAL CONTROL APPROACH FOR FLEXIBLE VEHICLE CONTROL

A. INTRODUCTION

The selection of the Ref. 9 flexible aircraft data for our continuous and discrete controller examples also provides an unusual opportunity to compare the results of conventional and optimal design approaches. The primary purpose of Ref. 9 was to demonstrate a method for applying linear optimal control theory to the design of a regulator for flexible aircraft. Several optimal and suboptimal controllers were developed and presented. It will be instructive to compare certain of these results with the continuous controller version of the system synthesis presented here. This comparison will be made in the next subsection.

When optimal control procedures are applied routinely (without special care and consideration) to the flexible aircraft control problem the resulting systems are quite complex in that feedbacks are required from all of the states to all of the control points. As will also be seen below for the flexible aircraft control case these complicated systems do not compare favorably with the far simpler conventional system. This result is not unusual as far as flexible mode control is concerned. In fact a survey of the literature indicates that attempts to apply optimal control procedures in a direct, straightforward, and routine way to the control of flexible modes do not fare well in general. Typically the controllers synthesized involve feedbacks of all states to all control points and often the controller is unusually sensitive and requires a high degree of calibration to precisely known characteristics. Some of the reasons for these features are explored in the second subsection using an approximation to a flexible beam as an example. Some of the deficiencies introduced by routine application of optimal control procedures are then rectified by introducing additional, none routine, considerations. For instance, we show that it is possible to construct a

97

performance index (cost function) which will result in a sawtooth Bode type controller as a consequence of an optimal control design exercise. As might be expected, the performance index is unusual. However, because optimal control procedures are so computationally efficient, the ability to synthesize a sawtooth-Bode-like controller with optimal techniques offers a potentially fruitful new direction for such systems.

B. COMPARISON OF CONVENTIONAL AND OPTIMAL CONTROLLER RESULTS FOR THE FLEXIBLE AIRCRAFT CONTROL PROBLEM

Reference 9 develops several optimal and suboptimal controllers which can be compared with the results of the present study. The optimal controllers are all based on the minimization of the cost functional

$$J = \frac{1}{2} \int_0^\infty \left[Q_{a_{n_p}} a_{n_p}^2 + Q_{M_{B_W}} M_{B_W}^2 + R_\delta \left(\delta_e^2 + \delta_f^2 + \delta_a^2 \right) \right] dt \qquad (39)$$

Here $Q_{a_{n_p}}$ and $Q_{M_{B_W}}$ are weightings on the acceleration at the pilot station and on a modified wing bending moment, respectively.

A large number of systems were synthesized on a preliminary basis to explore the effects of different cost combinations. Some of the regulators synthesized had:

    costs attached only to a_{n_p} and the control surface
        deflections, with no attention paid to M_{B_W};

    costs attached only to M_{B_W} and the control surface
        deflections, with no attention paid to a_{n_F};

    costs attached to both a_{n_p} and M_{B_W}, together with the
        control surface deflections.

For these basic criteria variation studies the Ref. 9 optimal systems synthesized used only the short period, wing bending, and wing torsion in the definition of the airplane. This reduction from the twelfth order complete model to the sixth order simplified model was made because "the twelfth is difficult to manage" (presumably from a computational standpoint — which would no longer be a major problem).

98

This truncation of the vehicle dynamics by simply ignoring the high frequency modes was, with the benefit of hindsight, unfortunate. Not only was the controlled element not truncated using residual stiffness concepts (Refs. 11, 12) but the insignificant third and fourth modes could have been eliminated not arbitrarily, but on the basis of their non-controllability and non-observability (as was demonstrated in Section IV). As a practical matter, with the sensors and locations available, the third and fourth modes (inboard store yaw mode and inboard store pitch mode) are insignificant but the fifth (outboard store yaw mode) is significant and ideally should have been retained. In any event the various results achieved in Ref. 9 for the vehicle with three modes do not compare very well with the six mode case for the flexible modes common to both representations.

One of the more interesting developments of Ref. 9 is shown on Fig. 40. This illustrates the effect on the closed-loop modes of the reduced system of varying the performance criterion weighting parameters. The solid-line curves are the result of varying the weighting $Q_{a_{n_p}}$ (with $Q_{M_{B_W}} = 0$) while on the dashed-line curves the weighting factor $Q_{M_{B_W}}$ for the wing root bending moment M_{B_W} varied (with $Q_{a_{n_p}} = 0$). Between $Q_{M_{B_W}} = 5$ and 10 the damping ratio for the short period mode is maximized, while the damping of the wing bending mode is increased monotonically as $Q_{M_{B_W}}$ increases. Thus a weight $Q_{M_{B_W}}$ approximately = 10 should provide benefits to both. As might be expected the variation of $Q_{a_{n_p}}$ directly affects the short period damping. This weighting parameter primarily modulates the gains of the $a_{n_p} \rightarrow \delta_1$ feedbacks. The maximum damping ratio for the wing bending mode, as affected by $Q_{a_{n_p}}$, occurs for a value of 2-3. Based on these secondary effects of weighting parameter variations for the reduced system, a reasonable set of weights for the cost functional might be

$$
\begin{aligned}
Q_{a_{n_p}} &\doteq 3 \\
Q_{M_{B_W}} &\doteq 10 \\
R_\delta &= 0.01
\end{aligned}
\tag{40}
$$
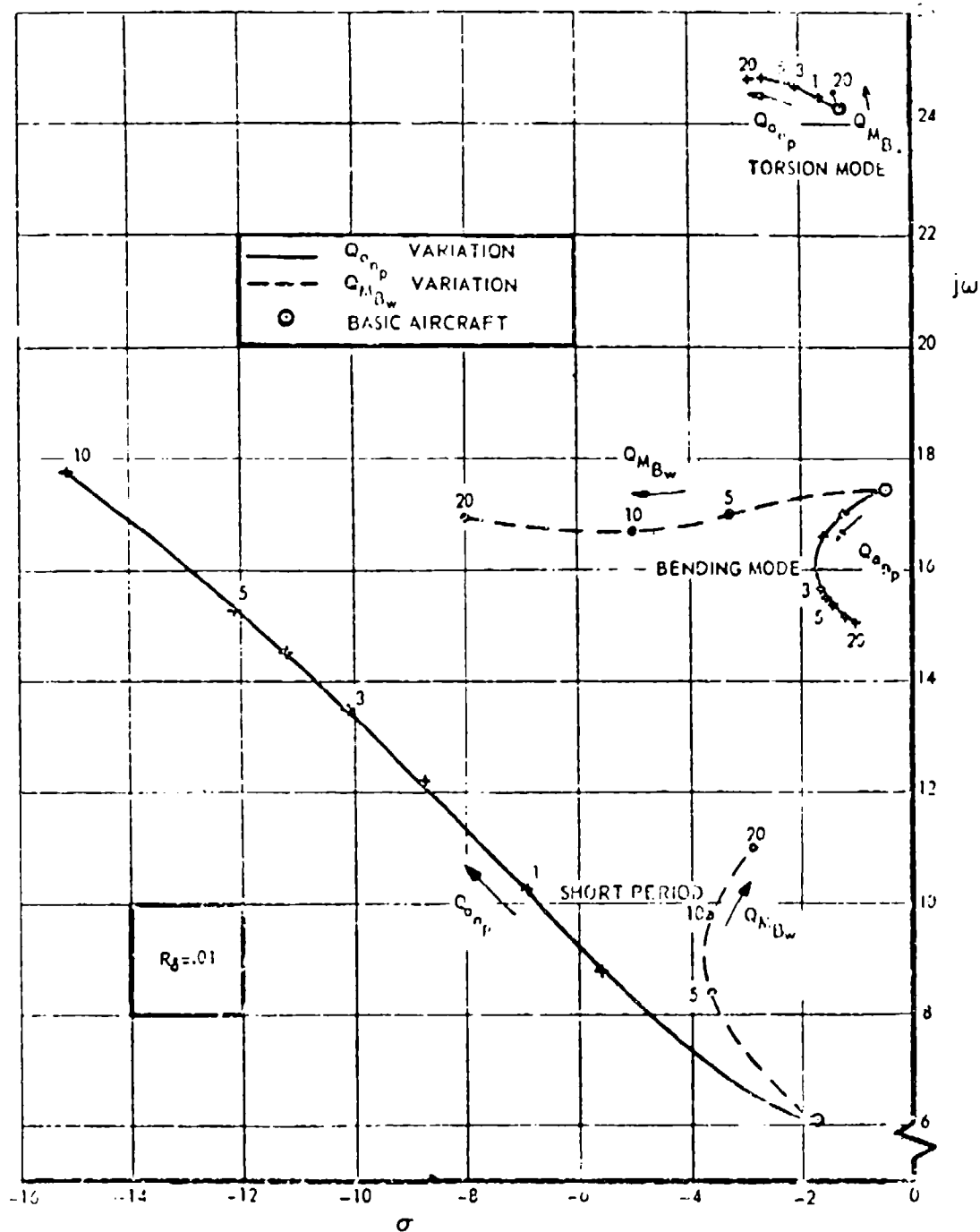
Figure 40. Pole Locations for Varying Weighting Factors of a_{n_p} and M_{B_w} for Reduced Model (Ref. 9)

As noted, these values correspond to near maximum damping ratios in the short period and wing bending modes when the weights are considered as single variations. A weight of $Q_{a_{n_p}} = 3$ (when $Q_{M_{B_W}} = 0$) gives a bending mode characteristic of [0.11, 15.74]. Similarly a weighting of $Q_{M_{B_W}} = 10$ (when $Q_{a_{n_p}} = 0$) gives a short period mode of [0.35, 10.52].

The primary effect of varying $Q_{a_{n_p}}$ is on the short period, where a value of 3 results in a damping ratio of approximately 0.6 when the bending moment weighting factor is zero. Similarly, the bending mode is predominantly dependent upon the weighting $Q_{M_{B_W}}$; a value of 10 improves the damping ratio of first wing bending mode by a factor of four (ζ = 0.027 to ζ = 0.10). The authors of Ref. 9 selected the weights given in Eq. 40 as an appropriate compromise.

Reference 9 also shows the results of a calculation of an optimal controller using all aircraft modes and the weightings based on the reduced aircraft model systems developments. These results are shown as pole locations of the closed-loop aircraft regulator system in Fig. 41. The most profound changes occur with the short period, first symmetrical wing bending, and outboard store yaw modes. First symmetrical wing torsion is barely affected and, as would be expected, neither the inboard store yaw mode nor the inboard store pitch mode are modified at all.

The eigenvalues for the rigid body and flexible modes of the aircraft-alone, aircraft plus optimal regulator, and aircraft plus conventional controller (from Section 4) are given in Table 6. The most dramatic differences between the controllers occur in the short period and first symmetric wing bending modes. For the optimal regulator the short period undamped natural frequency is pushed to a higher value than the first wing bending, leaving some doubt as to which mode should be considered the effective short period. However, neither the closed-loop short period nor the wing bending quadratic characteristics would be satisfactory as far as flying qualities are concerned. For this flight condition the MIL-F-8785C requirements for Level 1 short period characteristics for Category A flight phases would require

$$\zeta_{sp} > 0.35$$

$$3 < \omega_{sp} < 10 \text{ radians per second}$$

(41)
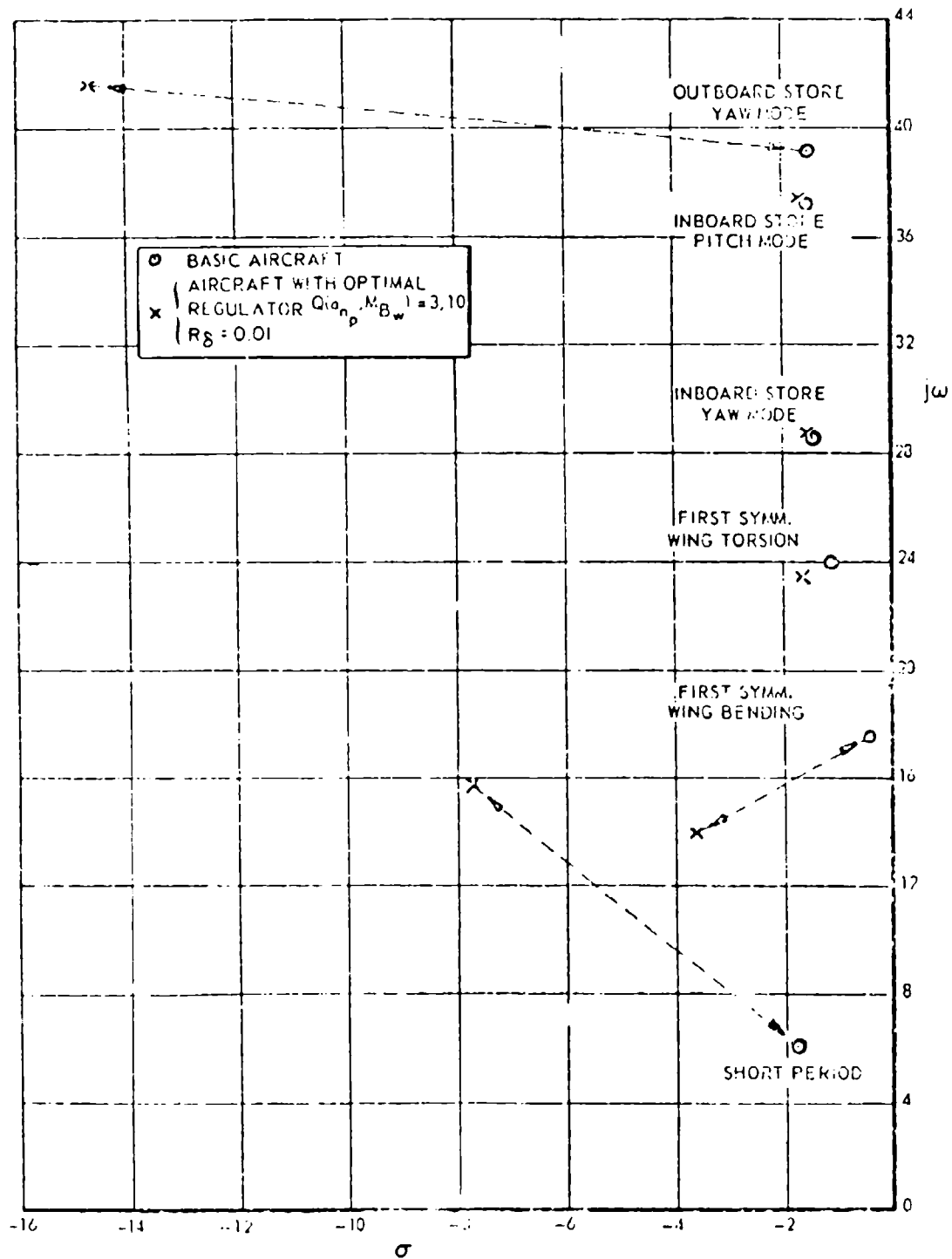
Figure 41. Pole Locations for the Basic Aircraft and
the Aircraft with Optimal Regulator (Ref. 9)

102

TABLE 6.   COMPARISON OF CLOSED-LOOP EIGENVALUES FOR OPTIMAL
AND CONVENTIONAL CONTROLLERS

MODE	AIRCRAFT-ALONE $[\zeta, \omega]$	AIRCRAFT + OPTIMAL REGULATOR	AIRCRAFT + CONVENTIONAL CONTROLLER
Short Period (Rigid Body)	[0.28, 6.3]	[0.44, 17.5]	[0.35, 7.4]
1st Symmetric Wing Bending (Mode 1)	[0.027, 17.6]	[0.255, 14.5]	[0.097, 16.1]
1st Symmetric Wing Torsion (Mode 2)	[0.046, 24.1]	[0.070, 23.6]	[0.073, 23,4]
Inboard Store Yaw Mode (Mode 3)	[0.051, 28.7]	---	---
Inboard Store Pitch Mode (Mode 4)	[0.042, 37.3]	---	---
Outboard Store Yaw Mode (Mode 5)	[0.038, 39.3]	[0.33, 44.09]	[0.05, 38.8]

If the modified short period is considered to be the effective short period mode, the damping ratio is Level 1 but the undamped natural frequency is 70 percent too high at best. Alternatively if the now lower frequency first symmetric wing bending is identified with the short period, the damping ratio is too low for Level 1 and the undamped natural frequency is almost 50 percent too high.

The mere fact that the lowest frequency closed-loop oscillatory modes range from 2.3 to 2.8 Hz when the aircraft-alone short period is about 1 Hz indicates that the optimal controller gains are extraordinarily high indeed. The controller will accordingly saturate at quite low levels of the feedback quantities.

At first glance the optimal regulator would appear to offer a significant advantage over the aircraft plus conventional controller as far as stabilization of the outboard store yaw mode is concerned. This is chimerical because the optimal controller does not take into account in any way the surface actuators and other high frequency filtering. With the surface actuator at 20 rad/sec the closed-loop outboard store yaw mode will hardly be affected by the controller. The results for the first symmetric wing torsion mode are quite similar for the optimal and conventional controller. Neither controller is suitable to modify the inboard store yaw and or pitch modes.

The optimal control of Fig. 41 cannot be mechanized using only the sensors at their current locations since these are insufficient to, by themselves, provide full state feedback for all six modes. Consequently the regulator design is based upon a full set of state vector components developed somehow. These could be achieved with observers, Kalman filters, or pseudo-inverse techniques. In any event, the effective controller will be of even higher order than the pure regulator discussed here. The optimal design also assumes that all three available control effectors are used and that the actuators at these locations have very large bandwidths compared to the highest frequency modes. When all of these points, together with the comparison with the conventional controller, are taken into account it is apparent that the optimal regulator of Ref. 9 has little viability as a practical system. Instead, it must be considered to be an academic exercise which illustrates a procedure. This was, of course, the fundamental purpose of the Ref. 9 report -- a purpose which it serves admirably. The generally unfavorable comparison of the highly complex and unrealistic optimal design with the conventional controller should also be viewed as an academic illustration which indicates some of the problems which must be accounted for if an optimal design is also to be practical.

C. A TRUNCATED FLEXIBLE BEAM EXAMPLE

With both flexible aircraft and large space structures there can be an overlap of the rigid body and bending mode frequencies which require

explicit consideration of the bending modes in the control system syn-
thesis procedure. An extensive literature exists in which the control
synthesis tools employed for control law development for such vehicles
and structures are predominantly based on a continuous optimal regulator
for control and estimation of the state vector using filter/observer
theo·y. A direct consequence of this approach is, typically, to require
n control points and n sensors if the plant equations contain n modes.
Thus the optimal results are at variance with the classical approach of
phase stabilization, which can conceivably increase the damping of many
modes using only one control point and one sensor. Clearly some trans-
lation of the classical ideas into the optimal setup, perhaps coupled
with modifications to optimal procedures, is indicated. In this subsec-
tion we will explore these points using a low order flexible system as
an example. It will serve to demonstrate that

- many physical plants are naturally in a favorable
  sawtooth format

- this sawtooth Bode format is best revealed when
  physical coordinates (as opposed to generalized
  coordinates) are used.

The simple example will then be used in the next subsection to explore
an optimal control approa   which is capable of forcing the sawtooth
Bode form.

Consider the example system comprising three masses coupled by
springs, with the possibility of a control effector at each node, shown
in Fig. 42.
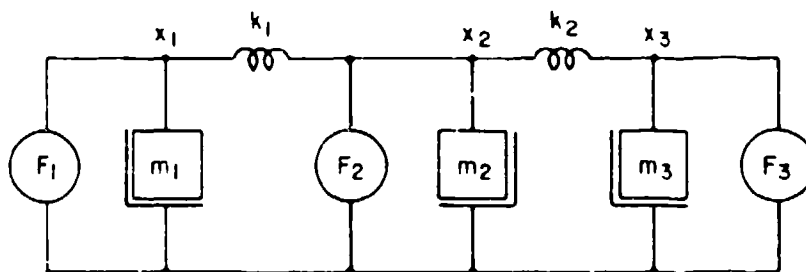
Figure 42. A Three Point-Mass System

The Laplace transformed equations of motion of this system are given by

$$
\begin{bmatrix}
(m_1 s^2 + k_1) & -k_1 & 0 \\
-k_1 & [m_2 s^2 + (k_1 + k_2)] & -k_2 \\
0 & -k_2 & (m_3 s^2 + k_2)
\end{bmatrix}
\begin{bmatrix}
X_1 \\
X_2 \\
X_3
\end{bmatrix}
=
\begin{bmatrix}
F_1 \\
F_2 \\
F_3
\end{bmatrix}
\tag{42}
$$

Equation 42 is a truncated form of the more general discrete mass approximation for conservative flexible systems, which would have the form,

$$
\begin{bmatrix}
(m_1 s^2 + k_1) & -k_1 & 0 & \cdots & \cdots & 0 \\
-k_1 & m_2 s^2 + (k_1 + k_2) & -k_2 & & 0 & \\
0 & -k_2 & m_3 s^2 + (k_2 + k_3) & & & \\
0 & 0 & -k_3 & & & \\
\cdot & & & & & \\
\cdot & & & & & \\
\cdot & & & & & \\
0 & 0 & & \cdots & -k_{n-1} & m_n s^2 + k_{n-1}
\end{bmatrix}
\begin{bmatrix}
X_1 \\
X_2 \\
X_3 \\
\cdot \\
\cdot \\
\cdot \\
X_n
\end{bmatrix}
=
\begin{bmatrix}
F_1 \\
F_2 \\
F_3 \\
\cdot \\
\cdot \\
\cdot \\
F_n
\end{bmatrix}
\tag{43}
$$

The diagonal terms in the plant matrix have a second order format, and the matrix is sparse and symmetric with only diagonal, upper diagonal, and lower diagonal elements. The characteristic function of Eq. 42 is the sixth order expression given by,

$$
\Delta = m_1 m_2 m_3 s^2 \left[s^4 + \left(\frac{k_2}{m_3} + \frac{k_1}{m_1} + \frac{k_1 + k_2}{m_2} \right) s^2 + k_1 k_2 \left(\frac{1}{m_1 m_2} + \frac{1}{m_2 m_3} + \frac{1}{m_1 m_2} \right) \right]
$$

$$
= m_1 m_2 m_3 s^2 \left[s^2 + \omega_1^2 \right] \left[s^2 + \omega_2^2 \right]
\tag{44}
$$

To make the example more specific consider that the system comprises unit masses interconnected with unit springs. Then the matrix equation becomes Eq. 45.

$$\begin{bmatrix} s^2 + 1 & -1 & 0 \\ -1 & s^2 + 2 & -1 \\ 0 & -1 & s^2 + 1 \end{bmatrix} \begin{bmatrix} X_1 \\ X_2 \\ X_3 \end{bmatrix} = \begin{bmatrix} F_1 \\ F_2 \\ F_3 \end{bmatrix} \tag{45}$$

Solving for [X] involves the inverse of the system matrix, which is shown as part of the solution below.

$$\begin{bmatrix} X_1 \\ X_2 \\ X_3 \end{bmatrix} = \frac{\begin{bmatrix} s^4 + 3s^2 + 1 & s^2 + 1 & 1 \\ s^2 + 1 & (s^2 + 1)^2 & s^2 + 1 \\ 1 & s^2 + 1 & s^4 + 3s^2 + 1 \end{bmatrix} \begin{bmatrix} F_1 \\ F_2 \\ F_3 \end{bmatrix}}{s^2(s^4 + 4s^2 + 3)} \tag{46}$$

In factored form this bec·mes

$$\begin{bmatrix} X_1 \\ X_2 \\ X_3 \end{bmatrix} = \frac{\begin{bmatrix} [s^2+(0.618)^2][s^2+(1.618)^2] & [s^2+1] & 1 \\ [s^2 + 1] & [s^2+1]^2 & [s^2+1] \\ 1 & [s^2+1] & [s^2+(0.618)^2][s^2+(1.618)^2] \end{bmatrix} \begin{bmatrix} F_1 \\ F_2 \\ F_3 \end{bmatrix}}{s^2[s^2 + 1][s^2 + (\sqrt{3})^2]} \tag{47}$$

All of these equations describe the plant in physical coordinates, i.e., x_1, x_2, and x_3. One can visualize placing sensors on the physical

107

masses and measuring position, velocity, acceleration, etc., and then feeding such sensed signals to control effectors imposing forces F_1, F_2, and F_3. With velocity or rate sensors (or their equivalent in terms of position sensors followed by lead equalization or acceleration sensors followed by lag equalization) there are a variety of single sensor, single actuator control systems which can stabilize the plant. A cross section of possibilities is shown in Figs. 43 and 44. In the first of these the sensors and actuators are co-located. As can be seen from Fig. 43(a) sensors and actuators co-located at the end points x_1 or x_3 can stabilize all modes with simple pure gain velocity feedbacks. On the other hand a velocity sensor at x_2 is not capable of observing and controlling the mode [0, 1]. This corresponds to the situation where a rate gyro is located at a fuselage station where the [0, 1] mode shape has zero slope. The [0, 1] mode will not be excited by controller inputs but it will be influenced by disturbances. The other modes are well controlled for both commands and disturbances. As seen by examining Fig. 44, for the condition where sensors and actuators are not co-located, it is virtually impossible to exert effective control over all modes with a pure gain single sensor/actuator system. Thus again we see in this example the fundamental sawtooth Bode, phase stabilization concept and application. Just as with the sawtooth Bode concept for flexible aircraft control, these principles for flexible beam stabilization go back many years. For example, Ref. 12 indicated "for vehicles which can be characterized as beams it is unlikely that all flexible modes can be stabilized without structural damping unless the rotational sensor and the control force for each axis are placed where the signs of the slope and deflection are the same for all modes, such as the beginnings or ends of the mode shapes."

These fundamental principles of beam stabilization, co-location etc., aside, the important point to be made for the current discussion is that it is possible with single sensor/actuator combinations to create a highly robust, extremely simple controller and that a cross section of these controllers is easily determined by considering the plant equations in physical coordinates.
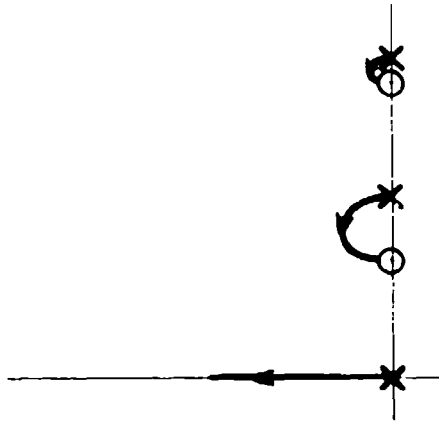
a) $\dfrac{\dot{x}_1}{F_1} = \dfrac{\dot{x}_3}{F_3} = \dfrac{[0,0.618][0,1.618]}{(0)[0,1][0,\sqrt{3}]}$
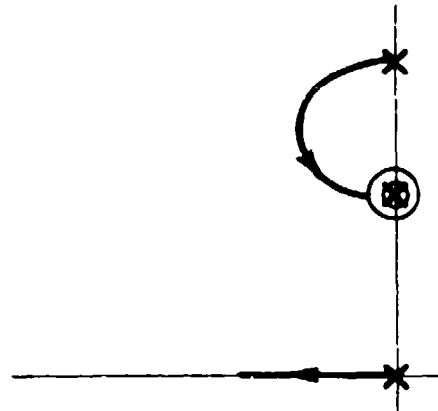
b) $\dfrac{\dot{x}_2}{F_2} = \dfrac{[0,1]^2}{(0)[0,1][0,\sqrt{3}]}$

Figure 43. Single-Sensor/Actuator System
Possibilities for Co-located Systems

109
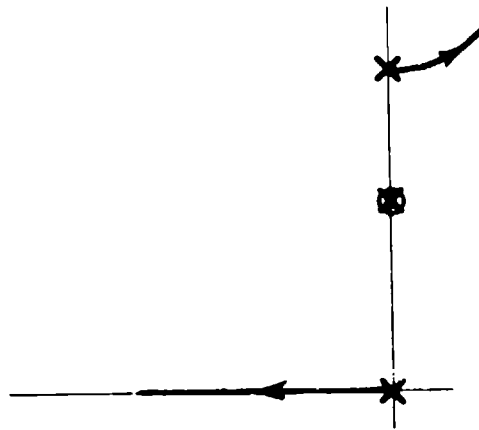
a) $\dfrac{\dot{x}_1}{F_2} = \dfrac{\dot{x}_3}{F_2} = \dfrac{\dot{x}_2}{F_1} = \dfrac{\dot{x}_2}{F_3} = \dfrac{[0,1]}{(0)[0,1][0,\sqrt{3}]}$
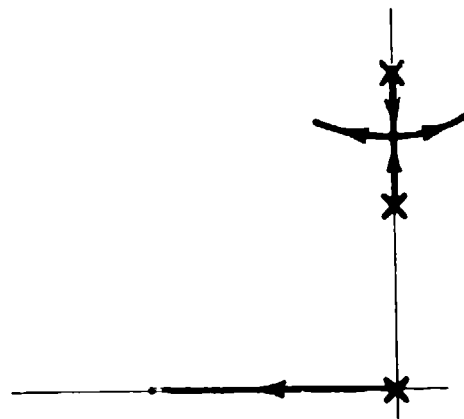
b) $\dfrac{\dot{x}_1}{F_3} = \dfrac{\dot{x}_3}{F_1} = \dfrac{1}{(0)[0,1][0,\sqrt{3}]}$

Figure 44.   Single-Sensor/Actuator System Possibilities
for Non Co-located Systems

The system of Fig. 42 can also be placed into a canonic form in terms of generalized coordinates by using the transformation

$$x = \phi q \tag{48}$$

where the column vectors of ϕ are the eigenvectors corresponding to the eigenvalues related to the eigenvectors of the system,

$$s^2 = 0, \quad s^2 = -1, \quad s^2 = -3 \tag{49}$$

The eigenvectors can be found by substituting the values given in Eq. 49 into Eq. 45 and solving for three constants which force the three equations to be identically zero. To illustrate, for the eigenvector corresponding to $s^2 = -3$, substitute $s^2 = -3$ into Eq. 45:

$$\begin{bmatrix} -2 & -1 & 0 \\ -1 & -1 & -1 \\ 0 & -1 & -2 \end{bmatrix} \begin{bmatrix} a \\ b \\ c \end{bmatrix} = \begin{bmatrix} 0 \\ 0 \\ 0 \end{bmatrix} \tag{50}$$

Since $s^2 = -3$ defines an eigenvalue, the determinant of the matrix of Eq. 50 is zero. Therefore, use Gaussian elimination to eliminate the dependent equations:

$$\begin{bmatrix} -2 & -1 & 0 \\ -1 & -1 & -1 \\ 0 & -1 & -2 \end{bmatrix} \rightarrow \begin{bmatrix} 1 & 1/2 & 0 \\ 1 & 1 & 1 \\ 0 & 1 & 2 \end{bmatrix} \rightarrow \begin{bmatrix} 1 & 1/2 & 0 \\ 0 & 1/2 & 1 \\ 0 & 1 & 2 \end{bmatrix} \rightarrow \begin{bmatrix} 1 & 1/2 & 0 \\ 0 & 1 & 2 \\ 0 & 1 & 2 \end{bmatrix} \rightarrow \begin{bmatrix} 1 & 1/2 & 0 \\ 0 & 1 & 2 \\ 0 & 0 & 0 \end{bmatrix}$$

$$\tag{51}$$

Therefore the independent relationships are,

$$a + b/2 = 0$$

$$b + 2c = 0 \tag{52}$$

Then if $a = 1$, $b = -2$, $c = 1$, the eigenvector $\phi_{s^2 = -3}$ becomes

$$\phi_{s^2=-3} = \begin{bmatrix} 1 \\ -2 \\ 1 \end{bmatrix} \tag{53}$$

Proceeding in a similar manner for $s^2 = 0$ and $s^2 = -1$ yields the transformation matrix

$$\phi = \begin{bmatrix} 1 & 1 & 1 \\ 1 & 0 & -2 \\ 1 & -1 & 1 \end{bmatrix} \tag{54}$$

Premultiply Eq. 45 by ϕ' to form

$$\phi' \begin{bmatrix} s^2+1 & -1 & 0 \\ -1 & s^2+2 & -1 \\ 0 & & s^2+1 \end{bmatrix} \phi q = \phi'F \tag{55}$$

Since all the eigenvectors in the ϕ matrix are mutually orthogonal, the operations indicated by Eq. 55 produce a diagonal (decoupled) matrix on the left hand side:

$$\begin{bmatrix} 3s^2 & 0 & 0 \\ 0 & 2(s^2+1) & 0 \\ 0 & 0 & 6(s^2+3) \end{bmatrix} \begin{bmatrix} q_1 \\ q_2 \\ q_3 \end{bmatrix} = \begin{bmatrix} 1 & 1 & 1 \\ 1 & 0 & -1 \\ 1 & -2 & 1 \end{bmatrix} \begin{bmatrix} F_1 \\ F_2 \\ F_3 \end{bmatrix}$$

$$\tag{56}$$

112

The solution of Eq. 56 for the generalized coordinates is easily written:

$$
\begin{bmatrix} q_1 \\ q_2 \\ q_3 \end{bmatrix} = \begin{bmatrix} \dfrac{1/3}{s^2} & \dfrac{1/3}{s^2} & \dfrac{1/3}{s^2} \\ \dfrac{1/2}{s^2+1} & 0 & \dfrac{-1/2}{s^2+1} \\ \dfrac{1/6}{s^2+3} & \dfrac{-1/3}{s^2+3} & \dfrac{1/6}{s^2+3} \end{bmatrix} \begin{bmatrix} F_1 \\ F_2 \\ F_3 \end{bmatrix} \qquad (57)
$$

It should be clear from the diagonal character of Eq. 56 that feedbacks involving the rates (or their equivalents) of <u>all</u> the generalized coordinates are needed to stabilize and control the three basic modes. For example, a controller which comprises

$$\dot{q}_1 \rightarrow F_1$$

$$\dot{q}_2 \rightarrow F_2 \qquad (58)$$

$$\dot{q}_3 \rightarrow F_3$$

will suffice. With no additional considerations, such as combining the $\dot{q}$'s to form physical coordinates, this controller implies signals from 3 state components fed to 3 actuators to control 3 modes.

Any control system based on generalized coordinates will then appear inherently to be more complicated than the simplest ones for physical coordinates. Again this can be, of course, only a matter of appearance, for the particular combinations of generalized coordinates being used could amount to a single appropriate physical coordinate. Nonetheless there will in general be n feedbacks required for stabilization of n modes <u>if</u> the system states used for feedback control are defined in generalized rather than physical coordinates.

D. OPTIMAL CONTROLLER TO GENERATE SAWTOOTH BODE CONDITIONS

As noted above the majority of optimal control studies for flexible structures use generalized coordinates to describe the plant, resulting typically in the requirement of feedback from all states to all control points. In particular, the use of the quadratic index

$$
J = \frac{1}{2} \int_0^\infty (u'Ru + x'Qx) \, dt = \frac{1}{2\pi j} \int_{c-j\infty}^{c+j\infty} (U^*RU + X^*QX) ds \tag{59}
$$

$$
R > 0, \quad Q \geqslant 0
$$

with diagonal Q and R with non zero elements will always result in feedback from all states to all control points. This result is unsatisfactory when one considers that a sawtooth Bode solution, requiring only one sensor and one co-located actuator, can be set up directly in physical coordinates.

Further, typical optimal control studies involving flexible craft (e.g., Refs. 13-15) appear to yield controller characteristics which contain lightly damped numerator and denominator quadratics. In the words of Ref. 13, "Right-half plane zeros are rarely used in classical compensation networks, but they appear to be common in optimal controllers for systems with poles near the imaginary axis."

None of these features which appear as consequences of routine applications of optimal control are especially attractive. We would like to get around them, while retaining the computational efficiencies available with optimal approaches. To do this we will explore, using the simple three-mode truncated flexible beam example, several aspects of optimal control application. The results will indicate that:

- optimal control procedures using the performance index of Eq. 59, with diagonal elements only (although some equal to zero), can generate a sawtooth Bode control law in physical coordinates;

- this same control law can be induced using gener-
  alized coordinates, but the Q matrix in the per-
  formance index will be quite peculiar -- still
  symmetric but non-diagonal.

The first key question is whether the performance index of Eq. 59
can be used to generate a control law in generalized coordinates which
will transform into a sawtooth Bode control law in physical coordinates.
For the simple beam example, the answer to this question is in the
affirmative. To see this, imagine that only MASS #1 has a co-located
sensor and actuator and rewrite the physical coordinate set (Eq. 45) as

$$
\begin{bmatrix} s^2 + 1 & -1 & 0 \\ -1 & s^2 + 2 & -1 \\ 0 & -1 & s^2 + 1 \end{bmatrix}
\begin{bmatrix} x_1 \\ x_2 \\ x_3 \end{bmatrix}
=
\begin{bmatrix} 1 \\ 0 \\ 0 \end{bmatrix} U +
\begin{bmatrix} F_1' \\ F_2' \\ F_3' \end{bmatrix}
\tag{60}
$$

Here the control vector U is a part of the general applied force vector
F in Eqs. 42 or 45, e.g., $F_1 = U_1 + F_1'$. Otherwise Eq. 60 and Eq. 45
are identical.

One may treat the system of Eq. 60 as a regulator problem by drop-
ping the external force vector F' and replacing it with the transform of
the initial condition vector. When this is done, a Wiener-Hopf approach
to the optimization immediately suggests a performance index of the form

$$
R = 1; \quad Q = \begin{bmatrix} -s^2 & 0 & 0 \\ 0 & 0 & 0 \\ 0 & 0 & 0 \end{bmatrix}
\tag{61}
$$

For those more comfortable with first-order notation (as opposed to
degree-of-freedom), the setup of Eqs. 60 and 61 can be restructured into
a first-order format by defining

$$
\dot{x}_1 = x_4
$$

$$
\dot{x}_2 = x_5 \tag{62}
$$

$$
\dot{x}_3 = x_6
$$

Thus

$$
\begin{bmatrix} \dot{X}_1 \\ \dot{X}_2 \\ \dot{X}_3 \\ \dot{X}_4 \\ \dot{X}_5 \\ \dot{X}_6 \end{bmatrix} = \left[\begin{array}{ccc|ccc} & & & 1 & 0 & 0 \\ & 0 & & 0 & 1 & 0 \\ & & & 0 & 0 & 1 \\ \hline -1 & 1 & 0 & & & \\ 1 & -2 & 1 & & 0 & \\ 0 & 1 & -1 & & & \end{array} \right] \begin{bmatrix} X_1 \\ X_2 \\ X_3 \\ X_4 \\ X_5 \\ X_6 \end{bmatrix} + \begin{bmatrix} 0 \\ 0 \\ 0 \\ 1 \\ 0 \\ 0 \end{bmatrix} U \tag{63}
$$

and

$$
R = 1; \qquad Q = \left[\begin{array}{ccc|ccc} 0 & & & & 0 & \\ & & & & & \\ \hline & & & 1 & 0 & 0 \\ & 0 & & 0 & 0 & 0 \\ & & & 0 & 0 & 0 \end{array} \right] \tag{64}
$$

with (3×3) and (3×3) labels above, and (3×3) and (3×3) below.

Application of any standard time domain optimal solution program based on either eigenvalue decomposition or a Riccati-based solution will yield a feedback K matrix

$$
K = [0 \quad 0 \quad 0 \quad 1 \quad 0 \quad 0] \tag{65}
$$

and thus produce the sawtooth Bode solution in physical coordinates.

Next, we explore the structure of the R and Q matrix needed to achieve the equivalent result in generalized coordinates. In generalized coordinates one has a formulation, equivalent to Eq. 60, of

$$
\begin{bmatrix} s^2 & 0 & 0 \\ 0 & s^2 + 1 & 0 \\ 0 & 0 & s^2 + 3 \end{bmatrix} \begin{bmatrix} q_1 \\ q_2 \\ q_3 \end{bmatrix} = \begin{bmatrix} 1/3 \\ 1/2 \\ 1/6 \end{bmatrix} U + \begin{bmatrix} 1/3 & 1/3 & 1/3 \\ 1/2 & 0 & -1/2 \\ 1/6 & -1/3 & 1/6 \end{bmatrix} F \tag{66}
$$

116

Again, one may switch to a first-order form by the assignment

$$
\begin{aligned}
\dot{q}_1 &= q_4 \\
\dot{q}_2 &= q_5 \\
\dot{q}_3 &= q_6
\end{aligned}
\tag{67}
$$

giving

$$
\begin{bmatrix} \dot{q}_1 \\ \dot{q}_2 \\ \dot{q}_3 \\ \dot{q}_4 \\ \dot{q}_5 \\ \dot{q}_6 \end{bmatrix}
=
\left[
\begin{array}{ccc|ccc}
 & & & 1 & 0 & 0 \\
 & 0 & & 0 & 1 & 0 \\
 & & & 0 & 0 & 1 \\
\hline
0 & 0 & 0 & & & \\
0 & -1 & 0 & & 0 & \\
0 & 0 & -3 & & &
\end{array}
\right]
\begin{bmatrix} q_1 \\ q_2 \\ q_3 \\ q_4 \\ q_5 \\ q_6 \end{bmatrix}
+
\begin{bmatrix} 0 \\ 0 \\ 0 \\ 1/3 \\ 1/2 \\ 1/6 \end{bmatrix}
U
\tag{68}
$$

The Wiener-Hopf degree-of-freedom Q matrix, when translated into the first-order format, will appear as

$$
Q =
\begin{bmatrix}
0 & 0 & 0 & 0 & 0 & 0 \\
0 & 0 & 0 & 0 & 0 & 0 \\
0 & 0 & 0 & 0 & 0 & 0 \\
0 & 0 & 0 & 1 & 0 & 0 \\
0 & 0 & 0 & 0 & 0 & 0 \\
0 & 0 & 0 & 0 & 0 & 0
\end{bmatrix}
\tag{69}
$$

117

What is the equivalent in generalized coordinates? In physical coordinates (using Wiener-Hopf)

$$X'QX = [X_1, X_2, X_3] \begin{bmatrix} -s^2 & 0 & 0 \\ 0 & 0 & 0 \\ 0 & 0 & 0 \end{bmatrix} \begin{bmatrix} X_1 \\ X_2 \\ X_3 \end{bmatrix} = q'\phi'Q\phi q'$$

$$= [q_1, q_2, q_3] \begin{bmatrix} 1 & 1 & 1 \\ 1 & 0 & -1 \\ 1 & -2 & 1 \end{bmatrix} \begin{bmatrix} -s^2 & 0 & 0 \\ 0 & 0 & 0 \\ 0 & 0 & 0 \end{bmatrix} \begin{bmatrix} 1 & 1 & 1 \\ 1 & 0 & -2 \\ 1 & -1 & 1 \end{bmatrix} \quad (70)$$

$$X'QX \to Q_{gen} = \begin{bmatrix} -s^2 & -s^2 & -s^2 \\ -s^2 & -s^2 & -s^2 \\ -s^2 & -s^2 & -s^2 \end{bmatrix} \quad (71)$$

In first-order format, using $\dot{q}_1 = q_4$, etc., Eq. 71 becomes

$$Q_{gen} = \left[\begin{array}{ccc|ccc} 0 & 0 & 0 & 0 & 0 & 0 \\ 0 & 0 & 0 & 0 & 0 & 0 \\ 0 & 0 & 0 & 0 & 0 & 0 \\ \hline 0 & 0 & 0 & 1 & 1 & 1 \\ 0 & 0 & 0 & 1 & 1 & 1 \\ 0 & 0 & 0 & 1 & 1 & 1 \end{array} \right] \quad (72)$$

Also, $R = 1$, as before. Application of time domain optimal control to the system defined by Eq. 68, using the Q matrix of Eq. 69, gives the gain matrix

$$K = [0 \quad 0 \quad 0 \quad 1 \quad 1 \quad 1] \quad (73)$$

118

The closed-loop system will be the same (when transformed back to physical coordinates) as the closed-loop system synthesized with the Q matrix of Eq. 64.

For each system, the closed-loop eigenvalues are

$$s = 0$$

$$s = -0.416283541$$

$$s = -0.233676852 \pm j\, 0.885556760 \qquad (74)$$

$$s = -0.058181377 \pm j\, 1.691279149$$

We also note, in passing, that the sawtooth Bode for this system can be invoked in physical coordinates by the selection of

$$H' = [0 \quad 0 \quad 0 \quad 1 \quad 1 \quad 1] \qquad (75)$$

where $\qquad Q = H\, H'$

A critical point in this development is that, for generalized coordinates, the Q matrix defined in Eq. 72 is non-diagonal but still symmetric. This unusual Q matrix is one secret to the evolution of a simple, pure gain, single sensor/actuator system from an optimal control procedure. We believe that this exercise is novel in that a Q, R formulation has been given for a phase-stabilizable sawtooth Bode configuration. As such, these results provide insight as to the formulation of co-located actuator/sensor controllers as optimal control problems, whether formulated in physical coordinates or in generalized coordinates.

SECTION VI

CONCLUSIONS

In this report we have examined, on an exploratory case study basis, the application of some prominent direct digital design procedures to the analysis of control systems for vehicles with flexible modes. Conclusions have been provided in the main text in the discussion for each of the examples, but some of the more interesting are worthy of reprise for emphasis. These are summarized below.

w-Domain Analysis Procedures

- The w-domain transfer function approach permits a direct carryover of classical frequency response synthesis procedures and stability analyses.

- The additional zeros introduced in w-domain transfer functions by the sampling and hold operations of digital systems:

  -- directly show the phase lag associated with sampling as the result of a rhp zero at w = 2/T;

  -- indirectly lead to some stability conditions for the sampled system which have no parallels in their continuous counterpart.

- The w-domain transfer function poles and zeros which transfer from the s-domain continuous case are only slightly affected by the fact of sampling until the sampling frequency, 1/T, approaches their magnitude. Thus, for pole and zero magnitudes less than about 1/T, the w-domain poles and zeros are closely approximated by those in the s-domain.

Hybrid Frequency Response Analysis

- The understanding of digital system response questions, as contrasted to stability, requires consideration of the modulation products associated with the impulse train amplitude modulation features of digital systems. The hybrid frequency response is an excellent approach to study these questions.

120

- A lightly damped flexible mode subjected to sampling gives rise to "resonances" at frequencies which are sums and differences of the flexible mode natural frequency and n times the sampling frequency. The lowest difference frequency may reflect a "resonance" to a value which may have an impact within the control bandwidth. Similarly, "notches" are reflected from transfer function numerator quadratics.

- The hybrid frequency response, by delivering all the output components for a sinusoidal input, permits the simple calculation of output waveforms. These can be particularly instructive in showing the non-periodic response and waveform distortion present as a consequence of the sampling process.

- As sampling rates are lowered the output distortion revealed by the hybrid frequency response will ordinarily become critical well before the effects of sampling and hold on stability.

Control Systems for Flexible Vehicles

- The straightforward survey of control possibilities using the sawtooth Bode concept as a guide reduces the total number of reasonable feedback possibilities to a small number of feasible contenders.

- The flying quality, bending mode relief, and pilot station excitation requirements, coupled with the desire to improve the flexible mode characteristics, combine to dictate a very small number of feasible system feedback architectures.

- The sawtooth Bode concept for phase stabilization of flexible modes is one of the continuous control schemes which carry over directly into the w-domain.

- An attempt to apply optimal control procedures in a routine fashion, without taking into account the flying qualities, actuation, and other practical considerations, will result in a design which has little practical relevance.

121

Optimal Control Applications to Flexible
Mode Controller Designs

- The highly robust, extremely simple, controller designs permitted by application of the sawtooth Bode concept cannot be realized by straightforward and routine application of optimal control procedures using a positive definite performance index with diagonal Q and R weighting matrices. The controller synthesized in this fashion will typically have feedbacks from all states to all control points, and will often have lightly damped right-half plane zeros.

- The consideration of physical coordinates in contrast to generalized coordinates can be very handy in the apparent simplification of controller feedback quantities. For example, the requirement to feedback all generalized coordinates to affect all the flexible modes may conceivably be translated into a requirement to feedback as little as one physical coordinate.

- A sawtooth Bode controller, can be readily achieved using optimal control procedures by selecting a special form of performance index. For example, using physical coordinates in the simple truncated beam case, a performance index using $R = 1$ and Q having only a single non-zero component will provide a pure gain, sawtooth Bode controller which damps all modes.

- A sawtooth Bode controller for the truncated beam example expressed in generalized coordinates can be induced by a Q matrix which is <u>non-diagonal</u> but symmetric. This unusual Q matrix is one secret to the evolution of a simple, pure gain, single sensor/actuator controller using an optimal control procedure.

REFERENCES

1. Franklin, Gene F., and David Powell, _Digital Control of Dynamic Systems_, Addison-Wesley, Menlo Park, CA, 1980.

2. Whitbeck, Richard F., and L. G. Hofmann, _Analysis of Digital Flight Control Systems with Flying Qualities Applications._ _Volume II -- Technical Report_, AFFDL-TR- 78-115, vol. II, Sept. 1980.

3. Whitbeck, Richard F., and Dennis G. J. Didaleusky, _Multi-Rate Digital Control Systems with Simulation Applications._ _Volume I: Technical Report_, AFWAL-TR-80-3101, Sept. 1980.

4. Whitbeck, Richard F., _Elements of Simulation Error Analysis_, AFWAL-TR-82-3022, June 1982.

5. Johnston, Donald E., and Walter A. Johnson, _Feasibility of Conventional Control Techniques for Large Highly Coupled Elastic Boost Vehicles_, NASA CR-88760, Mar. 1967.

6. Ashkenas, Irving L., Raymond E. Magdaleno, and Duane T. McRuer, _Flight Control and Analysis Methods for Studying Flying and Ride Qualities of Flexible Transport Aircraft_, NASA CR-172201, Aug. 1983.

7. McRuer, Duane T., and Donald E. Johnston, _Flight Control Systems Properties and Problems, Volume I_, NASA CR-2500, Feb. 1975.

8. Andrew, G. M., and J. M. Johnson, Jr., "Automatic Control of Aeroelastic Modes," IAS Paper 62-86, June 1962.

9. Erkelens, L. J. J., and J. L. Simons, _A Method for Applying Linear Optimal Control Theory to the Design of a Regulator for a Flexible Aircraft_, National Aerospace Lab., NLR TR-80032 U, Mar. 1980.

10. Schwendler, Robert G., and Richard H. MacNeal, _Optimum Structural Representation in Aeroelastic Analyses_, ASD-TR-61-680, Jan. 1962.

11. Pearce, B. F., _Topics in Flexible Airplane Dynamics, Part 1. Residual Stiffness Effects in Truncated Modal Analysis_, ASD-TDR-63-334, Part I, July 1963.

12. Gevarter, William B., "Basic Relations for Control of Flexible Vehicles," _AIAA Journal_, Vol. 8, No. 4, Apr. 1970, pp. 666-672.

13. Martin, Gary Don, and Arthur E. Bryson, Jr., "Attitude Control of a Flexible Spacecraft," A Collection of Technical Papers; Proc. of the AIAA Guidance and Control Conference, Palo Alto, CA, Aug. 1978.

14. Newsom, Jerry R., A Method for Obtaining Practical Flutter Suppression Control Laws Using Results of Optimal Control Theory, NASA TP-1471, Aug. 1979.

15. Mukhopodhyay, V., J. R. Newsom, and I. Abel, "Reduced-Order Optimal Feedback Control Law Synthesis for Flutter Suppression," J. Guidance, Control, and Dynamics, Vol. 5, No. 4, July-Aug. 1982.

APPENDIX A

EQUATIONS OF MOTION FOR EXAMPLE FLEXIBLE AIRCRAFT

Feedback Controls Survey and Closed-Loop Design Example

This appendix presents the system equations of motion in the frequency domain for both the feedback controls survey and the selected loop closure. The basic airframe and sensor equations are those of Ref. 9 for a contemporary, flexible, light fighter aircraft equipped with heavy external stores. The data base comprised two rigid body modes (pitch and heave) and five structural modes responding to elevator, flap and aileron inputs. The supplied sensor equations include acceleration and pitch rate at four stations (nose, tail, wing tip and pilot seat) as well as wing-root bending moment.

Figure A-1 presents the controls survey equations of motion using the general second order form

$$[A_2 s^2 + A_1 s + A_0] x = [B_2 s^2 + B_1 s + B_0] f$$

where the "cell" components of each row and column are stacked vertically, i.e.

$$
\begin{matrix} a_2 \\ a_1 \\ a_0 \end{matrix} \qquad \text{represents } a_2 s^2 + a_1 s + a_0
$$

The system variables, x, and forcing functions, f, are defined in Table A-1 as well as the corresponding column codes used in Fig. A-1.

The results of the controls survey indicated that feedback of shaped a_{n_w} and q_p to the elevator was relatively simple and gave the best performance potential. The block diagram is given in Fig. A-2 and the closed-loop system equations of motion are given in Fig. A-3.

	1 ALF	2 CIO	3 CV1	4 CV2	5 CV3	6 CV4	7 CV5	8 M1	9 M2	10 M3	11 M4	12 M5	13 DE	14 DF
1	3.54 / 4.81	-0.413E-03 / -434.	0	0	0	0	0	0.113E-02 / -0.785	0.640E-02 / 3.11	-0.332E-02 / 5.23	-0.673E-02 / -3.26	-0.742E-02 / -2.38	0.740	0.650
2	0.149E-01 / 1.18	3.78 / 8.74	·	0	0	0	0	-0.373E-02 / -0.230	0.972E-02 / 0.480	0.243E-02 / 1.04	-0.454E-02 / -0.510	-0.972E-03 / -0.470	1.33	-0.270
3	-0.113E-02 / 0.460	-0.519E-02 / -0.230	0.839 / 0	0	0	0	0	0.758E-02 / 2.01	0.194E-02 / 1.28	-0.105E-02 / 1.75	-0.600E-02 / -2.16	-0.527E-02 / -1.31	-0.350	0.140
4	-0.219E-02 / 0.480	-0.247E-02 / 0.200	0	1.46 / 0	0	0	0	0.219E-02 / -0.230	0.245E-01 / 7.15	0.486E-03 / 1.57	-0.102E-01 / -1.91	-0.802E-02 / -1.16	-0.240	0.330
5	0.137E-01 / -2.18	0.122E-01 / -0.650	0	0	41.8 / 0	0	0	-0.440E-02 / 0.610	0.332E-02 / -2.87	1.48 / 414.	0.211E-02 / 3.46	0.543E-02 / -2.30	0.340	-0.500
6	0.235E-02 / -1.54	0.478E-02 / -1.09	0	0	0	3.18 / 0	0	-0.178E-02 / 0.420	-0.729E-02 / -1.87	0.211E-02 / -2.93	0.934E-01 / 36.3	0.102E-01 / 1.49	0.400E-01	-0.510
7	0.648E-02 / -1.47	0.754E-02 / -0.550	0	0	0	0	4.28 / 0	-0.308E-02 / 0.410	-0.583E-02 / -2.05	0.818E-02 / -3.11	0.883E-02 / 2.14	0.800E-01 / 52.5	0.400	-0.730
8	0	0	0 / -1.0	0	0	0	0	0.810E-02 / 0	0	0	0	0	0	0
9	0	0	0	0 / -1.0	0	0	0	0	0.810E-02 / 0	0	0	0	0	0
10	0	0	0	0	0 / -1.0	0	0	0	0	0.810E-02 / 0	0	0	0	0
11	0	0	0	0	0	0 / -1.0	0	0	0	0	0.810E-02 / 0	0	0	0
12	0	0	0	0	0	0	0 / -1.0	0	0	0	0	0.810E-02 / 0	0	0
13	0	0	0	0	0	0	0	0	0	0	0	0	0 / 1.0	0
14	0	0	0	0	0	0	0	0	0	0	0	0	0	0 / 1.0
15	0	0	0	0	0	0	0	0	0	0	0	0	0	0
16	1.0 / 0	-1.13 / -123.	-0.230 / 0	0.129 / 0	0	0.542 / 0	0.223 / 0	0	0	0	0	0	0	0
17	1.0 / 0	-2.96 / -123.	1.0 / 0	1.0 / 0	-1.0 / 0	-1.0 / 0	-0.470 / 0	0	0	0	0	0	0	0
18	1.0 / 0	0.550 / -123.	-0.120 / 0	2.55 / 0	0	0.727 / 0	0.554 / 0	0	0	0	0	0	0	0
19	1.0 / 0	1.99 / -123.	-0.489 / 0	-0.401 / 0	0.455 / 0	0.238 / 0	0.628 / 0	0	0	0	0	0	0	0
20	0	0 / -1.0	0.400E-03	0.440E-02	0	0.960E-02	0.170E-02	0	0	0	0	0	0	0
21	0	0 / -1.0	0.700E-02	-0.270E-01	-0.390E-01	0.680E-01	0.390E-01	0	0	0	0	0	0	0
22	0	0 / -1.0	0.100E-02	0.210E-01	0	-0.110E-01	-0.100E-02	0	0	0	0	0	0	0
23	0	0 / -1.0	0.100E-02	0.500E-02	0	-0.120E-01	-0.400E-02	0	0	0	0	0	0	0

Figure A-1. Controls Survey Equations of Motion

126

15 DA	16 ANP	17 ANM	18 ANN	19 ANT	20 QP	21 QW	22 QN	23 QT			1 DEC	2 DFC	3 DAC	4 ALC	
0 0 0.580	0	0	0	0	0	0	0	0	ALF	1	0	0	0	0 0.534E-02 -4.81	DEC
0 0 0.310	0	0	0	0	0	0	0	0	TTQ	2	0	0	0	0 0.932E-02 -1.18	DFC
0 0 0.600E-01	0	0	0	0	0	0	0	0	CV1	3	0	0	0	0 0.729E-02 -0.440	DAC
0 0 0.220	0	0	0	0	0	0	0	0	CV2	4	0	0	0	0 0.543E-02 -0.480	ALC
0 0 -0.170	0	0	0	0	0	0	0	0	CV3	5	0	0	0	0 -0.352E-02 2.18	
0 0 -0.350	0	0	0	0	0	0	0	0	CV4	6	0	0	0	0 -0.162E-01 1.54	
0 0 -0.410	0	0	0	0	0	0	0	0	CV5	7	0	0	0	0 -0.162E-01 1.47	
0	0	0	0	0	0	0	0	0	M1	8	0	0	0	0	
0	0	0	0	0	0	0	0	0	M2	9	0	0	0	0	
0	0	0	0	0	0	0	0	0	M3	10	0	0	0	0	
0	0	0	0	0	0	0	0	0	M4	11	0	0	0	0	
0	0	0	0	0	0	0	0	0	M5	12	0	0	0	0	
0	0	0	0	0	0	0	0	0	DE	13	0 0 1.0	0	0	0	
0	0	0	0	0	0	0	0	0	DF	14	0	0 0 1.0	0	0	
0 0 1.0	0	0	0	0	0	0	0	0	DA	15	0	0	0 0 1.0	0	
0	0 0 0.338E-01	0	0	0	0	0	0	0	ANP	16	0	0	0	0	
0	0	0 0 0.338E-01	0	0	0	0	0	0	ANM	17	0	0	0	0	
0	0	0	0 0 0.338E-01	0	0	0	0	0	ANN	18	0	0	0	0	
0	0	0	0	0 0 0.338E-01	0	0	0	0	ANT	19	0	0	0	0	
0	0	0	0	0	0 0 0.810E-02	0	0	0	QP	20	0	0	0	0	
0	0	0	0	0	0	0 0 0.810E-02	0	0	QW	21	0	0	0	0	
0	0	0	0	0	0	0	0 0 0.810E-02	0	QN	22	0	0	0	0	
0	0	0	0	0	0	0	0	0 0 0.810E-02	QT	23	0	0	0	0	

Figure A-1.   Controls Survey Equations of Motion (Concluded)

127

TABLE A-1. SYSTEM AND FORCING FUNCTION VARIABLES
USED IN CONTROLS SURVEY AND/OR CLOSED-LOOP
SYSTEM DESIGN EXAMPLE

System Variables

	COL CODE	EOM Var.	Units	Definition
	ALF	α	rad	angle of attack
	C1Q	$c_1 q$	rad	pitch rate (normalized by c_1)^
	CV1	$c_1 v_1$	m	
	CV2	$c_1 v_2$	m	generalized co-ordinate for
	CV3	$c_1 v_3$	m	structural mode deflection rate
	CV4	$c_1 v_4$	m	(normalized by c_1)^
	CV5	$c_1 v_5$	m	
	N1	n_1	m	
	N2	n_2	m	generalized co-ordinate for
	N3	n_3	m	structural mode deflection
	N4	n_4	m	
	N5	n_5	m	
	DE	ζ_e	rad	elevator
**	DF	ζ_f	rad	flaps
**	DA	ζ_a	rad	symmetric ailerons
	ANP	a_{n_p}	g	pilot station acceleration
	ANW	a_{n_w}	g	wing station acceleration
**	ANN	a_{n_n}	g	nose station acceleration
**	ANT	a_{n_t}	g	tail station acceleration
	QP	q_p	rad/sec	pilot station pitch rate
**	QW	q_w	rad/sec	wing station pitch rate
**	QN	q_n	rad/sec	nose station pitch rate
**	QT	q_t	rad/sec	tail station pitch rate
++	MBW	MBW	N-m	wing root bending moment
++	DEF	ζ_{e_f}	rad	net feedback to elevator
++	DEA	ζ_{e_a}	rad	a_{n_w} feedback to elevator
++	DEQ	ζ_{e_q}	rad	q_p feedback to elevator

Forcing Functions

	COL CODE	EOM Var.	Units	Definition
	DEC	ζ_{e_c}	rad	elevator command
**	DFC	ζ_{f_c}	rad	flap command
**	DAC	ζ_{a_c}	rad	aileron command
	ALG	α_{g_c}	rad	gust input

++   variables not used for controls survey

**   variables not used for closed-loop system design example
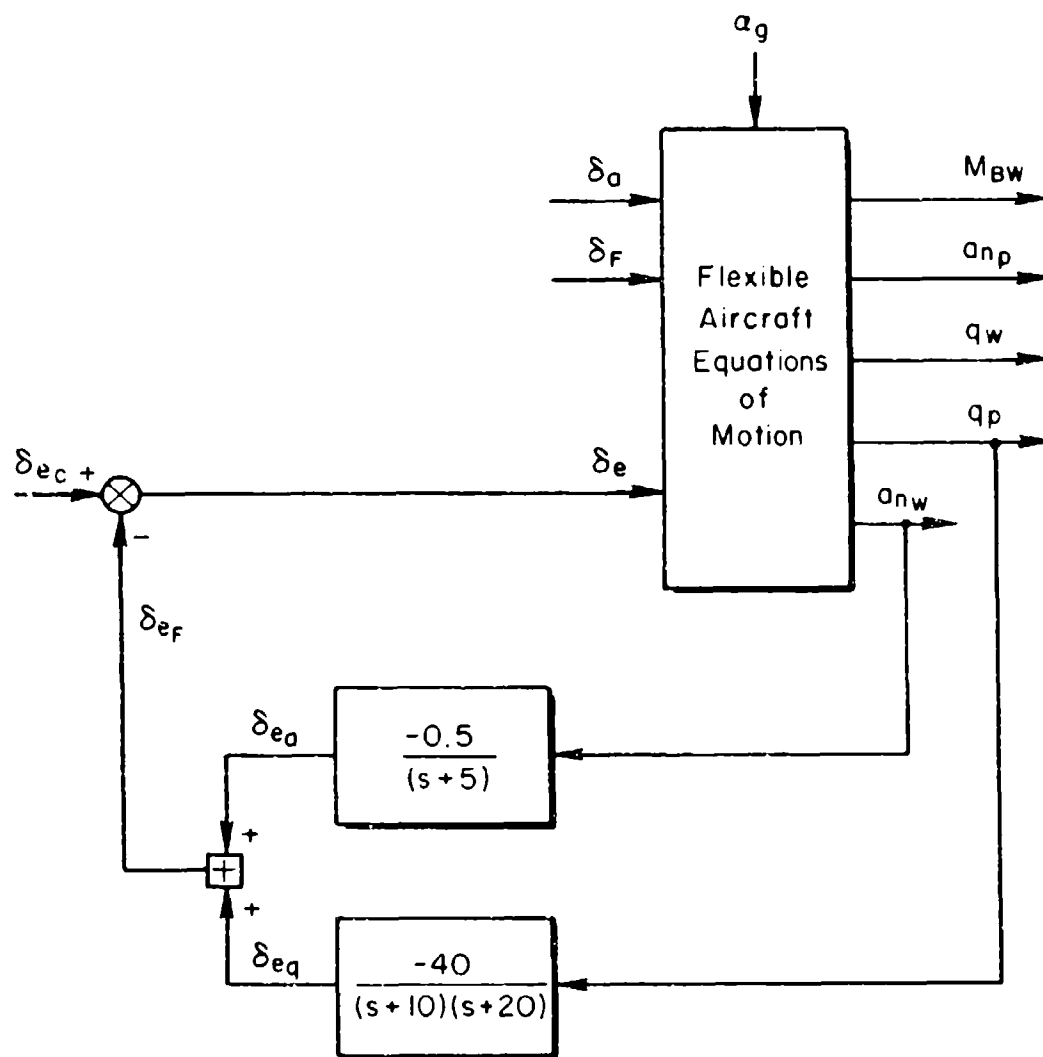
^   normalization constant is c_1 = 2.35/290. sec

128

Figure A-2. Closed-Loop System for Flexible Mode
and Short Period Damping Augmentation

	1 ALF	2 CI3	3 CV1	4 CV2	5 CV3	6 CV4	7 CV5	8 M1	9 M2	10 M3	11 M4
1	0 3.56 4.81	0 -0.413E-02 -434.	0	0	0	c	0	0 0.113E-02 -0.780	0 0.440E-02 3.11	0 -0.332E-02 5.23	0 -0.773E-02 -3.26
2	c 0.169E-01 1.18	0 3.78 6.24	0	0	0	0	c	0 -0.373E-02 -0.205	0 0.972E-02 0.480	0.243E-02 1.04	-0.454E-02 -0.510
3	0 -0.713E-02 0.460	0 -0.519E-02 -0.230	0 0.839 0	0	0	0	0	0 0.758E-02 2.01	0.194E-02 1.28	-0.105E-02 1.75	-0.600E-02 -2.16
4	0 -0.219E-02 0.480	0 -0.247E-02 0.200	0	0 1.46 0	0	0	0	0 0.219E-02 -0.230	0.265E-01 7.15	0.486E-03 1.57	-0.102E-01 -1.91
5	0 0.137E-01 -2.18	0.122E-01 -0.650	0	0	0 61.8 0	0	0	0 -0.640E-02 0.610	0.332E-02 -2.87	1.48 414.	0.211E-02 3.46
6	0 0.235E-02 -1.54	0.478E-02 -1.09	0	0	0	c 3.18 0	0	c -0.178E-02 0.420	-0.729E-02 -1.87	0.211E-02 -2.93	0.934E-01 36.3
7	0 0.648E-02 -1.47	0.754E-02 -0.550	0	0	0	0	0 4.28 0	-0.308E-02 0.410	-0.563E-02 -2.05	0.818E-02 -3.11	0.883E-02 2.14
8	0	0	0 0 -1.0	0	0	0	0	0.810E-02 0	0	0	0
9	0	0	0	0 0 -1.0	0	0	0	0	0.810E-02 0	0	0
10	0	0	0	0	0 0 -1.0	0	0	0	0	0.810E-02 0	0
11	0	0	0	0	c	0 0 -1.0	0	0	0	0	0.810E-02 0
12	0	0	0	0	0	0	0 0 -1.0	0	0	0	0
13	0	0	0	0	0	0	0	0	0	0	0
14	0 1.0 0	0 -1.13 -123.	0 -0.230 0	0 0.129 0	0	0 0.542 0	0 0.223 0	0	0	0	0
15	0 1.0 0	0 -2.96 -123.	0 1.0 0	0 1.0 ?	-1.0 0	-1.0 0	-0.470 0	0	0	0	0
16	0	0 0 -1.0	0.400E-03	0.440E-02	0	0.960E-02	0.170E-02	0	0	0	0
17	c 0.865E+06 0.184E+07	0 0.162E+06 -0.106E+09	0.485E+06 0.459E+06	-0.474E+05 0.632E+06	-0.950E+06 -0.107E+07	-0.993E+05 -0.102E+07	-0.452E+06 -0.192E+07	0 0 -0.536E+06	0 0 0.235E+07	0 0 0.362E+07	0 0 -0.304E+07
18	0	0	0	0	0	0	0	0	0	0	0
19	0	0	0	0	0	0	0	0	0	0	0
20	0	0	0	0	0	0	0	0	0	0	0

Figure A-3. Closed-Loop System Equations of Motion for Elevator Control of Flexible Mode and Short Period Damping Augmentation

12 MS	13 DE	14 ANF	15 ANW	16 QP	17 MBW	18 DEF	19 DEA	20 DEQ			1 DEC	2 ALG	
0 -0.762E-02 -2.38	0 0 0.740	0	0	0	0	0	0	0	ALF 1		0	0 0.534E-02 -4.81	DEC
0 -0.972E-03 -0.470	0 0 1.33	0	0	0	0	0	0	0	C10 2		0	0 0.932E-02 -1.18	ALG
0 -0.527E-02 -1.31	0 0 -0.350	0	0	0	0	0	0	0	CV1 3		0	0 0.729E-02 -0.460	
0 -0.802E-02 -1.18	0 0 -0.240	0	0	0	0	0	0	0	CV2 4		0	0 0.543E-02 -0.480	
0 0.543E-02 -2.30	0 0 0.340	0	0	0	0	0	0	0	CV3 5		0	0 -0.352E-02 2.18	
0 0.103E-01 1.49	0 0 0.400E-01	0	0	0	0	0	0	0	CV4 6		0	0 -0.162E-01 1.54	
0 0.800E-01 52.5	0 0 0.400	0	0	0	0	0	0	0	CV5 7		0	0 -0.162E-01 1.47	
0	0	0	0	0	0	0	0	0	M1 8		0	0	
0	0	0	0	0	0	0	0	0	M2 9		0	0	
0	0	0	0	0	0	0	0	0	M3 10		0	0	
0	0	0	0	0	0	0	0	0	M4 11		0	0	
0 0.810E-02 0	0	0	0	0	0	0	0	0	M5 12		0	0	
0	0 0 1.0	0	0	0	0	0 0 1.0	0	0	DE 13		0 0 1.0	0	
0	0	0 0 0.338E-01	0	0	0	0	0	0	AMP 14		0	0	
0	0	0	0 0 0.338E-01	0	0	0	0	0	ANW 15		0	0	
0	0	0	0	0 0 0.810E-02	0	0	0	0	QP 16		0	0	
0 0 -0.203E+07	0	0	0	0	0 0 1.0	0	0	0	MBW 17		0	0 0.199E+05 -0.184E+07	
0	0	0	0	0	0	0 0 1.0	0 0 -1.0	0 0 -1.0	DEF 18		0	0	
0	0	0	0 0 0.100	0	0	0	0 0.200 1.0	0	DEA 19		0	0	
0	0	0	0	0 0 0.200	0	0	0	0.509E-02 0.150 1.0	DEQ 20		0	0	

APPENDIX B

MAPPING BETWEEN THE s, z, and w-DOMAINS

This appendix presents a variety of graph forms suitable for interpreting and/or converting roots from one domain to another. These were prepared using the transformations

$$z = e^{Ts} = \frac{1 + Tw/2}{1 - Tw/2} = -\frac{(w + 2/T)}{(w - 2/T)}$$

The figures provided are:

Fig. B-1   w-domain with s-domain contours of ζ, ω_n

Fig. B-2   z-domain with s-domain contours of ζ, ω_n

Fig. B-3   s-domain with w-domain contours of ζ, ω_n

Fig. B-4   z-domain with w-domain contours of ζ, ω_n

Generally the user enters a plot with the rectangular coordinates of a root and interpolates within the contours for the ζ and ω_n of the other domain.

Figures B-1 and B-3 are sized to illustrate that roots well below the folding frequency are essentially equal (numerically) in s or w.
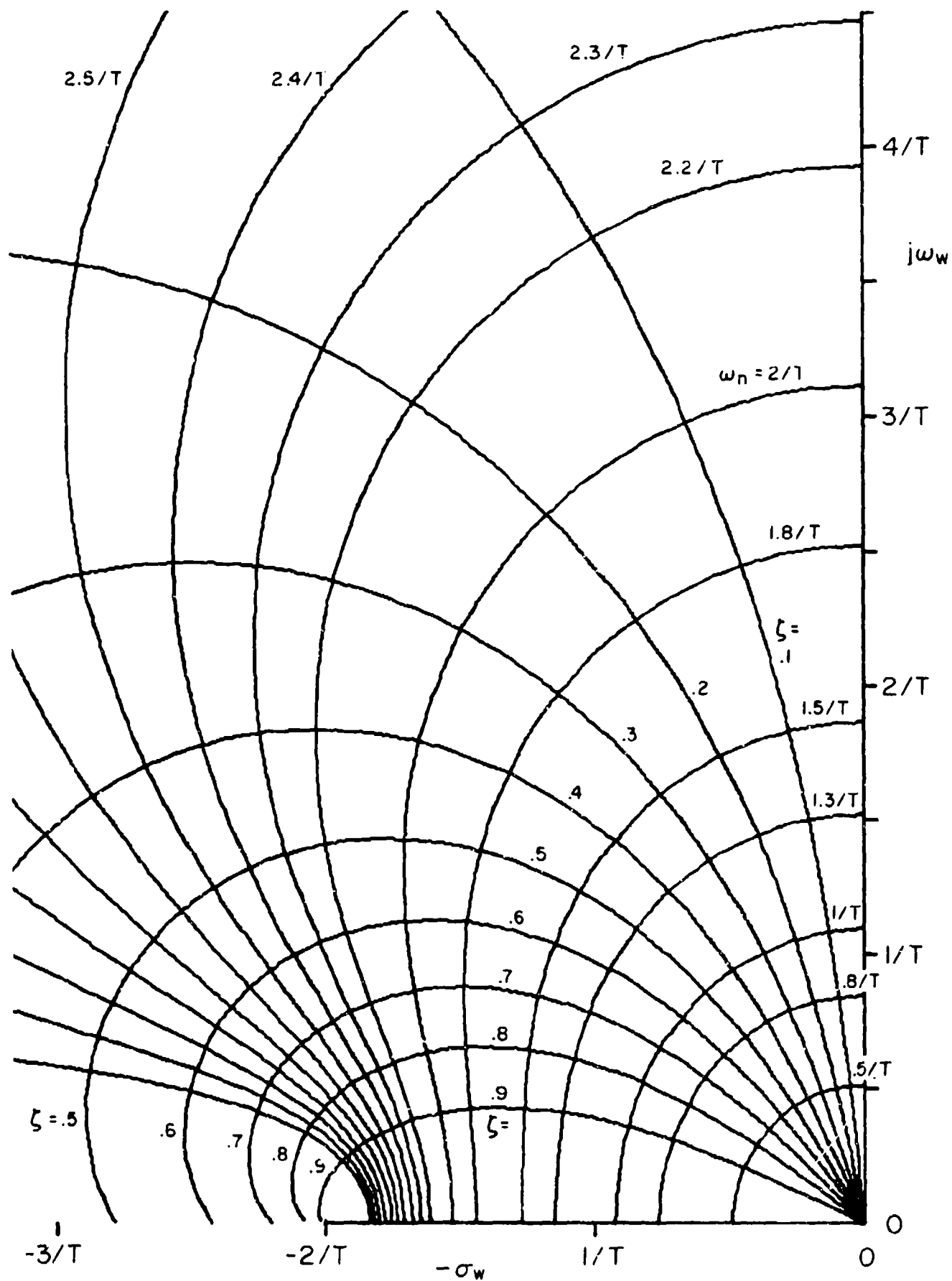
Figure B-1. w-Domain with s-Domain Contours of ζ, ω_n
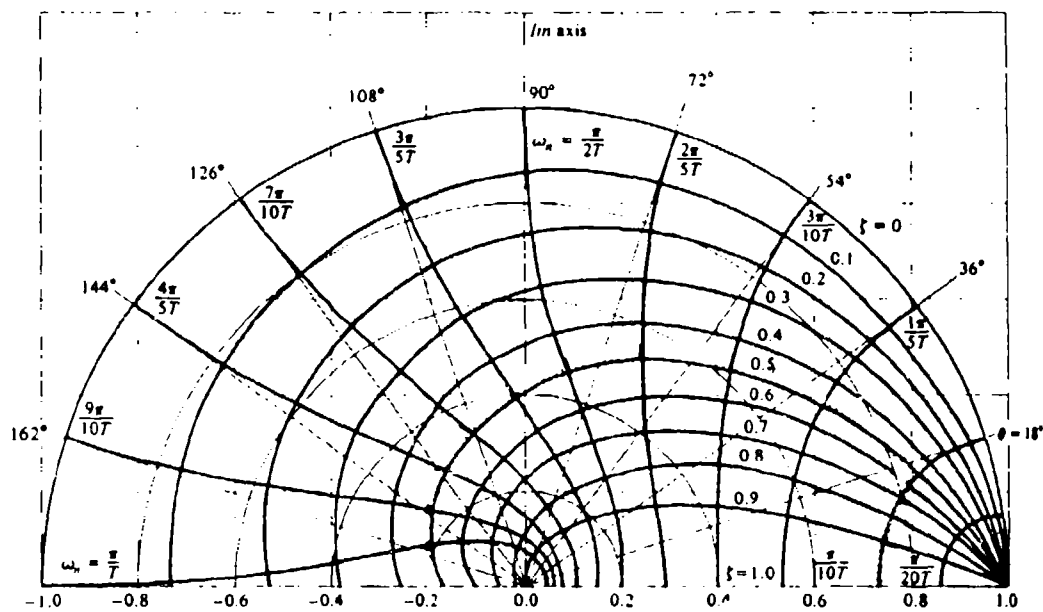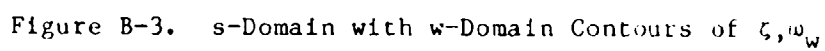
Figure B-2. z-Domain with s-Domain Contours of ζ, ω_n
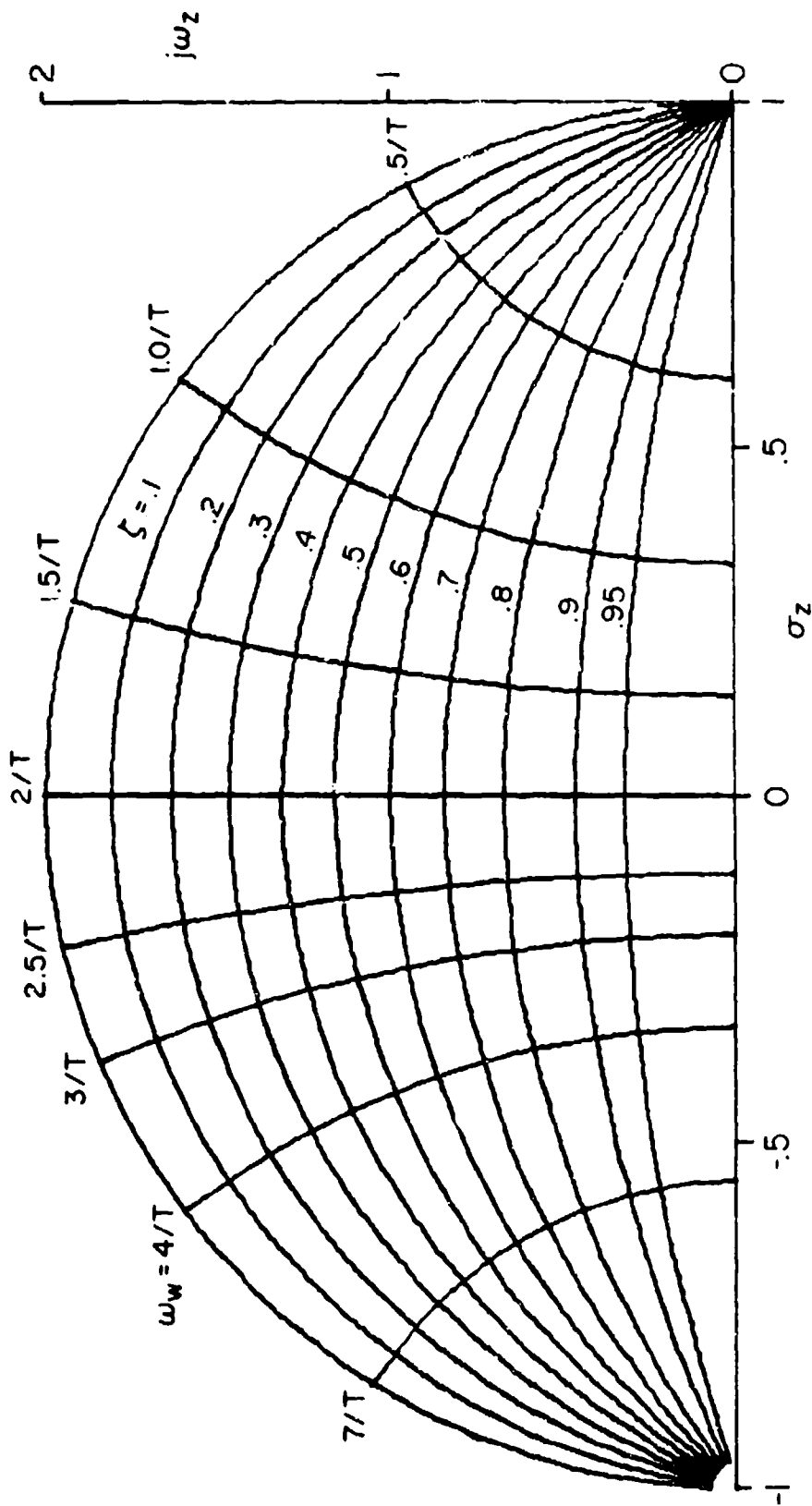(adopted from Ref. 1)

Figure B-3.   s-Domain with w-Domain Contours of ζ, ω_w

Figure B-4. z-Domain with w-Domain Contours of ζ, ω_w